POLITECNICO DI MILANO

School of Industrial Process Engineering

Master of Science in Materials Engineering and Nanotechnology

Department of Chemistry, Materials and Chemical Engineering "Giulio Natta"

DAMAGE SENSING AND SELF-HEALING MATERIALS THROUGH MICROENCAPSULATION PROCESS

Supervisor: Prof. Stefano TURRI

Co- Supervisor: Ing. Giovanni POSTIGLIONE

Master of Science Thesis by:

Oriana FERRULLI

ID.:787113......

Anno Accademico 2013 – 2014

Summary

GLOSSARY OF TERMS

X_c - Core Fraction

X_c^{TGA} - Core Fraction calculated by TGA analysis

η_{encaps} - Encapsulation efficiency

η_r - Reaction efficiency

7MC - 7-Methoxycoumarin

ACBP - 2-Amino-5-chlorobenzophenone

Acripol - Acrylpolyurethane from EP Vernici

Ant. - Dipentaerythritol pentaacrylate, SR399 from Sartomer Co

BuOAc - Butyl acetate

C120 - 7-Amino-4-Methylcumarin

C1 - Methacrylate matix coating with S1 microcapsules

C2 - Methacrylate matix coating with S2 microcapsules

C3 - P56 matix coating with S2 microcapsules

C4 - Acripol matix coating with S3-L microcapsules

C5 - P56 matix coating with S3-L microcapsules

C6 - P56 matix coating with S3-EPy microcapsules

CB - Chlorobenzene

DABP - 4-4' Diaminobenzophenone

Dar. - 2-Hydroxy-2- methylpropiophenone (trade name: Darocure 1173®)

DL75 - Desmodur L75

DMF - N,N-Dimethylformamide

DSC - ethoxylated trimethylolpropane triacrylate from Sigma-Aldrich®

ECC - 3,4-epoxycyclohexylmethyl 3,4 epoxycyclohexane carboxylate from Sigma Aldrich®

EPy - 1-Ethenylpyrene

FN408 - Eu Complex

FTIR - Infrared spectroscopy

H1A - microcapsules with DABP based polyurea shell/ SR499 core

H1B - microcapsules with DABP based polyurea shell/ TMPTA428 core

H2	-	microcapsules with DABP based polyurea shell/ SR399 core
H3	-	microcapsules with DABP based polyurea shell/ ECC core
LUM	-	Lumoge FViolet
MeOH	-	Methanol
MPy	-	1-Methylpyrene
O/W	-	Oil in Water
OM	-	Optical microscopy
P56	-	FLUOROLINK® P56 (Solvey)
p-DSC	-	Photo-differential scanning calorimetry
PEGMA		PEG monomethacrylate
PUrea	-	Polyurea
S1	-	microcapsules with ACBP based polyurea shell/ sp-dye in sunflower oil core
S2	-	microcapsules with DABP based polyurea shell/ sp-dye in sunflower oil core
S3	-	microcapsules with DABP based polyurea shell/ fluorescent dye in sunflower oil core
SEM	-	Scanning Electron Microscopy
SP-dye	-	1',3'-dihydro-1',3,3'-trimethyl-6-nitrospiro[2H-1-benzopyran-2,2'-(2H)-indole]
SR499	-	ethoxylated trimethylolpropane triacrylate from Sartomer Co
SR399	-	dipentaerythritol pentaacrylate, from Sartomer Co
TEGDMA	-	tetraethylenglycol dimethacrylate
TGA	-	Thermogravimetric analys
TMPTA428/612	-	ethoxylated trimethylolpropane triacrylate from Sigma-Aldrich®
UV-VIS	-	UV-VIS spectroscopy

LIST OF FIGURES

LIST OF TABLES

Table 1.1 Possible external stimuli, which include a chromatic or non-chromatic response into the material.

Table 1.2: Classification of polymeric smart materials based on non cromatic response[11].

Table 1.3: Classification of polymer smart materials based on chromatic response[11]

Table 1.4: Classification of polymeric smart materials based on color response with intrinsic smart functionality[11].

Table 1.5: Different important microencapsulation techniques

Table 1.6: Advantage and Disadvantages of Emulsion-Based Methods for Preparing Microcapsules. *: SEM images of (A) core-shell microcapsules with poly(urea-formaldehyde) wall and dicyclopentadiene core (scale bar = 100 μm),[162] (B) hollow PSS/PAH capsules (scale bar = 1 μm),[37] (C) microcapsule formed from gum arabic/gelatin coacervation (scale bar = 500 μm),[163] and (D) microcapsules formed from the internal phase separation of PMMA (scale bar =10 μm).

Table 1.7: Classification of self-healing meterials based on activating stimulus

Table 2.1: Properties of luminescent dyes. Where λ_{ex} is the maximum absorption wavelength and λ_{em} maximum emission wavelength.

Table 2.2: The chemical structures and important physical properties of reactive monomers.

Table 2.3: Quantities of chemicals used to prepare damage sensing microcapsules. ACBP: 2-Amino-5-chlorobenzophenone; DABP: 4-4' Diaminobenzophenone; DL75:DesmodurL75; CB: Chlorobenzene; DMF: N,N-Dimethylformamide.

Table 2.4: : Quantities of chemicals used to prepare self-healing microcapsules. ACBP: 2-Amino-5-chlorobenzophenone; DABP: 4-4' Diaminobenzophenone; DL75:DesmodurL75; CB: Chlorobenzene; DMF: N,N-Dimethylformamide; Dar: Darocure1173; Ant: Triarylsulfonium hexafluoroantimonate salt.

Table 3.1: Chemicals used for microencapsulation

Table 3.2: Average Diameter and Size Distribution of Microcapsules Synthesized by Different Experimental Conditions

Table 3.3: Reaction efficiencies, encapsulation efficiencies and core fractions of damage sensing microcapsules.

ABSTRACT

Smart materials are a class of materials able to respond to stimuli and environmental changes and to activate their functions according to these changes. The design, fabrication, and construction of smart structures is one of the ultimate challenges for engineering researchers today.

With the aim to extend materials lifetime two types of smart materials are knowing a growing interest especially in the coating field: damage sensing and self-healing materials. The first ones allows the damage identification whilst the second ones possess the intrinsic capability to heal small cracks. A method for the production of materials with those advanced properties includes the microencapsulation, which is the process of enclosing a liquid core within a polymeric shell.

The present work reports the fabrication of novel microcapsules characterized by a UV-screening shell and examples of composite coatings containing such microcapsules. After a mechanical damage is applied, the microcapsules rupture leads to the core diffusion into the matrix. The smart material functionality is then triggered by the UV light.

In the damage sensing application a photochromic or fluorescent dye was encapsulated so that the corresponding composite could act as a damage sensor, showing a fluorescent signal when a scratch was applied on its surface to simulate a real damage and after subsequent exposure to UV light.

The self-healing material has a similar action mechanism but differs in the encapsulated core. Experimentally, a UV-absorbing polyurea shell was obtained by reacting a polyisocyanate with an amine via a interfacial polymerization process. The influence of two types of amine on the UV-screening ability of the shell was investigated. Differential scanning calorimetry (DSC), thermo-gravimetric analysis (TGA), scanning electronic microscopy (SEM), rheological analyses, optical microscopy and IR analyses demonstrated the successful encapsulation of various core materials. For the self-healing coatings fabrication, different photocurable resins were chosen as core material in the synthesis of microcapsules

ESTRATTO IN ITALIANO

Negli ultimi anni gli smart materials (letteralmente "materiali intelligenti") hanno attratto grande interesse in tutta la comunità scientifica per la loro capacità di rispondere agli stimoli esterni tramite un segnale leggibile. La progettazione, la fabbricazione e la costruzione di strutture intelligenti è una delle sfide più attraenti nell'ambito dell'attuale ricerca scientifica. Al fine di estendere il tempo di vita dei materiali, sempre più crescente è l'interesse verso lo sviluppo di due tipi sistemi *smart*: sistemi *damage-sensing* e sistemi *self-healing*. I primi permettono l'individuazione di un danno, mentre i secondi possiedono la capacità intrinseca di riparare piccole cricche.

Uno dei processi più studiati per la produzione di questi materiali è la microincapsulzione che consiste nell'inglobare all'interno di una parete polimerica (*shell*) un agente liquido (*core*).

Il presente lavoro di tesi riporta la fabbricazione di una nuova tipologia di microcapsule costituite da un *shell* UV-schermante e alcuni esempi di rivestimenti in materiale composito contenenti le suddette microcapsule. L'applicazione di un danno meccanico provoca la rottura delle microcapsule all'interno del rivestimento, con conseguente fuoriuscita del materiale incapsulato che diffonde sulla superficie della zona fratturata della matrice rendendo possibile la visualizzazione del danno ed eventualmente la sua riparazione.

Un colorante fotocromico e pigmenti fluorescenti sono stati scelti come materiali da incapsulare per ottenere microcapsule che aggiunte ad una matrice polimerica diano un composto che funga da sensore meccanico.

Uno shell di poliurea in grado di assorbire la radiazione UV è stato ottenuto mediante la reazione di un poliisocianato a base TDI con un amminobenzofenone sfruttando il processo di polimerizzazione interfacciale. L'effetto di due differenti ammine con proprietà UV-schermanti (2-Amino-5-chlorobenzophenone, ACBP e 4-4' Diaminobenzophenone, DABP) è stato, cosi, inizialmente investigato. Le microcapsule sintetizzate con le due tipologie di *shell* poliureico sono state ampiamente caratterizzate mediante tecniche di calorimetria differenziale a scansione (DSC), analisi termogravimetrica (TGA), microscopia a scansione di sonda (SEM), microscopia ottica (MO) e analisi IR. Tali analisi hanno permesso di dimostrare che il colorante fotocromico, disciolto in olio di girasole, è stato correttamente incapsulato in entrambi i sistemi. Tuttavia, le microcapsule con *shell* a base di DABP

presentano una maggiore resistenza ad ambienti aggressivi, ciò rende possibile il loro utilizzo in tutti i comuni *coatings* disponibili in commercio. L'uso, invece, di microcapsule con *shell* a base ACBP resta limitato ad applicazioni in rivestimenti a base acquosa.

Quindi sono stati sviluppati sistemi *smart* a risposta cromatica, alcuni basati sul colorante UV-sensibile, incapsulato in microsfere, disperse in una matrice foto-polimerizzabile a base acrilica ed altri con microcapsule contenenti *dye* fluorescenti disperse in matrici sia a base acquosa sia a solvente. Grazie a questi sistemi, è possibile constatare, in modo non invasivo, se il materiale ha subito un danneggiamento meccanico. Una frattura del materiale provoca la rottura delle microcapsule, con conseguente fuoriuscita del colorante. Tramite irraggiamento UV è possibile localizzare la zona in cui è avvenuto il danno, e successivamente riparare o sostituire il materiale. Utilizzando un'ammina con proprietà schermanti nella regione UV, è possibile ottenere microcapsule con parete in grado di schermare il pigmento UV-sensibile in condizioni normali. Quando invece si verifica un danno, il colorante fuoriesce e permette di visualizzare la lesione attraverso un cambiamento di colore, dovuto a una reazione chimica attivata da luce UV per il benzo-pirano indolo, colorante organico utilizzato, che passa alla corrispondente forma aperta di merocianina se irradiato a 365 nm, oppure ad emissione di luce da parte di una molecola fluorescente per rilassamento radiativo in seguito ad assorbimento di una radiazione elettromagnetica.

Questi sistemi sono potenzialmente applicabili a qualsiasi tipo di matrice polimerica e quindi risultano un potente metodo di controllo non distruttivo (CND), cioè un metodo finalizzato alla ricerca ed identificazione di difetti strutturali senza alterare il materiale e non richiede la distruzione o l'asportazione di campioni dalla struttura in esame.

I materiali autoriparanti hanno un meccanismo di funzionamento simile, utilizzando materiali di core differenti. La stessa tecnica di sintesi è stata quindi utilizzata per ottenere microcapsule per sistemi *self-healing*. In questo caso, resine foto-reticolabili sono state scelte come agenti da incapsulare ed una analisi reologica è stata condotta per determinare la loro compatibilità con il processo di incapsulazione. Analisi chimiche e morfologiche mostrano che tutte le tipologie di resine prescelte sono state incapsulate con successo. Un rapido curing del core estratto è stato inoltre osservato in seguito ad irraggiamento UV, ciò dimostra la capacità di queste resine di mantenere la proprietà reticolante anche dopo essere state processate. Questi sistemi rappresentano una soluzione promettente nel campo dei materiali autoriparanti, da sviluppare in futuro. Microcapsule contenenti resine *UV-curing* aprono la strada ad una nuova chimica dei polimeri autoriparanti, che si presentano come sistemi

altamente resistenti e stabili, che non richiedono l'aggiunta di un catalizzatore per attivare il processo di healing.

1. STATE OF ART

1.1. Smart materials

Smart materials are a broad class of materials which have been developed in recent years thanks to a combined effort of different scientific disciplines like chemistry, physics, material science, mechanical and electrical engineering. These new materials are labelled as "smart" because they are able to interact in real time with their surrounding environment, producing a detectable change in a specific property (output) in response to an external stimulus (input) (Figure 1.1)[1]. The nature of external stimulus can be different: physical, mechanical, electrical, chemical, thermal, optical etc. Similarly the change due to the input can vary: modification of shape, mechanical resistance, colour, porosity, flexibility and electrical conductivity. In most cases, properties changes are reversible[2].
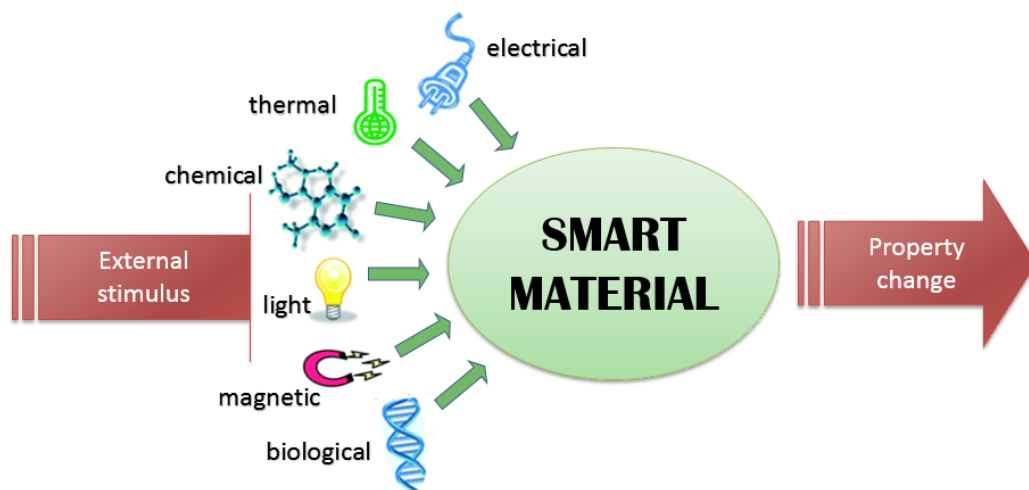
Figure 1.1: Schematic representation of smart material operating principle

Due to their innovative properties, smart materials are used not only as advanced functional materials but can also be integrated in more complex "smart" systems composed by sensors, actuators, control algorithm, control hardware and structural parts[3]. In the last 20 years, a growing interest has been given to smart materials applications thanks to the chance to design smart materials with unique functionality suitable for specific functions[4,5]. Therefore, different typologies of smart technologies have been developed, well documented and applied in industrial and commercial context: most important examples are shape memory alloys[6,7], fibre optic sensors[8], electro and magneto-rheological fluids[9], piezoelectric materials[10], thermochromic materials and electrochromic materials (Figure 1.2).
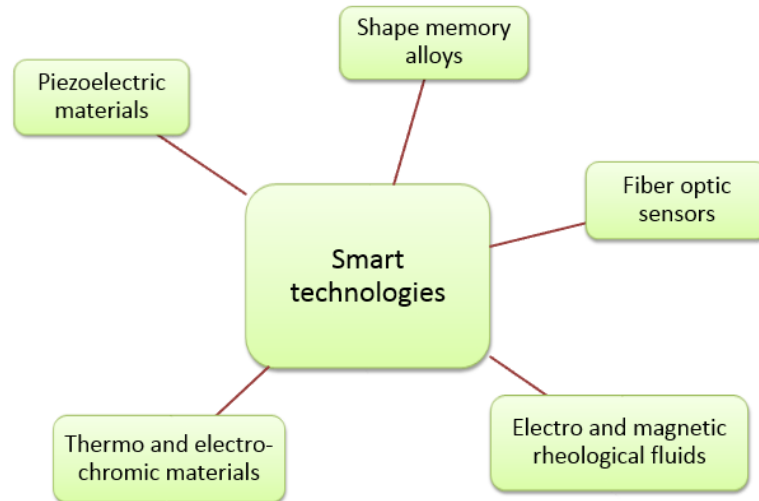
Figure 1.2 Examples of different smart technologies

A possible and effective way to develop and design smart materials is to take inspiration from nature. In fact, natural elements, systems and processes have been developed and optimized through very slow but extremely efficient evolutionary steps and constitute a continuous source of inspiration to create new artefacts. For this reason, a particular field of science called biomimetics (literally from Greek "imitation of life") studies and analyses biological structures, forms and functions in order to adapt and transfer it to artificial materials and processes. Over the past few years, biomimetics has contributed to the development of several study fields like engineering, chemistry, physics and material science. Moreover, the study of nature has allowed the designing of a new class of smart materials called "bioinspired" or "biomimetic" materials. For example, a self-cleaning biomimetic material has been designed taking inspiration from vegetal world, specifically from lotus leaves: this material is able to maintain itself clean through the action of atmospheric agents (rain, wind). Indeed, the presence on its surface of many nanometric asperities guarantees hydrophobicity and prevent impurities from reaching underlying surface (Figure 1.3a). Similarly, self-healing and self-mending materials could be designed taking inspiration from natural tissues and organisms, which are able to self-repair through spontaneous processes. For example, rhino's horn, when damaged, is self-mended thanks to a keratin-based resin, which seals scratches and wounds (Figure 1.3b). Another possible biomimetic materials is an adhesive that mimic gecko's foot: in fact, gecko has incredible adhesive ability and can climb also on vertical surfaces thanks to particular setae placed on its feet which bonds with different surfaces through Van der Waals forces (Figure 1.3c).
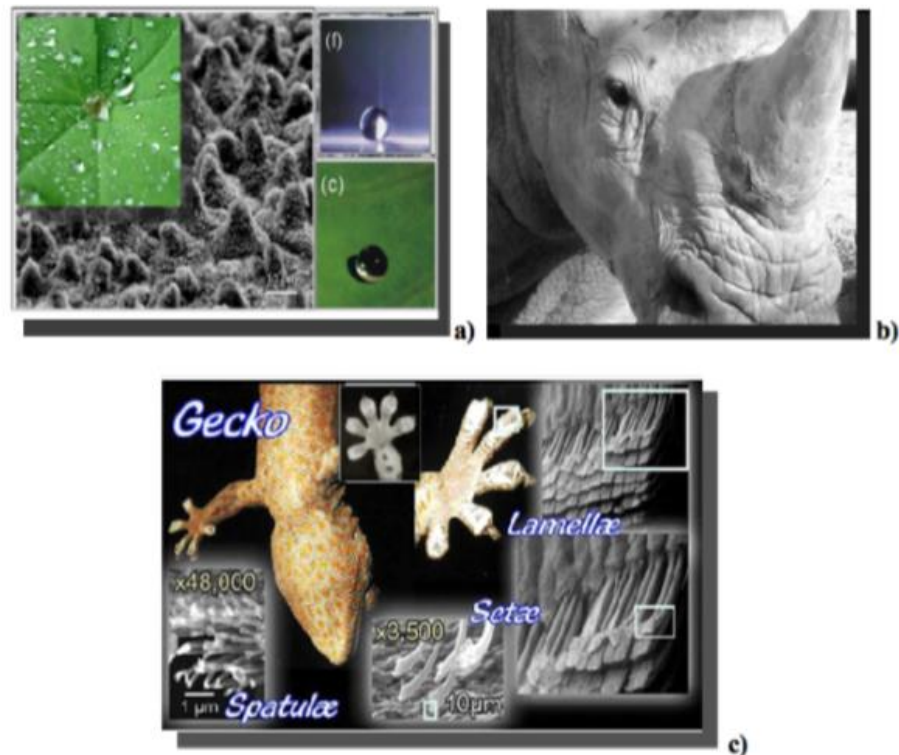
Figure 1.3 Example of natural systems, which inspirates new biomimetic smart materials: (a) Lotus leaves, (b) Rhinoceros hotn, (c) Gecko's feet.

Along with biomimetic smart materials, a growing interest has risen in recent years for the conversion of conventional "dumb" coating systems into innovative "smart" coatings; with "smart" we intend coatings able to modify properties and structure, in response to changes in their surrounding environment. Particular attention has been given to the development of smart polymeric coatings; indeed polymeric structures can be modified through organic or inorganic additives and so they are very versatile and adapt for becoming "intelligent" coatings.[11]

A possible classification of smart polymeric coatings can be done on the type of response given to an external stimulus. On this base, we can identify two broad classes of smart coatings: smart polymer coatings based on color response and smart polymer coating based on noncolor response. For both classes, smart functionality may be imparted by functional additives added separately into the coating or be intrinsically built in the polymeric structure. For smart sensors based on color response, the response may be visible color change, fluorescence, or phosphorescence. In general, the type of stimuli needed to activate smart functionality could be varied as can be seen in Table 1.1.

Smart coating based on color response	Smart coating based on non color response
STIMULUS	STIMULUS
• pH change • redox reaction • the presence of heavy metals • sorption of chemicals • radiation • mechanical action • temperature change • electrical current	• mechanical action • presence of gases • light • temperature change • neutralizing agent(e.g. NH_2) • ageing

Table 1.1 Possible external stimuli, which include a chromatic or non-chromatic response into the material.

In the following three tables, other examples of smart polymer coatings are listed and classified on the basis of external stimulus, response, sensor type, sensing and actuation mechanism and potential application. Table 1.2is referred to smart coatings based on noncolor response while Table 1.3 and Table 1.4are referred to smart coatings based on color response.

SMART POLYMER BASED ON NONCOLOR RESPONSE

STIMULUS	RESPONCE	SENSOR TYPE	SENSOR MECHANISM	APPLICATION
Mechanical action	Capsule Ropture-Healing	U/F capsules containing DCPD	DCPD-catalysed polymerization	Crack self-healing of coating
Gases; ammonia; acetaldehyde	Selective absorption	PP copolymer, PC, acrylates	Match solubility parameters	Coating on quarz crystal resonator, electronic noise
Light	Surface Wettability	Azobenzone derivates	Cis-Trans isomerization	Coating with reversible absorptive capacity for biological agents
Temperature	Hydrophilicity/ hydrophobicity	N-isopropyl acrylamide	Transition from random coil to dehydrated form	Coating on Biomaterials (nonprotein absorptive or protein retentive)
Neutralizing agents (NH_3, $(NH_4)_2CO_3$)	dissolution	Carboxylated copolymer	Water soluble neutralized form	Temporary protective coating
Aging deterioration	Mechanical properties, water resistance	Frequency dependent dielectric measurements sensor	Dielectric sensing of molecular mobility	Monitor durability of coatings

Table 1.2: Classification of polymeric smart materials based on non cromatic response[11].

SMART POLYMER MATERIALS BASED ON COLOR RESPONSE

STIMULUS	RESPONCE	SENSOR TYPE	SENSOR MECHANISM	APPLICATION
pH change	Color	pH indicator	Ionic form of different color	Corrosion detection
Oxidation	Fluorescence	Fluorescin. Shiff bases	Redox reaction with fluorescent oxidized form	Corrosion detection
Sorption, diffusion	Fluorescence	Fluorescence probe	Decrease fluorescence	Follow degradation of coating
Mechanical action	Capsule ropture-healing, color change	U/F capsules with flm former on dry marker	Release of healing or dye material	Sel healing, crack detection
Light and temperature	Color	Photocromic dyes, thermocromic pigments or dye marker	Polymerization, structural transition	Printing inks and battery tester
TNT, nerve gas presence	Quenching fluorescence	Fluorescent polymer fibres, reactive sensor	TNT bonds to reception on chromophores, reducing signal, nerve gas reacting with sensor	Location of land mines; sensor for chemical wafare gas

Table 1.3: Classification of polymer smart materials based on chromatic response[11]

SMART POLYMER MATERIALS BASED ON COLOR RESPONSE WITH INTRINSIC SMART FUNCTIONALITY

STIMULUS	SENSOR TYPE	SENSING MECHANISM	APPLICATION
Temperature	Polymers with crystallisable side chains	Passage from crystalline to amorphous structure	Controlled germination of seeds through modification of permeability
Radiation	dyacetilenes	Polymerization	Radiation sensor
Oxidation	Conductove polimeric film (Polyaniline, Polypirrole, Polythiopene)	Passage to charge to neutral state	Corrosion monitoring

Table 1.4: Classification of polymeric smart materials based on color response with intrinsic smart functionality[11].

1.2. Smart Materials and Damage Management

The development of strong durable materials along the 20th century has always followed the path of designing stiffer materials able to withstand high loads for the longest possible time, up to the point when failure inevitably occurs. This design philosophy is based on creating microstructures which oppose the formation or extension of micro-cracks by tuning the atoms configurations and production processes. It is possible to argue that the development of those materials was progressing along the paradigm of damage prevention. An alternative concept to that of damage prevention is damage management, which forms the basis of the field of smart materials. The paradigm is based on the notion that the formation of damage is not problematic as long as it is counteracted by a subsequent autonomous process of "managing" or "healing" the damage[12].

Damage in general terms can be described as changes introduced to a system that affect its function and/or performance. That means that damage is not meaningful without a comparison of two different states of the system in question, one of which is assumed to be the initial (and often un-damaged) state. The term damage does not necessarily imply a total loss of system functionality, but rather a departure in level of system operation from optimal. A fundamental challenge is the fact, that damage is typically a local phenomenon and may be therefore difficult to detect (in time). Most systems lose their integrity, their value, operation or usefulness over time due to degradation processes where defects grow and coalesce to cause component and finally system level damage (e.g. fatigue or corrosion damage accumulation). On a relatively short time scale, damage can also result from scheduled discrete events such as aircraft landing and from unscheduled discrete events such as an impact. As damage grows, it will reach a point where it affects the system operation to a level, which is not any longer acceptable for a user; this point is referred to failure. The main causes of deterioration of materials may be summarized as: 1) Harmful materials, substances and agents such as oxygen, oxidizing agents, water, salts, poisons, active materials, and living bodies such as virus, bacteria, fungi, insects, animals, human beings and others; 2) Factors from the surroundings such as heat, visible light, external mechanical force e.g. strong wind, radiation, pressure, rain, collapse of the adjacent structure, a sudden impact and others. Such deterioration are in general irreversible, they occur progressively and exponentially in time until a certain threshold is reached where either significantly high costs for repairs are necessary or a failure is going to occur. Increased lifetime and reliability

of materials systems and devices can be critical requirements in traffic, construction, information transfer, medicine, military, space missions as well as in ordinary daily life.[13]

If defects can be easily detected in the initial stage, this could help users heal or replace the damaged materials before their complete destruction. Because of the importance of crack sensing from the economic and safety aspects, some types of defects sensor have been developed. Piezoelectric films were developed to monitor crack initiation and growth by measuring the output voltage signals from the sensors[14]. The change in electrical resistance of a carbon powder-glass fiber reinforced plastic sensor was used for fracture detection[15]. Optical fibers have been embedded in materials for structural condition monitoring[16]. Electrically conductive wires or ribbons were used for detecting cracking in concrete structures[17]. All these sensors cannot measure damage directly, features need to be extracted through data processing and in a learning process type of damage and severity of damage can be identified.

Indicators in polymers and composite materials can reveal mechanical damage and the need for repair before damage becomes catastrophic.

Self-healing or remendable polymers have the built-in capability to heal microcracks formed within the structure and substantially recover their aesthetic appearance and load transferring ability after a mechanical damage. Such recovery can occur autonomously or be activated after the application of a specific stimulus (e.g. heat, radiation)[18]. This is a very valuable material characteristic since it effectively extends the lifetime of the product and has desirable economic and human safety value[19]. Indeed, reliability and long-term durability of polymeric materials are still problematic when they are used for structural or coatings application due to the formation of microcracks within the structure. Moreover, especially for thermoset polymers, conventional repair methods are not very effective for healing of microcracks and require high costs for continuous active monitoring of the structure. For these reasons, the design of self-healing polymers has become fundamental for a new approach of damage management[20], in which the structures are able to control and retard crack formation without continuous monitoring and external repair. Use of remendable polymers is expected to make structure safer, more reliable and durable while reducing the cost of maintenance; so, the development of this new class of materials offers great opportunities for broadening the application of polymers into manufacture of structural and critical components[21].

In this thesis work, the attention was focused on two types of smart materials activated by a mechanical stimulus: damage sensing and self- healing polymeric materials. The smart functionality of the systems developed in the present work is due to the presence of microcapsules that are added into a polymeric coating. UV-screening shell microcapsules containing a stimuli-sensitive core material were successfully manufactured by an interfacial polymerization process. The same synthesis technique was used to produce the microcapsules used in the self-healing material. Photochromic and fluorescent dyes were adopted as core material for damage sensing capsules whilst the self-healing system is based on the presence of photocurable resins.

In this work both the synthesis process and the microcapsules characterization are fully described. A preliminary spectroscopy analysis was carried out on the photochromic and fluorescent dyes; similarly rheological analysis of the photocurable resins were performed in order to assess their suitability for the encapsulation process. An extensive study of the microcapsules properties is also reported. IR analysis, optical microscopy, SEM images and TGA/DSC tests were used to this end. Finally examples of smart coatings show the promising functionality of this systems in future applications.

The next paragraph shows an introductive overview on microencapsulation principles, explaining various synthesis methods and the key parameters involved in their functionality. In the following paragraphs different typologies of damage sensing and self-healing materials, either based on microcaspules or on different systems, are presented. Different healing mechanisms are also explained as it is possible to achieve healing, either intrinsically via reversible bonds present in the material itself (intrinsic self-healing polymers), or extrinsically via a pre-added healing agent (extrinsic self-healing polymers), in response to some external stimulus[22].

1.3.Microencapsulation overview

Microencapsulation is described as a process of enclosing micron-sized particles of solids or droplets of liquid or gasses in an inert shell, which in turn isolates and protects them from external environment. The products obtained by this process are called microparticles, microcapsules and microspheres which differentiate in morphology and internal structure. When particle size is below 1 μm they are known as nanoparticles, nanocapsules, nanospheres, respectively, and particles having diameter between 3-800 μm are known as microparticles, microcapsules or microspheres particles larger than 1000 μm are known a macroparticles.

In its simplest form, a microcapsule is a small sphere with a uniform wall around it (Figure 1.4). The material inside the microcapsule is referred to as the core, internal phase, or fill, whereas the wall is sometimes called as shell, coating, or membrane. Most microcapsules can be a common alternative to using fibers for reinforcement in polymer composites.
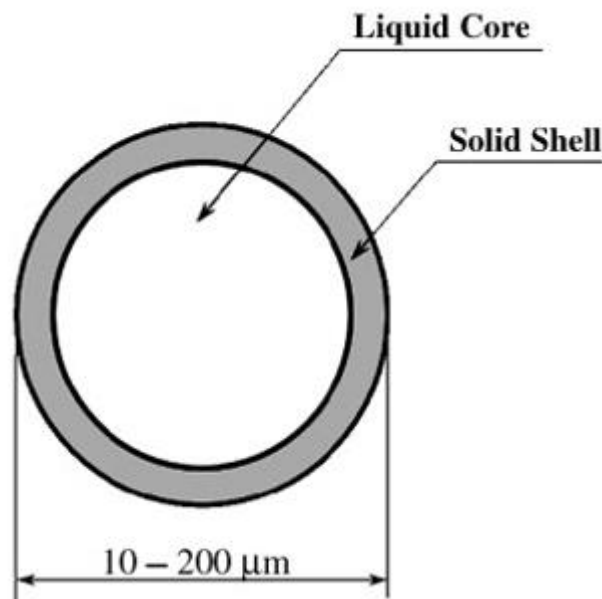
Figure 1.4: A simplified illustration of a microcapsule.

Spanoudakis et al.[23] reported in the mid-1980s that the incorporation of compliant rubbery particles or rigid inorganic fillers can enhance the fracture toughness of epoxy composites without compromising other mechanical properties of the system. The introduction of an additional component to the composite system, however, increases complexity and brings with it a new set of parameters to keep in mind and interactions to account for. A different option from the use of rubber is the use of hollow polymeric microcapsules, which are a lightweight alternative to achieve toughening of a brittle polymer matrix. These reinforcing

fillers are analogous to the reinforcing fibers, as they can not only strengthen the matrix material but also provide a reservoir space to contain a healing agent.There are many complex parameters to think about when incorporating these microspheres into a composite system, and each has to be addressed when optimizing a stimuli-responsive healable composite material.

Many mechanisms can initiate changes in a capsule shell wall that results in the release of capsule contents (Figure 1.5)[24]. In drug delivery, light-activated mechanisms are relevant for targeted release in biological tissues (Figure 1.5, photo). Tissues show negligible absorption in the 800-1200 nm region, providing a window for laser irradiation of near-IR-sensitive capsules. UV- and visible light-sensitive capsules are also used in the cosmetic and agricultural industries where solar irradiation triggers release. Biological triggers are used for drug therapy and vitamin delivery (Figure 1.5, biological). Slight changes in pH or the presence of certain chemicals (e.g., insulin) cause appropriately designed capsule store lease their contents in a patient, requiring only in vivo stimuli (Figure 1.5,chemical).Thermally induced release is useful in applications where subtle changes in temperature occur (Figure 1.5, thermal). For example, in agricultural applications, an increase in soil temperature can initiate delivery of nutrients. Deodorant and antiperspirant materials can be released upon reaching targeted temperatures, allowing for delivery only where a person perspires. Magnetically induced release is useful for drug delivery, activating capsules only in tissues subjected to oscillating magnetic fields (Figure 1.5, magnetic). Electric field release is useful in delivering anti-corrosive materials only when a metallic surface is compromised (Figure 1.5,electrical) and may be useful in battery materials that experience a higher voltage than standard operating potentials.
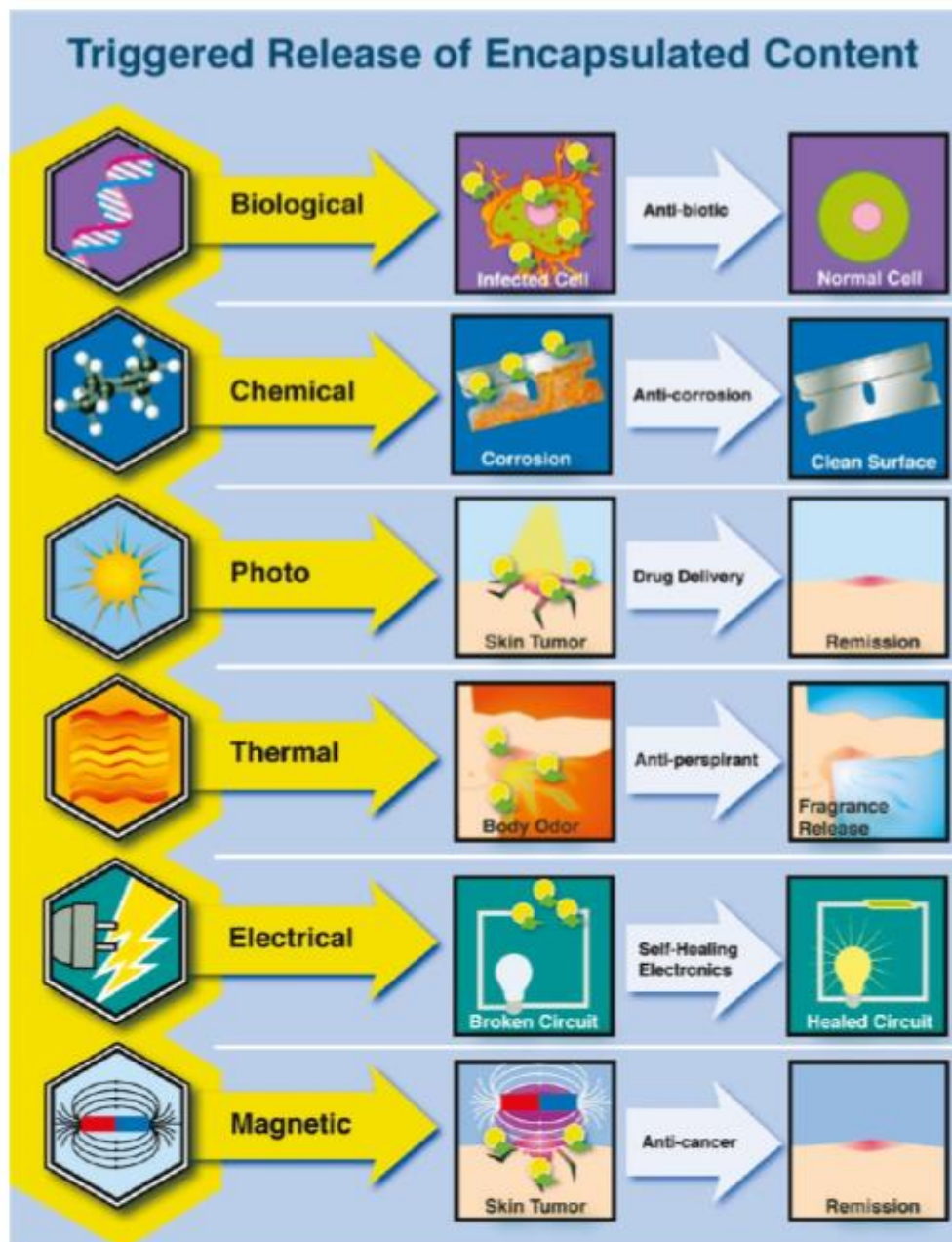
Figure 1.5: Triggering mechanisms for microcapsule release include biological, chemical, photo, thermal, electrical and magnetic stimuli[24].

1.3.1. Encapsulation techniques

Various techniques are available for the encapsulation of core materials. In general, the process of microencapsulation can be categorized into two groups: chemical processes and physical processes. Examples of important microencapsulation techniques are summarized in Table 1.5.

MICROENCAPSULATION PROCESSES	
Chemical processes	**Physical processes**
Emulsion	Spray drying
Coacervation and phase separation	Spray cooling
Interfacial polymerization	Fluid bed coating
Thermal gelation	Electrostatic method

Table 1.5: Different important microencapsulation techniques

Each method has advantages for specific applications, which depend on a variety of capsule characteristics. These include shell wall thickness and permeability, chemical composition of the shell wall, mechanical integrity of the shell wall, and capsule size. Of equal importance in choosing a preparation method is the ability to incorporate specific materials within the capsule, whether the core is aqueous, organic, or inorganic. The core material and method for preparation also affects whether capsules are spherical or ellipsoidal. A capsule's ultimate shape results from the shape of its liquid droplet precursor in the emulsion, which depends on the viscosity and surface tension of the core liquid, the direction of flow in the emulsion, and the choice of the surfactants used for droplet stabilization.

Table 1.6 highlights the major pros and cons of the most common methods: emulsion polymerization, layer-by-layer assembly of polyelectrolytes, coacervation, and internal phase separation and Table 1.6 shows an overview of these techniques.

We note here that the pros and cons listed in Table 1.6 and throughout our discussion are generalizations for these capsule types, and improvements in capsule preparation have overcome some of the disadvantages listed.
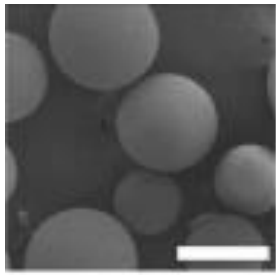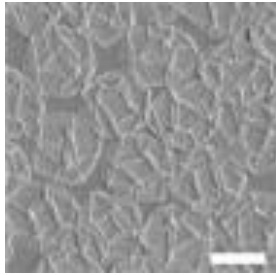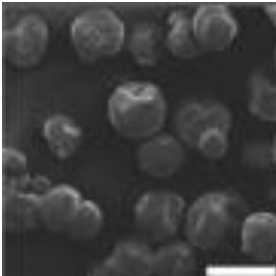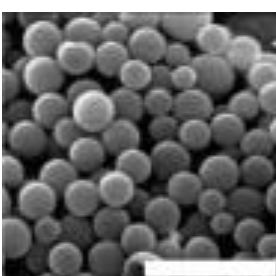
Methods	Representative image*	Advantages	Disadvantage
A: Emulsion polymerization		High strength capsule shell walls; Large scale synthesis; Thick shell wall; Narrow size distribution.	Difficult to encapsulate aqueous cores; Can only be loaded once; Surfactant and polymerization specific; Often large size distribution.
B: Layer-by-Layer Assembly		Compatible with aqueous or organic cores; Easy trigger incorporation; Post-fabrication core loading; Narrow size distribution if sacrificial core particles are uniform in size.	Laborious fabrication; Often poor structural integrity; Dry isolation difficult; Some cores require strong acid in preparation.
C: Coacervation		Easy of use in time-release applications; Simple fabrication.	Hydrophobic cores and required; Low strength shell wall; Slow shell formation; Can only be loaded only; Often large size distribution.
D: Internal Phase Separation		High strength shell walls; Carbon rich polymers can be used; Ideally suited for thermal triggers.	Limited triggering capabilities; Hydrophobic cores are required; Limited core/shell polymer combination; Can only be loaded once; Often large size ditribution.

Table 1.6: Advantage and Disadvantages of Emulsion-Based Methods for Preparing Microcapsules. *: SEM images of (A) core-shell microcapsules with poly(urea-formaldehyde) wall and dicyclopentadiene core (scale bar = 100 µm),[162] (B) hollow PSS/PAH capsules (scale bar = 1 µm),[37] (C) microcapsule formed from gum arabic/gelatin coacervation (scale bar = 500 µm),[163] and (D) microcapsules formed from the internal phase separation of PMMA (scale bar =10 µm).

Emulsion Polymerization. Many capsules are prepared through the polymerization of monomer units at the aqueous/organic interface of droplets in an emulsion. Emulsions of oil in water or water in oil are typically produced by vigorous agitation or sonication of a biphasic liquid. Stirring or sonication creates droplets, and it is these droplets that become the core material of the capsules. The formation of a polymer at the aqueous/organic interface creates the capsule shell wall that encases the droplet. Polymers may form from condensation reactions at the interface between the two phases (Figure 1.6A). The stability of emulsions depends largely on the miscibility of the organic and aqueous materials and the surface tension of the core liquid.

Layer-by-Layer Assembly. Layer-by-layer (LBL) assembly is used to prepare a variety of capsule materials. Initially metal oxide particles are suspended in an aqueous solution. In a stepwise fashion, negatively and positively charged polyelectrolytes are deposited onto these particles, forming layers of polymers held together by electrostatic interaction. After the multi-layering is complete, an acid is usually employed to remove the metal oxide core, leaving behind hollow, semipermeable capsules (Figure 1.6B). More recently, De Geest and others have reported less harsh conditions for core dissolution, such as the removal of $CaCO_3$ cores with ethylenediaminetetraacetate (EDTA)[25]. Pastoriza- Santos et al. have reported the use of polystyrene particles as a core in LbL assembly that can be removed by exposing capsules to tetrahydrofuran[26]. Another method for avoiding strong acids involves the use of small organic molecules as cores including toluene and dodecane. Khapli et[27] al. reported the use of frozen cyclohexane as the core material, which was removed after LbL deposition when the capsules were brought to room temperature. Because of the high permeability of the shell walls, capsule cores can be readily exchanged with external media, allowing for a variety of core materials to be introduced after capsule preparation. Upon isolation in the solid state, the capsules often resemble deflacted balloons owing to the weak structural integrity of their shell walls. Recent reports on incorporating cross-links between layers, such as azides, have improved the integrity of the shell walls, including resistance to changes in size and shape in response to changing solvents or the pH of an aqueous solution. Preparing air-stable capsules (capsules that do not deflate when dried) is a challenge recently overcome by the incorporation of inorganic nanoparticles as fillers to reinforce the otherwise soft LbL capsule shell walls.

Coacervation. Self-assembly can be extended to capsule systems using coacervation. Preparing microcapsules and microspheres (solid particles) using coacervation is a common method in materials for food and fragrance applications where time release or temperature induced delivery is a goal. Complex coacervation involves the neutralization of two oppositely charged polymers in aqueous solution, forming an entangled neutralized polymer shell wall. The oil phase contains one polymer, and the aqueous phase contains a polymer of the opposite charge. The attraction of one polymer to another results in the formation of coacervates, which migrate to the aqueous/organic interface, thus forming the shell wall (Figure 1.6C). Gelatin and gum arabic are common complementary components that have been used for capsule preparation.

Internal Phase Separation. Another method of preparing microcapsules is the controlled phase separation of a polymer within the droplets of an emulsion. In this method, a polymer is dissolved in a solvent mixture containing volatile and nonvolatile solvents. Droplets of the resultant solution are suspended in an aqueous layer, which is stabilized by continual agitation and the use of surfactants. As the volatile solvent evaporates, the polymer begins to precipitate and migrate toward the organic/aqueous interface. When the solvent has completely evaporated, the polymers coalesce to form a shell wall (Figure 1.6D). While this method is convenient for microcapsule preparation and has been demonstrated with PS, PMMA, and PTHF shell walls, it is not feasible if the desired polymer is soluble in its intended core or if the polymer is insoluble in the volatile solvent.
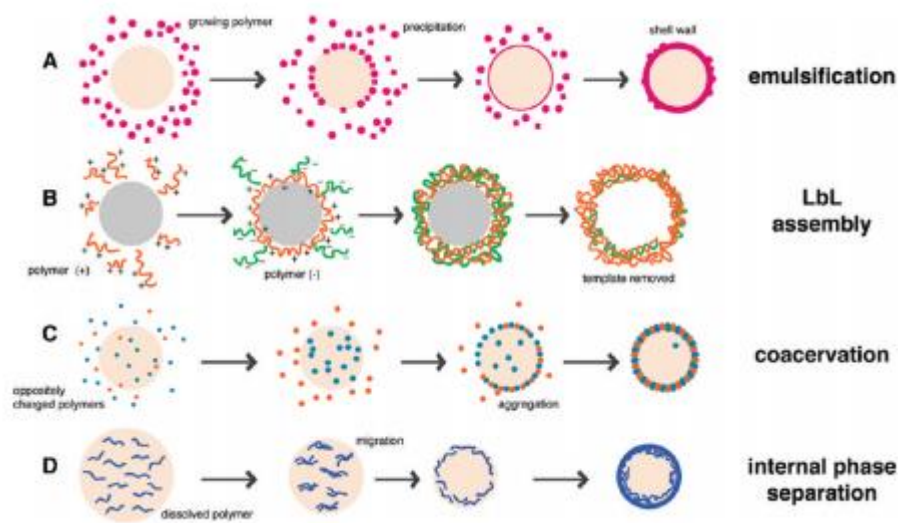
Figure 1.6: Methods for the dynamic self-assembly of nano-and microcapsules containing deliverable cargo. (A)an emulsification polymerization where a polymer is deposited at an aqueous/organic interface, yielding a polymer shell wall around a stabilized droplet, that becomes the core solution; (B)layer-by-layer(LbL) assembly of polyelectrolytes onto a metaloxide particle,that is removed using acid to create a permeable hollow capsule; (C) coacervation of two oppositely charged polymers that aggregate, forming coacervates, at the oil/water interface; (D) interphase separation in which a polymer is dissolved in a core material with a volatile solvent and precipitates, migrating to the aqueous/organic interface, thus creating the polymer shell wall[24].

For the majority of self-healing composite systems that have been studied, the microcapsules are a urea-formaldehyde polymer encapsulating dicyclopentadiene as the liquid healing agent (Figure 1.7). During the in situ polymerization process, urea and formaldehyde react in the water phase to form a low molecular weight pre-polymer; as the weight of this pre-polymer increases, it deposits at the dicyclopentadiene–water interface. This urea-formaldehyde polymer becomes highly cross-linked and forms the microcapsule shell wall. Nanoparticles of urea-formaldehyde pre-polymer then deposit on the surface of the microcapsules, providing a rough surface morphology that aids in the adhesion of the microcapsules with the polymer matrix during composite processing. Brown et al.[28] report that the microcapsules made in this manner average 10–1000 μm in diameter, with a smooth inner membrane that is 160–220 nm thick and a fill content of 83–92% liquid healing agent.
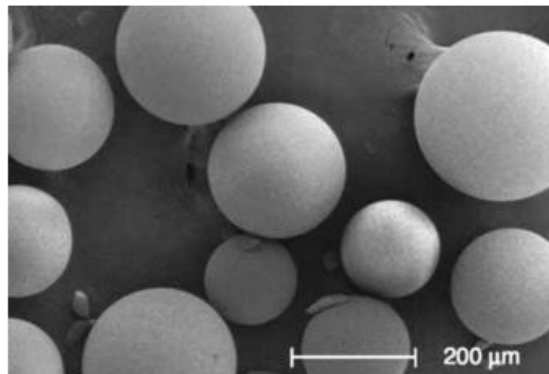
Figure 1.7 : Urea-formaldehyde microcapsules containing dicyclopentadiene prepared by emulsion in situ microencapsulation[28].

As shown in Figure 1.8, as a microcrack propagates through a matrix material, the microcapsules break releasing their contents. The liquid monomer is released into the crack plane by capillarity action, filling the crack volume. During the filling process the monomer flows and makes contact with the catalyst, dissolving the catalyst. The dissolved catalyst polymerizes the monomer repairing the crack by bonding the crack faces together. The crack become filled with a cured monomer and a large fraction (e.g. 90%) of the virgin mechanical strength is reported to be recovered.
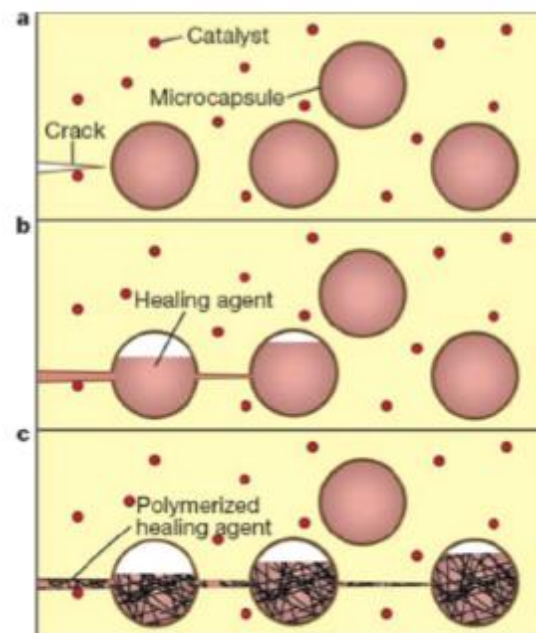
Figure 1.8: Autonomic healing concept incorporating encapsulated healing agent and embedded catalyst particles in a polymer matrix; (a) damage event causes crack formation in the matrix; (b) crack ruptures the microcapsules, releasing liquid healing agent into crack plane; (c) healing agent polymerizes upon contact with embedded catalyst, bonding crack closed[28].

During the years many other different kinds of microcapsules have been synthetized for self-healing applications. A microcapsule for a self-repairing anticorrosion coating based on a polydimethylsiloxane (PDMS) healing chemistry was proposed[29]. Huang et al.[30] demonstrated that polyurethane (PU) microcapsules, containing hexamethylene diisocyanate (HDI) as a core material embedded in polymeric composites, could achieve self-healing properties and improve the corrosion resistance of coatings. Linseed oil, epoxy resins, amine and inorganic particles have been used as the core healant of capsules for self-healing polymeric coatings and they will be discussed in more details in the following section. While melamine-formaldehyde, urea-formaldheyde or polyurea as shell materials.

In the present work of thesis, microcapsules are synthetized by a method that utilizes emulsion. The capsule shell will be formed at or on the surface of the droplet by interfacial polymerization (IFP) of the reactive monomers. The substance used is a multifunctional isocyanates monomer, which dissolved in liquid core material and it will be dispersed in aqueous phase containing dispersing agent. A co-reactant multifunctional amine will be added to the mixture. This results in rapid polymerization at interface and generation of polyurea capsule shell takes place.

1.3.2. Microcapsule parameters

The mechanical rupture of the microcapsule is the triggering event for the healing process; without it, no healing will occur. It is exceedingly important, therefore, to fabricate microcapsules with optimal mechanical properties and wall thickness. The relationship between the stiffness of the capsule and the stiffness of the surrounding matrix will determine how the crack will propagate in the sample. Keller and Sottos[31] have described how a capsule with a higher elastic modulus than the matrix material will create a stress field that tends to deflect cracks away from the capsule; a more compliant shell wall, on the other hand, will produce a stress field that attracts the crack towards the microcapsule (Figure 1.9). The image on the left in Figure 1.9 corresponds to an inclusions three times stiffer than the surrounding matrix, and the image on the right corresponds to an inclusion three times more compliant than the surrounding matrix. This latter relationship will facilitate the rupture, ensuring that the healing process will be triggered in the event of mechanical damage to the system.
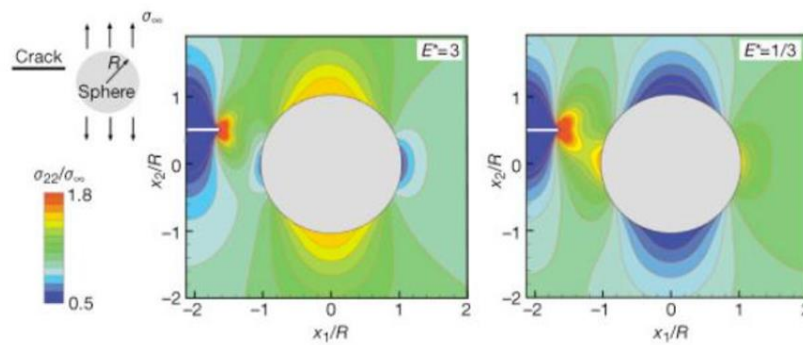
Figure 1.9: Stress state in the vicinity of a planar crack as it approaches a spherical filler particle embedded in a linearly elastic matrix[31]

As mentioned, the wall thickness of the microcapsule is another critical parameter to probe. If the shell wall is too thick, the microcapsule will not easily rupture, and healing will not occur. If the shell wall is too thin, however, the microcapsules can rupture during composite manufacture and processing, or the healing agent could leak or diffuse into the matrix over time. As noted by Brown et al.[32], the shell wall thickness is largely independent of manufacturing parameters and is typically between 160 and 220 nm thick; however, slight adjustments can be made during the encapsulation procedure to alter the resulting microcapsules.

The size of the microcapsule also plays a role in the performance of the system, in terms of the effect on toughness of the composite as well as the fill content and resulting amount of healing agent available during crack propagation. The microcapsule size is controlled mainly via the rate of agitation during the encapsulation process; typical agitation rates reported by Brown et al.[32] range from 200 to 2000 rpm, with finer emulsions and therefore smaller diameter capsules being produced with increasing rates. In 2004, Brown noted that smaller microcapsules exhibit maximum toughening at lower concentrations; on the other hand, Rule et al.[33] reported in 2007 that specimens that contain larger microcapsules perform better than those with smaller microcapsules at the same weight fraction, presumably due to the amount of healing agent present in the specimen. In the latter study, the best healing achieved was on a specimen containing 10 wt% of 386 μm capsules, which corresponds to 4.5 mg of healing agent being delivered per unit crack area (assuming all capsules in the crack plane rupture). In that report, Rule et al. postulated, based on measured crack face separation values (length and height of crack), that the crack volume is 2.6 μL/cm^2 over the damaged area in a sample; this means that at least 2.6 μL/cm^2 of healing agent would need to be delivered in order to completely fill the crack. Indeed, they found a rapid decline in effectiveness of

healing when the amount of healing agent delivered to the crack dropped below this value. The amount of healing agent available for delivery to the crack plane was calculated based on the microcapsule size and weight fraction incorporated into the composite, and verified by comparing the data from these autonomously healing samples with that of samples in which a known volume of healing agent was manually injected into the crack plane to initiate the healing process.

In addition to the parameters involving the microcapsule itself, the properties of the healing agent must also be investigated. As previously discussed, the relationship between the kinetics of the healing process and the mechanical crack growth are of the utmost importance. Jones et al.[34] described how if the crack grows too fast as compared to the healing polymerization process, then little or no healing will occur. However, if the healing agent cures too quickly and catalyst dissolution is slow, then there will be insufficient coverage of the crack plane and healing will occur in isolated locations around the catalyst particles; this will reduce the healing efficiency of the system. If the healing agent cures too slowly, rest periods will need to be introduced to allow for maximum recovery of mechanical strength between damage events. Brown et al.[28] have shown that the polymerization of the healing agent provides both a short term adhesion effect to retard crack growth and a long term closure effect to restore strength to the material. These dual advantages of a carefully optimized polymerization process allow for maximum healing efficiencies to be obtained in these composite samples.

1.3.3. Manufacture and characterization of self-healing microcapsules

The group of White et al., the pioneer in developing self-healing polymeric materials, systematically investigated self-healing strategy based on ring opening metathesis polymerization (ROMP) of microencapsulated dicyclopentadiene (DCPD) and reported a series of important findings[28,35,36].

DCPD was encapsulated in a poly (urea–formaldehyde) shell and embedded with the Grubbs' catalyst in an epoxy matrix. Healing is triggered when damage in the form of a crack ruptures the microcapsules, causing DCPD to be released into the crack plane where it comes in contact and mixes with the pre-embedded Grubbs' catalyst (Figure 1.10).
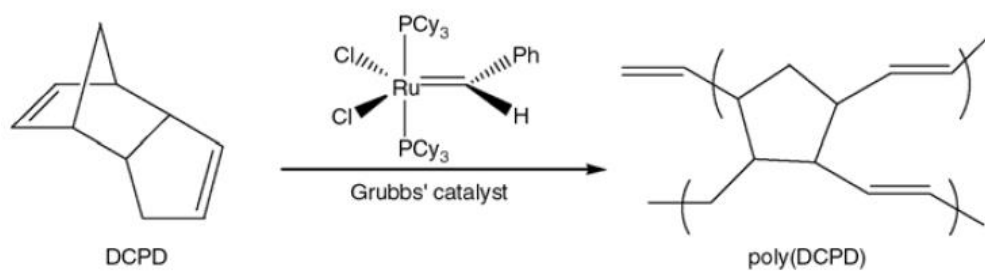
Figure 1.10: Ring opening metathesis polymerization of DCPD[37].

The choice of healing agent, dicyclopentadiene, was made based on its low cost, wide availability, long shelf life, low viscosity and volatility, and its rapid polymerization at ambient conditions upon contact with a suitable catalyst. The catalyst chosen, first generation Grubbs' catalyst: bis(tricyclohexylphosphine)benzylidene ruthenium (IV) dichloride is well known for promoting olefin metathesis, showing high activity while being tolerant of a wide range of functional groups. After failure, his system could recover up to 75% of its virgin fracture toughness; by optimizing various parameters (catalyst and microcapsule size and loading), it was found that up to 90% toughness recovery could be achieved. Also fatigue lifetime of these systems could be improved to over 30 times longer than that of a polymer without a self-healing functionality, and under certain conditions (low applied stress and short rest periods), fatigue crack growth was indefinitely retarded[35].

Kessler, Sottos, and White[36] introduced the same microcapsules and catalyst into a fiber reinforced polymer composite to test the healing ability on the most common mode of composite failure, delamination. The healing efficiency for the self-healing specimens under optimized conditions, was 66%. Brown, Sottos, and White[35] also examined the effect of the inclusion of microcapsules and catalyst particles on the mechanical properties of the epoxy matrix: the virgin fracture toughness increased with an increase in the concentration of microcapsules, reaching a maximum at 15 wt%, corresponding to a toughness more than double that of the neat epoxy. The catalyst particle size also affected the fracture toughness, with both virgin and healed toughness values increasing with an increase in particle size; the maximum increase in toughness was achieved with 180-355 μm catalyst particles. Much effort has been dedicated to optimizing existing microcapsule based self-healing that uses ROMP healing agents. A large amount of this effort has been focused on improving the kinetics of healing, which is a crucial factor when deciding the appropriate applications for self-healing polymers that may be subject to constant or frequent stress. Two ROMP based

monomers that have received significant attention as more rapid healing agents are ethylidene norbornene (ENB) and the exo-isomer of DCPD (Figure 1.11)

endo-DCP   exo-DCP   ethylidene norbornene
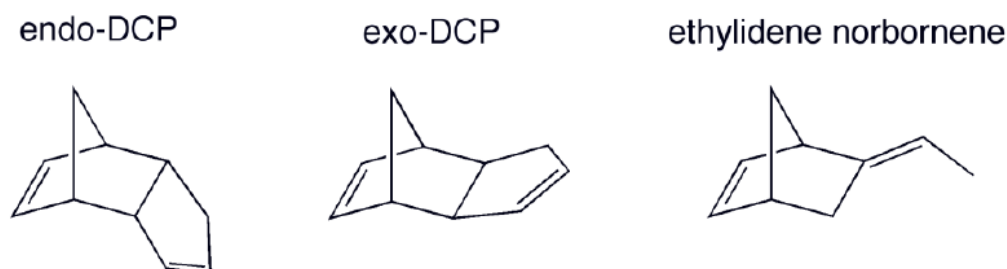
Figure 1.11: Monomers used as liquid healing agents[37].

DCPD is most easily obtained as the commercially available endo-isomer, and all ROMP based selfhealing systems. However, Rule and Moore[37] found that the exo-isomer, which can be prepared from endo-DCPD in a two-step isomerisation processis, undergo ROMP nearly 20 times faster than its endo-counterpart[38]. So when exo-DCPD was incorporated into a self-healing polymer steady-state healing was reached after only about 30 min, nearly 20 times faster than the time required to fully heal with the endo-isomer. ENB, a monomer also active towards the ROMP chemistry, is particularly attractive as a healing agent because it is a cheap, commercially available chemical with an extremely rapid bulk polymerisation rate. ENB also has a much lower freezing point than that of DCPD (15°C). The drawback to using this monomer, however, is that the resulting polymer is linear and thus has inferior mechanical properties as compared to polyDCPD.

Liu et al.[39] tested a system that used a blend of the two monomers as the liquid healing agent to increase the rate of polymerization and range of usable temperatures, while at the same time maintaining desirable mechanical properties. The polymerization was indeed faster with the addition of ethylidene norbornene and could be completed at a lower catalyst loading. Hence, a blend of DCPD with ENB was believed to provide a more reactive healing system with acceptable mechanical properties, making it more suitable for practical use. There are some issues regarding the stability and reactivity of the catalyst chosen for this systems. First generation Grubbs' catalyst is deactivated upon prolonged exposure to air and moisture and also loses its reactivity upon exposure to diethylenetriamine (DETA), the agent used to cure the epoxy matrix of these composites. Grubbs' catalyst can exist in different crystal morphologies and each has an effect on the dissolution kinetics and corresponding healing performance of the material. Smaller catalyst particles will have faster dissolution kinetics but will then have a larger reduction in activity due to exposure to DETA. Therefore,

the key to achieving optimal healing efficiency is to balance the competing effects of better catalyst protection during fabrication with the larger crystals and faster dissolution in the DCPD healing agent with the smaller crystals.

Rule and co-workers[40] proposed to encapsulate Grubbs' catalyst by wax to overcome the deactivation problem. This was achieved by a hydrophobic congealable disperse phase encapsulation process already established in pharmaceutical applications. The average diameters of the wax encapsulated catalyst ranged from 50 to 150 mm. The encapsulated Grubbs' catalyst was protected against deactivation by the DETA curing agent, retaining 69% of its reactivity. The wax microspheres also proved to aid in the dispersion of the catalyst within the epoxy matrix, leading to more uniform healing. The greater drawback of using ROMP based self-healing is economics, the Grubbs' catalyst uses ruthenium – a precious metal that is much expensive. One way this problem can be addressed is using the monomers described above with faster healing kinetics (such as ENB and exo-DCPD), which require lower loadings of catalyst to achieve high degrees of cure in a reasonable time period. Additionally, increasing the rate of catalyst dissolution in healing agent, either by treating the catalyst particles to have a larger surface area or selecting catalysts and healing agents with inherently matching chemical compatibilities, is known to reduce the amount of catalyst required in a self-healing polymer.

An alternative to the ruthenium catalysts was also recently explored, as they tend to be costly and have limited availability, and so would not be practical for larger scale commercial applications. Tungsten (VI) catalysts were investigated by Kamphaus et al.[41] as a cost-effective alternative to using Grubbs' Ru catalyst; in these systems WCl_6 would act as a catalyst precursor, becoming active either following alkylation with phenylacetylene or oxidation from contact with air. In addition to the alkylating agent, a dissolution agent (nonylphenol) would need be added to ensure miscibility with DCPD in order for polymerization to be initiated. The samples prepared with WCl_6 initially showed a 50% decrease in virgin fracture toughness, most likely due to poor bonding between the catalyst and the epoxy matrix. Upon addition of a silane coupling agent, the toughness was increased to 75% that of the neat epoxy. The as-received WCl_6 catalyst had a tendency to agglomerate into particle clusters within the matrix and so mechanical stirring was used to obtain a better catalyst distribution within the sample. The highest healing efficiency obtained was 20% for

a completely autonomous sample, which was achieved using 12 wt% WCl_6, 15 wt% exo-DCPD, 0.5 wt% phenylacetylene, and 1.0 wt% nonylphenol.

Cho et al.[29] developed a totally different healing system using di-n-butyltin dilaurate (DBTL) as the catalyst and a mixture of hydroxyl end-functionalized polydimethyl-siloxane (HOPDMS) and polydiethoxysiloxane (PDES) as the healing agent. The polycondensation of HOPDMS with PDES is alleged to occur rapidly at room temperature in the presence of the organotin catalyst even in open air. This system possesses some advantages, including (i) the healing chemistry remains stable in humid or wet environments, (ii) the chemistry is stable to an elevated temperature (>100°C), enabling healing in higher-temperature thermoset systems, (iii) the components are widely available and comparatively low in cost, and (iv) the concept of phase separation of the healing agent simplifies processing, as the healing agent can now be simply mixed into the polymer matrix.

In this system the catalyst was encapsulated instead of the siloxane-based healing agent, both of which were simply phase-separated in the vinyl ester matrix (VE) Polyurethane microcapsules containing a mixture of DBTL catalyst and chlorobenzene were formed (prior to embedding in the matrix) through interfacial polymerization. Despite the potentially more stable healing agent, this system actually achieved a healing efficiency value of 46%, which is lower than the 75–90% reported for the DCPD/Grubbs' catalyst-based healing system.

Keller et al.[42] investigated healing in a poly(dimethylsiloxane) elastomer (PDMS) with a healing agent that, when polymerised, is identical to the polymer matrix. In this system, a two-capsule healing agent was used: the first capsule contained a vinyl functionalised PDMS resin and a platinum catalyst, and in the second, capsule was a liquid initiator containing a hydrosiloxane copolymer diluted with 20% solvent to reduce its viscosity. Both components were encapsulated in urea–formaldehyde shells. Upon rupture of the microcapsules and release of the two shell materials into the damage area, the platinum catalyst adds the Si–H bonds of the hydrosiloxane copolymer across the vinyl groups of the PDMS resin to cure and heal damage. This system was shown to heal tear damage by recovering 70–100% of tear strength and significantly retard fatigue crack growth.

An alternative approach to self-healing systems containing an embedded healing agent utilizes epoxy as the encapsulated healing agent. This healing process would produce the same material that comprises the matrix of the composite, thus ensuring good adhesion between the healing material and the matrix, as well as allowing for recovery of the initial

mechanical properties. A second component, a hardener, would also need to be incorporated into the composite; in the event of crack formation and propagation the epoxy capsules would be ruptured and upon exposure of this epoxy to the hardener in the composite, polymerization would occur, filling the crack and restoring strength to the material. One of the first successful attempts to match a healing agent to its epoxy matrix was done by Rong et al.[43], in which a diglycidyl ether bisphenol-A (DGEBA) based epoxy resin was encapsulated in a urea–formaldehyde microcapsule and, along with a commercially available capsulated imidazole hardener, embedded in an epoxy matrix made from the same DGEBA epoxy resin as in the microcapsules. Healing with this system showed 100% recovery in fracture toughness.

Yin et al.[44] used uncured epoxy resin as a healing agent, utilizing a imidazole-metal complex as a latent hardener. This $CuBr_2(2\text{-}MeIm)_4$ hardener complex was soluble in the epoxy matrix and so could be evenly mixed in to form a homogenous matrix material capable of initiating healing at any point. The epoxy resin was encapsulated in urea-formaldehyde microcapsules and these were then embedded into the matrix material. This system shown to achieve up to 111% healing efficiency of , however, the main limitation is that it was not fully autonomous. In order for the imidazole complex to dissociate into its reactive species, it required heating to between 130-170°C.

Another system to be examined that integrates an encapsulated healing agent into a polymer matrix makes use of solvent-promoted healing. There are five stages to the healing process: surface rearrangement, surface approach, wetting, diffusion, and randomization. In 2007, Caruso et al.[45] transferred the previous research in solvent-promoted healing into the realm of mechanically stimulated self-healing materials. In this system, it is the solvent that is encapsulated and embedded into the polymer matrix. Solvents were screened for their healing ability by first manually injecting them onto a crack plane of a fractured epoxy specimen. It was found the healing efficiencies of these composites are highly correlated to solvent polarity, with the highest healing achieved by nitrobenzene, N-methyl pyrrolidone, dimethylacetamide, dimethylformamide, and dimethyl sulfoxide, which have dielectric constants between 32 and 47. These polar, aprotic solvents work well as healing agents while formamide and water, both polar protic solvents, showed no indication of healing. This is presumably due to the fact that the epoxy matrix contains a large number of free hydroxide groups and so the H-bond acceptor capability of these polar, aprotic solvents may play a

significant role in the healing process. The encapsulation procedure proved problematic, both in using urea-formaldehyde encapsulation and in using reverse-phase encapsulation techniques. The only solvent that was relatively easy to encapsulate was chlorobenzene, giving capsules with 160 μm average diameter; it was this encapsulated solvent that was used to demonstrate the self-healing capability of the system. Composites were fabricated with 20 wt% chlorobenzene microcapsules, which showed a maximum 82% healing efficiency. Similar composites using xylenes showed only 38% healing efficiency and composites using hexanes showed 0% healing efficiency, further demonstrating the dependence of healing efficiency on solvent polarity. Further work will be done to encapsulate the other solvents which showed high healing efficiencies as previously mentioned, as well as investigation into the mechanism of solvent-promoted healing.

Another example of monomers encapsulated to give self-healing property is isocyanate, which is capable of reacting with water in a humid or wet environment to enact healing. This would lead to a one-part, catalyst-free healing agent that could be incorporated into a matrix to create a healable composite material. In the recent past, the encapsulation of isocyanates has been limited to the solid state or blocked form[46,47] . Only two reports have appeared in the literature concerning the encapsulation of liquid isocyanates in the polyurethane shell walls by oil-in-water (O/W) emulsion method. For the first time, Sottos et al.[61] described the synthesis of PU microcapsules filled with IPDI. Spherical microcapsules with average diameter in the range of 40-400 μm were manufactured by adjusting agitation rate over the range of 500-1500 rpm (Figure 1.12). The mean diameter and agitation rate followed an inverse power law relationship. Once the microcapsules were filtered and dried, free-flowing powder was obtained with high yields. The average shell wall thickness ranged from 2 to 17 μm and increased linearly with capsule diameter, yielding a nearly constant wall thickness to diameter ratio of 0.05. IPDI content in capsules was above 60 wt % at agitation rates below 900 rpm, and weight loss was less than 10 wt % after half-year storage. Capsules were linear elastic in compression to failure and the average strength decreases with increasing diameter.
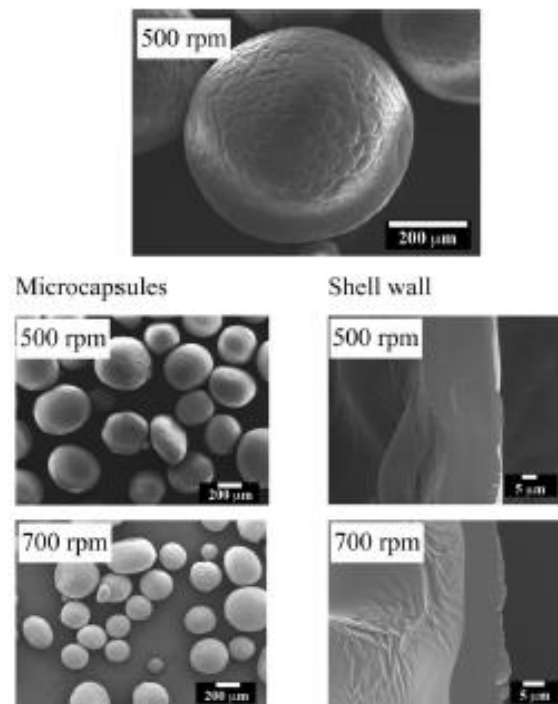
Figure 1.12: Surface and shell morphology of microcapsules obtained at various agitation rates[61].

This work opens the door for future studies that incorporate these capsules into a composite to create a material capable of healing under wet environmental conditions. Then Yang et al.[48] reported microencapsulation of more reactive hexamethylene diisocyanate (HDI) in the polyurethane spheres again and demonstrated its stability over time (Figure 1.13). They have studied the parameters associated with producing controlled microcapsule diameter and shell wall dimensions, as well as the associated mechanical properties of these capsules and reactivity of the liquid healing agent contained within. This work opens the door for future studies that incorporate these capsules into a composite to create a material capable of healing under wet environmental conditions.
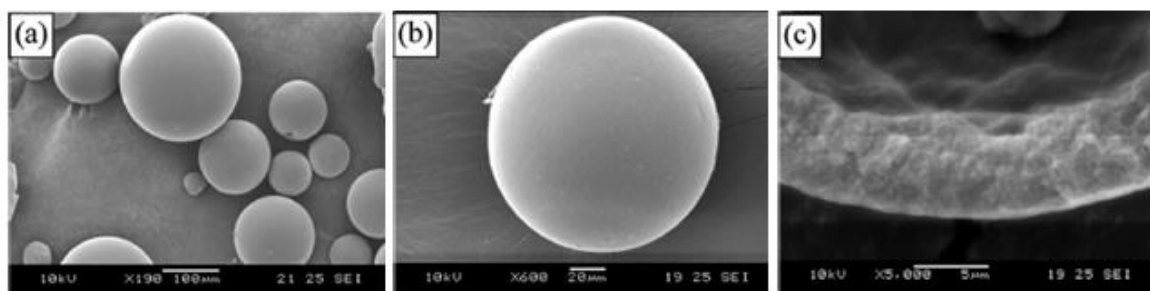
Figure 1.13: Morphology of HDI microcapsules. (a) Spherical shaped microcapsules, (b) zoomed in image showing smooth outer surface, and (c) shell wall profile.[62]

Although the endurance of polyurethane was a required characteristic to encapsulate reactive healing agents such as isocyanates, the capsule shell wall material must ensure a good

adhesion to the matrix in which the microcapsules will be incorporated to make the new selfrepairing composite. Since the capsule adhesion to the matrix affects the self-healing success, the goal of the modification is to improve dispersion and adhesion in spherical particle and to reinforce composites. Having been inspired by the above concept, Di Credico et al.[49] studied the microencapsulation process of a liquid IPDI with different polymeric shell and they identified an efficient method for the preparation of stable microcapsules with a liquid IPDI in large quantities, resilient and tailored to be embedded in epoxy matrices. The synthesis of new double layered polyurethane/poly(urea–formaldehyde) (PU/PUF) microcapsules filled with IPDI in a single batch process is reported (see Figure 1.14). The encapsulation of IPDI into PU/PUF double layered shell walls brings substantial improvements to the microcapsule properties. The PUF shell wall forms a stable protective layer around the sticky PU surface so that the double-walled shell shows to be hard and able to preserve the liquid IPDI, that instead diffuse outside of single UF shell microcapsule. At the same time the inner PU layer is soft and deformable for low mechanical strength, in order to impart flexibility and tightness to the microcapsules. Therefore these microcapsules combine the high shell strength, provided by the PU/PUF double wall component, with the more effective incorporation into bulk matrices, as verified during composite manufacture. In addition the PU shell wall was obtained by using commercially available TDI based pre-polymer, with effective improvement for large scale application.
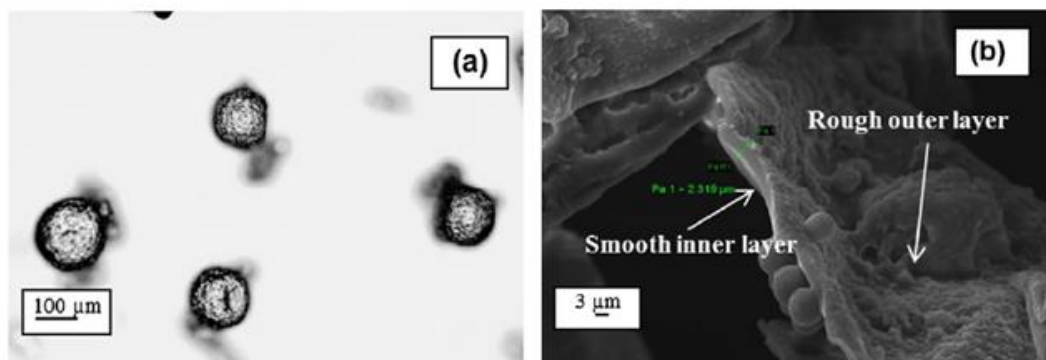
Figure 1.14: Morphology of PU/PUF microcapsules: (a) OM image, and (b) shell wall profile[49].

Urea–formaldehyde microcapsules filled with drying linseed oil were used for the healing of cracks in an epoxy coating.[50] Microcapsules were synthesized by in situ polymerization in an o/w-emulsion. Initially fully water-compatible urea and formaldehyde react in continuous aqueous medium to form poly(urea– formaldehyde). As the molecular weight of this polymer increases, the fraction of polar groups gradually decreases till the polymer molecules become hydrophobic and get deposited on the surface of o/w-emulsion droplets.

The obtained microcapsules were then incorporated in an epoxy resin coating. Since the outer shell surface of the microcapsules was very rough, strong binding to the coating matrix was provided. The encapsulated linseed oil is released by coating cracks and fills the cracks in a coating matrix (Figure 1.15). Finally, oxidation of linseed oil by atmospheric oxygen leads to the formation of a continuous film inside the crack.

Figure 1.15: Microscope photos of self-healing coating films with urea–formaldehyde microcapsules immediately after crack formation (left) and after 90 s (right)[50].

Corrosion of metallic substrate takes place when moisture and oxygen are transported through the cracks to the metal–coating interface. Healing of cracks, thus, provides an effective method to prevent corrosion. Performance of linseed oil as a healing material was assessed by exposing specimens coated with paint containing filled microcapsules to salt spray. Before exposure, coated surface was cross-cut up to the metal. Control specimens had the paint without microcapsules. Up to 72 h of exposure, specimens with paint containing capsules were found free from corrosion at the scribed lines (Figure 1.16). Control panels, however, suffered from corrosion after 48 h of exposure. Superior corrosion resistance performance of healed films is due to the reason that, linseed oil released from ruptured microcapsules filled the crack and formed a film by oxidative polymerization with atmospheric oxygen which prevented the ingress of moisture and oxygen and thus prevented corrosion.
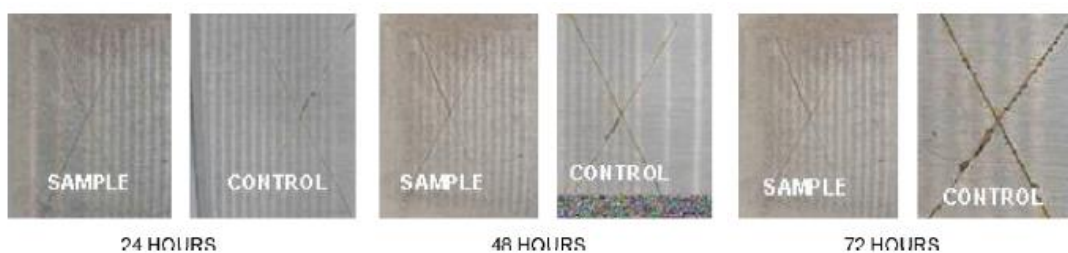
Figure 1.16: Salt spray performance of coatings at different exposure periods[50].

1.4. Damage sensing materials

Fundamental to the understanding and implementation of self-healing systems is the detection of damage and a trigger mechanism which initiates the repair action. This is done in nature efficiently e.g. in the case of wound healing by growth factors and matrix components that are available to provide these "start" signals, triggering relatively sedentary cell lineages at the wound margin to proliferate, to become invasive, and then to lay down a new matrix in the wound gap.

In order to deal with the phenomenon and the connected principles of self-healing in general, and even further to design and construct artificial self-healing functionalities for systems and devices, it is important to understand the nature and the consequences of damage and of degradation processes first.

One key aspect for achieving a successful microcapsule-based self-healing systems is that the liquid healing agent within microcapsules is effectively delivered into the crack planes after damage in order to provide efficient recovery of property. Therefore, it is beneficial to track the release of healing agent through invisible cracks from incorporated microcapsules for the development of self-healing. Toward this goal, a variety of research groups have introduced methods of detecting mechanical damage through color change. Mechanically active small molecules incorporated into polymer backbones or as crosslinks between polymer chains have shown changes in color and/or fluorescence upon fracture[35], tension[36,37] and shear[38]. The force-induced dissociation of dye aggregates has been used to change photoluminescent character in stretched polymers[55-57]. Changes in pH have been used to detect compression in polymer brushes[76], and microcapsules containing a pH-sensitive dye solution have also been utilized in carbonless copy paper, in which color change occurs upon a change in pH when ruptured microcapsule cores react with acidic clay or resin coatings[77]. Fluorescent dyes have been incorporated into filled hollow fibers to enhance damage visibility in the structure of the reinforced plastic[78]. None of these systems forms a colored product in tandem − or that is necessarily compatible − with a structural healing process.

Departing from these approaches, Urban[79] reports the development of copolymer colloidal particles that, upon coalescence, form films capable of sensing color changes upon mechanical scratches, but upon exposure to the visible (VIS) portion of the electromagnetic radiation (λ=580 nm), temperature, and/or acidic atmospheres, not only mechanical damage is repaired, but also mechanically induced red color scar vanishes. Figure 1.17 illustrates the

results obtained by Urban. It reports optical images of colorless film (A-1) which was mechanically damaged to result in a 10 mm wide scratch (A-2), followed by exposure to VIS radiation or temperature (A-3). As seen, initially colorless area a (A-1) turns reddish upon mechanical damage (A-2-a'), but when exposed to VIS radiation (λ=580 nm) or temperature (T = 95°C), turns back to its original undamaged and colorless state (A-3-a''). The undamaged area labeled b, b' and b'' remains unchanged. Exposure to acidic vapors turns the entire film reddish (A-4), but the damaged area a''' (A-4) is being repaired, and the original colorless state (A-3) can be retrieved back upon exposure to VIS radiation (λ=580 nm) or temperature (T = 95°C).
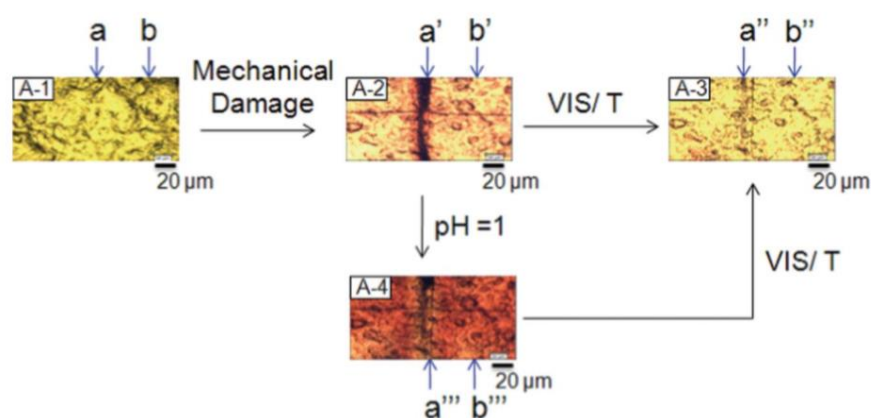
Figure 1.17: Optical images of p(MMA/nBA/SNO) films: undamaged (A-1), mechanically damaged (A-2), after exposure to VIS radiation or temperature (A-3) and after exposure to acidic vapors (A-4). Repair is achieved by either one of these conditions: visible light, temperature, or acidic pH vapors[79].

Moore et al.[80] report a new core-shell microcapsule system for the visual detection of mechanical damage using a red dye. Similarly, they sought to utilize ROMP of the cyclic monomer 1,3,5,7cyclooctatetraene (COT) to produce polyacetylene   an intensely colored conjugated polymer. 1,3,5,7-Cyclooctatetraene was incorporated into poly(ureaformaldehyde) core−shell microcapsules using an in situ emulsification condensation polymerization. To determine the potential for the COT capsules to visually indicate mechanical damage by color change, they gently mixed the thermally stable capsules with the Grubbs−Love catalyst without rupturing the capsules, and the mixture of catalyst and capsules was deposited onto a glass slide (Figure 1.18a). These capsules were ruptured by compression between two glass slides. Release of the core material was evident, and, immediately, a color change from pale yellow to red-orange was observed (Figure 1.18b). The color changed over 5 min to dark purple (Figure 1.18c,d,e). This color change

is consistent with an increase in the degree of polymerization (DP) of polyacetylene. As the conjugation length increases due to increasing DP, the polymer absorption should shift to the red and become more broad, eventually appearing almost black.
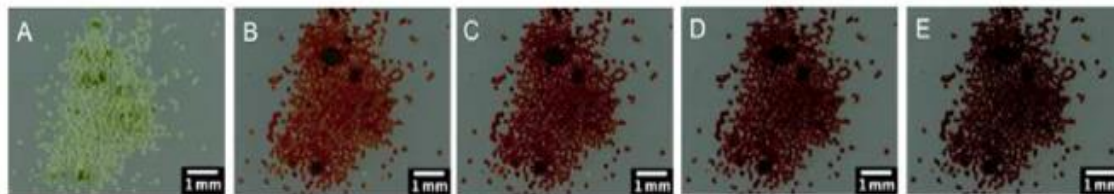
Figure 1.18: Photographs depicting color change of microcapsules mixed with 5 wt.% Grubbs-Love catalyst before and after crushing between two glass slides. (a) before damage, (b) t = 20 s, (c) t = 40 s, (d) t = 1 min, (e) t = 5 min[80].

To demonstrate damage indication by color change in a solid polymer film, COT microcapsules (15 wt %) and Grubbs-Love catalyst (1.5 wt %) were incorporated into poly(acrylic acid) (PAA) films ca. 500 μm thick. Aqueous PAA was chosen for processing in order to minimize catalyst degradation and leaching of the hydrophobic COT core into the polymer matrix during film deposition. Controls were prepared in which (1) only capsules were incorporated, (2) only catalyst was incorporated, and (3) neither catalyst nor capsules were incorporated. After curing overnight at room temperature (ca. 21 °C), the films were scratched with a razor blade. Within 1 min after damage, the scratched region displayed a red-orange color (Figure 1.19), consistent with the color change observed when crushing capsules and catalyst together.
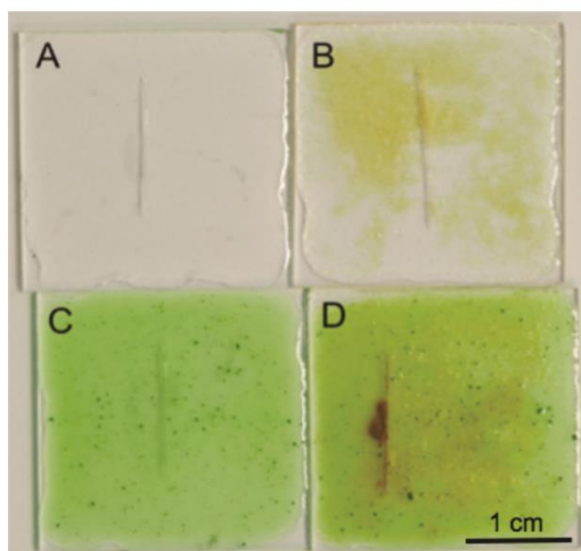
Figure 1.19: Photographs of PAA films containing (a) no microcapsules or catalyst, (b) 15 wt % COT microcapsules prepared by recipe C, (c) 1.5 wt % Grubbs−Love catalyst, and (d) 15 wt % COT microcapsules prepared by recipe C and 1.5 wt % Grubbs−Love catalyst. The 1 in. × 1 in. films are shown 2 min after being scratched with a razor blade[80].

Using this approach, a large amount of conventional materials could be converted into smart material that change colour in response to external stimuli. It is possible just by incorporating microcapsules containing cromophoric dye into the coating. The drawback of this system containing COT as core material is the necessity to use of too much expensive catalyst which cannot be used in industrial applications.

Noh and Lee[63] synthesized microcapsules with two different self-healing agents, *endo* diciclopentadiene (*endo*-DCPD) and 5-ethyldiene-2-norbornene (ENB), containing fluorescent dye surrounding by melamine-urea-formaldehyde (MUF) shell. The MUF microcapsules were dispersed in an epoxy coating layer and a fluorescence microscope was used to track the transport of liquid healing agent through cracks after inducing the damage on the epoxy coating. Figure 1.20 contains fluorescent microscope images (a), (b), and (c) before damaging and (d), (e), and (f) after damaging taken at different excitation wavelengths of 350, 480, and 546 nm, respectively. The vivid images could be viewed for all excitation wavelengths in different emission colors; blue at 350 nm, green at 480 nm, and red at 546 nm. . It is interesting to notice that the capsule shell is very bright, indicating the incorporation of fluorescent dye into the shell material. Note that the dye was mixed with self-healing agent, followed by dispersion in water and then in-situ polymerization of shell materials reaction at higher temperature. This is presumably due to the migration of dye to shell forming material during the initial stage of reaction. The images (d), (e), and (f) in Figure 1.20 for cracked coating layer embedded with 5 wt% of Grubbs catalyst and 5 wt% of microcapsules show a bright line starting from microcapsules. This is considered to be the trace of transport of self-healing agent between crack planes released from a microcapsule. The brightest fluorescence was observed in the vicinity of the microcapsules where the release of self-healing agent starts to the cracks because the larger amount healing agent is spread to the exit of crack. Also, it is shown that the propagating crack runs around one of small microcapsule at left-top in the image. The black spots shown in the images (d), (e), and (f) are believed to come from the Grubbs catalyst in the matrix. In this work, the addition of a fluorescent dye to self-healing agent enables to observe the track of the self-healing agent release into cracks from microcapsules at three different UV wavelengths. This means that the addition of fluorescent dye to self-healing agent may be useful in studying the details of cracks which are crucial in a microcapsule-based self-healing methodology.
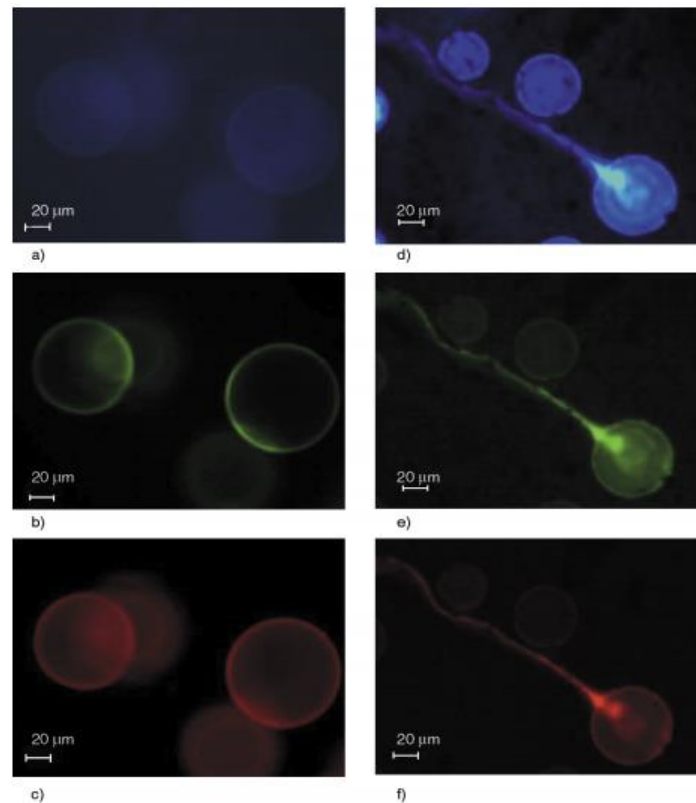
Figure 1.20: Fluorescent microscope images for a coating layer dispersed with endo-DCPD microcapsules containing a fluorescent dye (before damage, left) and a fluorescent dye in the presence of Grubbs catalyst (after damage, right) at different excited wavelengths; (a) and (d) at λ = 350 nm, (b) and (e) λ= 480 nm, (c) and (f) λ= 546 nm[63].

1.5. Self-healing materials

Polymer composites, when used as structural materials, often need to be repaired in order to restore pristine mechanical properties and increase their service-life. Ideal repair methods are those that can be executed quickly and effectively on site with minimum external human work; over the last few years, many attempts has been made to optimize mending process. One of the earlier healing methods for fractured surfaces is hot plate welding, where polymer pieces are brought into contact above the glass transition temperature (Tg) of the material, and this contact is maintained long enough for interdiffusion across the crack face to occur and restore strength to the material. However, this method present some disadvantages. Firstly, it has been demonstrated that the location of the weld remains the weakest point in the material and it becomes a preferential site for future damage; moreover this method can be used only for thermoplastics polymers, and therefore most of coatings and adhesives are excluded.[64] In laminate composites, when a delamination phenomenon occurred, a resin is

injected in order to repair damage and increase the durability of material. In case of fiber breakage, a reinforced patch is often used to partially restore strength to the material. In critical cases, both methods can be used simultaneously to increase healing efficiency and to restore the greatest amount of strength possible[65]. Unfortunately, none of these methods of repair is an ideal solution to restore damage in a structural composite material. These methods are just temporary solutions to prolong the lifetime of the material and each of these repair strategies requires monitoring of the damage and manual intervention to enact the repair. This greatly increases the cost of the material by requiring regular maintenance and service. In the perspective of damage management approach, a new healing method must be developed: an ideal healing process should be self-mending without need for external intervention or repair, it should be also realized directly in situ without the removal of the damaged part and it should be self-triggered by a particular external stimulus (i.e. mechanical breakage). The sum of these properties defines self-healing materials and recent studies have been conducted over the past few years to develop such type of materials. A unique parameter must be introduced to quantify the extent of healing within the same material and to compare it to different systems. It has become standard practice to assess the healing ability of a particular material/technique by comparing the fracture toughness K_{IC} of the material both before and after healing. The healing efficiency, η, can therefore be expressed as:

$$\eta = \frac{K_{IC}^{healed}}{K_{IC}^{virgin}} * 100$$

Where K_{IC}^{virgin} is the fracture toughness of the virgin specimen and K_{IC}^{healed} is the fracture toughness of healed specimen. Similar expressions of healing efficiency η can be written in terms of other mechanical properties like strain energy release rate G_{IC} or ultimate tensile stress[66]. An healing efficiency of 100% states that materials has completely recovered its mechanical resistance. In literature, healing systems with η≈90% have been reported[19,67], but values around 40% can be considered good and acceptable as well.

Self-healing materials can be classified according to type of stimulus that activate healing mechanism:

- **Mechanical stimulus** Self-healing materials based on mechanical stimulus are systems in which a polymeric agent is incorporated inside the structure by means of microcapsules or hollow fibers. Upon mechanical stimulus (fracture of the fibers or capsules), this agent would "bleed" into the damage site to initiate repair through a polymerization mechanism. Different polymeric agent and polymerization catalyst can be used. The most studied systems are: dyciclopentadiene (DCP) as liquid healing agent coupled with a ruthenium(IV) catalyst that will initiate ring opening metathesis polymerization (ROMP)[68]; polydimethilsiloxane (PDMS) system in which hydroxyl end-groups polycondensate by mean of tin catalyst[69]; system that utilizes epoxy as the encapsulated healing agent and an aminic hardener to trigger reaction[70]; encapsulation of solvent which cause swelling of the host polymeric matrix and help healing process[71]; encapsulation of isocyanates which are capable of reacting with water in humid or wet environment to form polyurethanes and enable healing[72].

- **Thermal stimulus** These self-healing systems are based on thermally reversible pericyclic reactions to repair damage. These reactions progress in a concerted fashion and the transition state of the molecule has a cyclic geometry, in which covalent bonds are repeatedly formed and destroyed, thanks to the heat given to the system. Between thermally activated pericyclic reactions, the most interesting and studied is the Diels-Alder cycloaddition: this reaction involves the concerted addition of a conjugated diene with a dienophile to form a cyclohexene ring containing two newly formed C–C bonds. The diene and dienophile components of this reaction can be altered to incorporate almost any functionality imaginable, and thus obtain specific properties for the materials. The most studied system in self-healing field is furan/maleimide. Furan compound act as diene and maleimide compound act as dienophile to form thermally reversible covalent bonds. Another interesting system is based on cyclopentadiene, which simultaneously acts as diene and dienophile and it is able to self-react to form a DA adduct. The great advantages of thermal self-healing system is the possibility to perform multiple healing process, exploiting the

reversibility of DA reactions, which can be theoretically repeated an infinite number of times.

- **Electrical stimulus** A particularly promising alternative system for healing that has been reported in recent years is the incorporation of a conductive component into the polymer matrix which can undergo resistive heating upon application of an electrical stimulus. When a crack forms in the material, the number of pathways available for the electrons to travel becomes limited; this results in a corresponding increase in resistance. With a constant applied electric field, heat is generated at the source of increased resistance, the site of damage. This localized heating initiates a built-in repair mechanism at the crack based on thermal reversible DA reaction, restoring sample's original mechanical and electrical properties. Not only does the inclusion of a conducting component into a polymer composite allow for localized healing but it also provides a non-destructive method of monitoring the material's structural integrity through an electronic feedback mechanism, allowing for detection of barely visible damage that otherwise can go unnoticed[73].

- **Electromagnetic stimulus** Conductive materials used in electrical healing system require electrical contacts to accomplish inductive heating. A feasible alternative is to incorporate magnetic compounds inside the polymer matrix and heat them without contact via electromagnetic induction. This technology has been intensively studied in biomedical field where the need to heat remotely is extremely important. Specifically, magnetic nanoparticles are directly injected in solid tumours and subsequently heated by exposure to a high-frequency magnetic field[74].

- **Photo stimulus** Reversible covalent bonding can be brought about through cycloaddition reactions, as previously discussed with the Diels-Alder reaction, which are thermally initiated. The alternative type of cycloaddition reactions is photoinitiated, undergoing cyclization upon irradiation of a certain wavelength of light and cleavage upon irradiation of a shorter wavelength of light. An example of these photosensitive groups can be found in some olefin-containing compounds that can undergo a [2+2] cycloaddition reaction upon irradiation with light to form cyclobutane. These newly formed covalent bonds can then be reversibly cleaved

upon irradiation with a shorter wavelength of light to give the starting olefins. Then, photoinduced cyclization can be exploited to form polymeric reversible cross-linked systems and many studies have been carried out on photoreactions of compounds containing cinnamic acid, coumarin, anthracene, maleimide and butadiene derivates[75].

- **Ballistic stimulus** Another type of reversible cross-linking system is based on ionic interaction. Ionomers are polymers that contain up to 15% of ionic content and have been studied for their ability to restore cross-linking after damage to a material, thereby restoring mechanical strength. A poly(ethylene-co-methacrylic acid) polymer subjected to projectile puncture showed healing ability, based on a viscoelastic recovery at the impact zone. Moreover, the hole generated by the projectile is filled and covered and ionic interactions are reformed to restore mechanical resistance of the material[76].

STIMULUS	TYPE OF SENSOR
Mechanical	Microcapsules
Thermal	Diene and Dienophile
Electrical	Conductive components
Electromagnetic	Electromagnetic materials
Photo	Olephine
Ballistic	Ionomers

Table 1.7: Classification of self-healing meterials based on activating stimulus

1.6.Healing by Mechanical stimulus

Presently, judging from the number of publications, self-healing systems utilizing mechanical stimulus, seem to be the most realistic approach to truly autonomous sel-healing polymeric coatings. Autonomous systems do not require any external input to repair. The most common approaches for autonomic self-healing materials involve incorporation of self-healing agents within a brittle vessel prior to addition of the vessels into the polymeric matrix. These vessels fracture upon loading of the polymer, releasing the low viscosity self-healing agents to the damaged sites for subsequent curing and filling of the microcracks. The exact nature of the self-healing approach depends on (i) the nature and location of the damage; (ii) the type of self-healing resins; and (iii) the influence of the operational environment.

Various approaches, such as microcapsule embedment, hollow fiber embedment, microvascular system and supramolecular network (see Figure 1.21) were applied to create autonomous self-healing coatings. Among these approaches, the microcapsule embedement is the most commonly used one for self-healing because of microcapsule's facile preparation and easy dispersion into the material matrix. Moreover, this method is the object of this dissertation and it will be discussed in more detail.
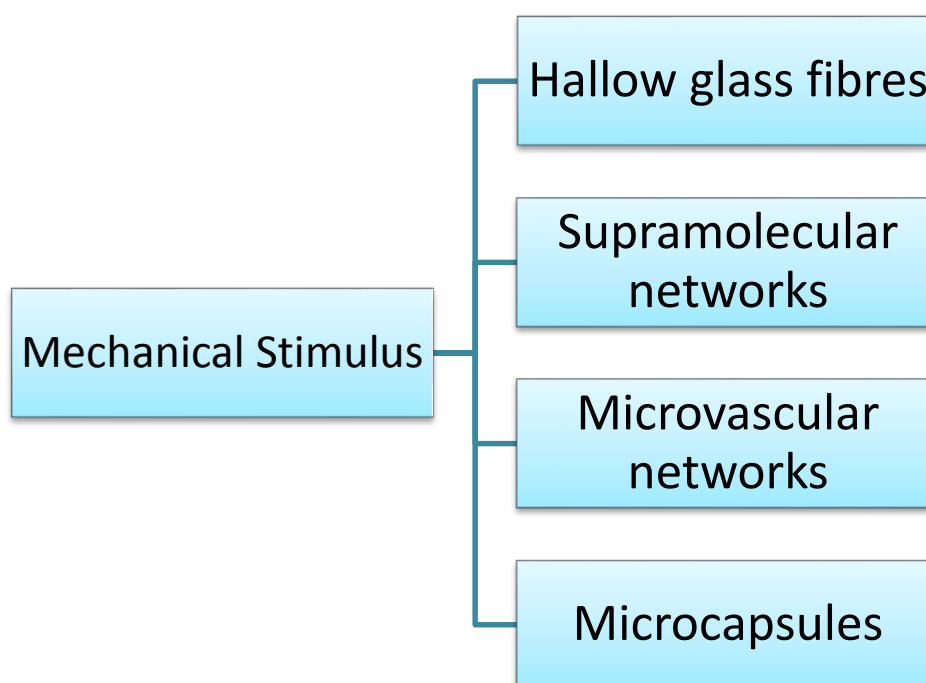
Figure 1.21: Mechanical stimuli response healing systems.

1.6.1. Hollow glass fibers

It is well known that the mechanical properties of polymeric materials can be greatly improved with the addition of a reinforcing fiber or other filler, giving the composite desired high strength and stiffness-to-weight ratios. The main disadvantage to these composites, however, is their poor performance under impact loading; this is an indication of their susceptibility to damage, which manifests mainly in the form of delamination. Utilizing reinforcing fillers that contain a healing agent would not only add the desired strength to the system but would also allow for self-repair of any damage that occurred via repair materials pre-embedded into the material.

Hollow glass fibers have been shown to augment structural performance of materials without creating sites of weakness within the composite. These hollow fibers offer increased flexural rigidity and allow for greater custom tailoring of performance by adjusting the thickness of the walls and degree of hollowness. By utilizing hollow glass fibers in these composites, alone or in conjunction with other reinforcing fibers, it would be possible to not only gain the desired structural improvements, but to also introduce a reservoir suitable for the containment of a healing agent.

In this sense, significant effort has been dedicated to incorporating healing agents into hollow fibres, which can be used both as a structural reinforcement and as large storage vessels. Once failure occurs in composites filled with these resin infused fibres, fibres rupture and healing agent(s) can diffuse into the damaged regions (Figure 1.22).
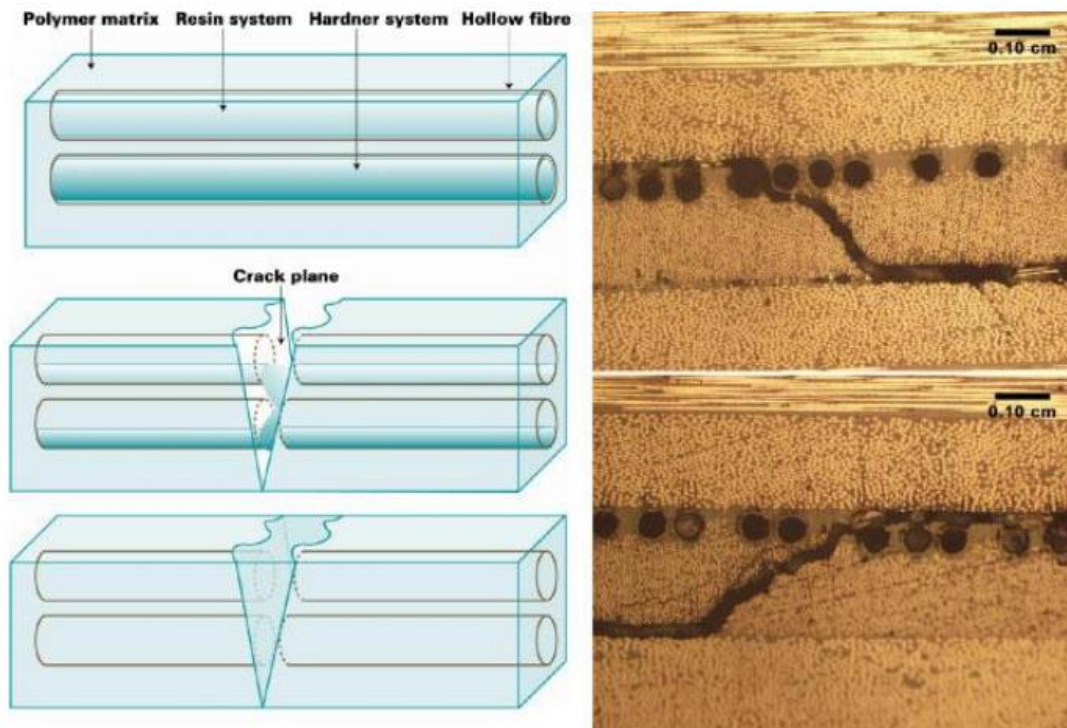
Figure 1.22: **Self-healing concept using hollow fibre storage vessels (left) and ruptured hollow vessels containing healing agent (right)**

These hollow fibres have been filled either through open ends, with either capillary action or vacuum assistance, or through surface pores, which need to be covered after resin infusion (Figure 1.23).
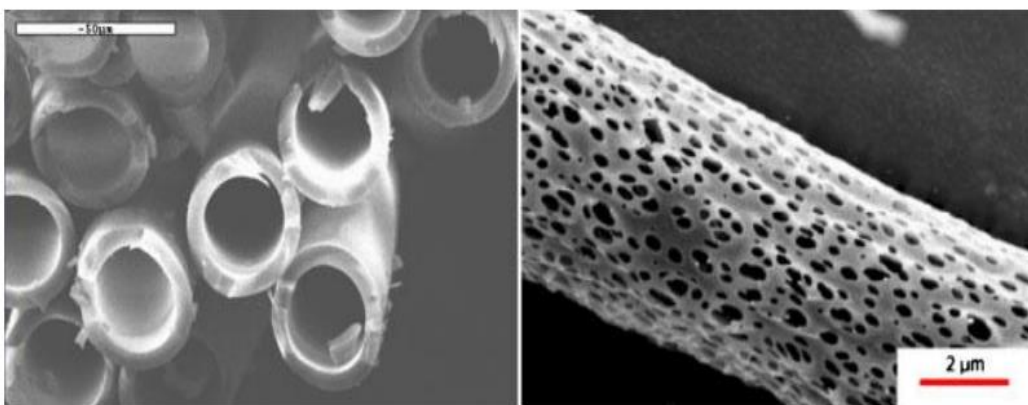
Figure 1.23: Hollow fibres with open ends (left) and hollow fibres with open surface pores (right)

Dry and Sottos[77,78] pioneered the concept of releasing healing chemicals stored in hollow fibers to repair damage. This concept has been initially applied to cementitious materials to

alter the cement matrix permeability, repair cracks, prevent corrosion. This first system utilized cyanoacrylate[79], ethyl cyanoacrylate[80], and methyl methacrylate as healing agents to repair cracks in concrete.

The feasibility of this approach was subsequently extended to polymeric materials by Motuku et al.[81] in the late 1990s. The healing agents contained within the glass fibers has been either a one-part adhesive, such as cyanoacrylate, or a two-part epoxy system containing both a resin and a hardener where either both are loaded in perpendicular fibers or one embedded into the matrix and the other inside fibers.

One of the initial challenges encountered when creating this type of self-healing system is the development of a practical technique for filling the hollow glass fibers with repair agent. When approaching this problem, the dimensions of the glass fiber itself must be considered, including diameter, wall thickness, and fiber hollowness, as well as the viscosity and healing kinetics of the repair agent. Bleay et al.[82] were among the first to develop and implement a fiber filling method involving capillary action that is assisted by vacuum, now a commonly utilized technique.

The glass fiber chosen must be also evaluated for its ability to withstand the composite manufacturing process without breakage, while still possessing the ability to rupture during a damage event in order to release the required agent(s) for healing. It was determined early on by Motuku et al.[81] that hollow glass fibers were best suited for this kind of application, as opposed to polymer tubes or those made of metal, which often did not provide controlled fracture upon impact damage. the next factor to investigate is the ability of the repair agent to adequately reach the site of damage and subsequently undergo healing; this will depend upon the viscosity of the healing agent, the kinetics of the repair process in relation to this viscosity, and the extent of cure of the healing agent within a given time period. Once this set of variables has been investigated, the last parameters to optimize are the concentration of healing fibers within the matrix, the most effective spacial distribution of these fibers, and the dimensions of the final specimen, all while keeping in mind the corresponding effects on the mechanical properties of the resulting composite material. These self-repair composites require a heat treatment to aid in delivery of the resin to damaged area as well as in curing of the healing agent. This can be a stong limitation from commercial point of view.

1.6.2. Microvascular networks

In conventional extrinsic self-healing composites it is hard to perform repeated healing, because rupture of the embedded healant-loaded containers would lead to depletion of the healing agent after the first damage.

Infusing larger storage vessels, such as the hollow fibres with healing agent, will likely result in multiple healing events of one damage site, but the total volume of liquid in each fibre is still finite. A logical progression to supplying even larger volumes of healing agent to damage sites is through a series of healing agent filled interconnected channels, which could potentially be linked to an external, refillable liquid pump to deliver a constant supply of healing agent. Healing with connected networks of healing agent is mechanistically similar to that of the hollow fibre approach, and conceptually similar to the vascular systems of many plants and animals.

Appropriately, connected networks of flowing healing agent is colled 'microvascular' networks (Figure 1.24a) Toohey et al.[83] proposed a self-healing system consisting of a threedimensional microvascular network capable of autonomously repairing repeated damage events.

Their work mimicked architecture of human skin. When a cut in the skin triggers blood flow from the capillary network in the dermal layer to the wound site, a clot would rapidly form, which serves as a matrix through which cells and growth factors migrate as healing ensues. The 3D microvascularm networks were fabricated by deposition of fugitive ink (a mixture of Vaseline/microcrystalline wax (60/40 by weight)) in terms of directwrite assembly through a cylindrical nozzle. Then, the yielded multilayer scaffold was infiltrated with epoxy resin. When the resin was consolidated, structural matrix was obtained. With the help of heating and light vacuum, the fugitive ink was removed and 3D microvascular networks were created. By inserting a syringe tip into an open channel at one end of the microvascular networks, fluidic polymerizable healing agent was injected into the networks. The healing chemistry of this method used ring opening metathesis polymerization of dicyclopentadiene (DCPD) monomer by Grubbs' catalyst, benzylidenebis(tricyclohexylphosphine) dichlororuthenium, which was used successfully in microencapsulated composites. In the crack plane, the healing agent interacted with the catalyst particles in the composites to initiate polymerization, rebonding the crack faces autonomously. After a sufficient time period, the cracks were healed and the structural integrity of the coating was restored. As

cracks reopened under subsequent loading, the healing cycle was repeated. By means of four-point bending configuration monitored with an acoustic-emission sensor (Figure 1.24b), the above approach proved to be feasible. The system showed up to 70% recovery of fracture toughness after damage in the four-point bending protocol.

The authors imagined extending this approach further to integrate pumps, valves and internal reservoirs, as well as to introduce new functionalities, including selfdiagnosis or self-cooling, through the circulation of molecular signals, coolants or other species.
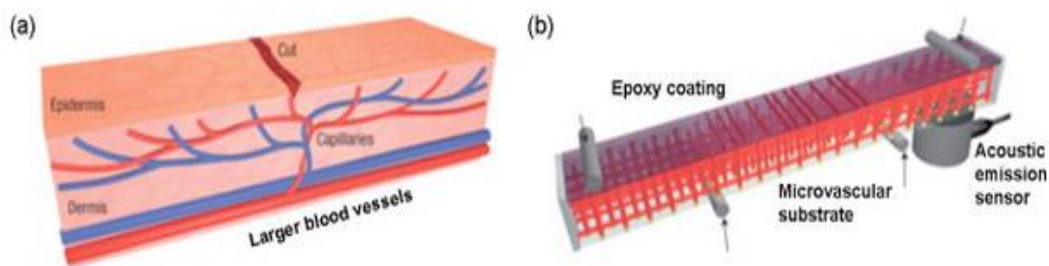
Figure 1.24: Microvascular based self-healing concept: a) a capillary network in the outer skin layer with a cut; b) schematic of an epoxy specimen containing a microvascular network, loaded in a four-point bending configuration monitored with an acoustic emission sensor.

During the same timeframe, Williams et al.[84] published their version of a microvascular-containing mechanically stimulated healable material in the form of a sandwich structure composite. Sandwich structures use high performing skin materials, such as glass or carbon fiber composites, separated by a lightweight core to obtain a material with very high specific flexural stiffness. A vascular network incorporated into a sandwich structure would address the larger damage volume expected of these systems, as well as allowing for multiple healing events to occur. Samples were fabricated with channels containing a healing agent, which had a negligible effect on the mechanical properties of the composite. Rupture of the vessels released the healing fluid, filling the void that formed as a result of impact damage on the sample. Initial tests were run on samples containing pre-mixed resin and hardener, to demonstrate the healing capability of the system. Indeed, these samples showed consistent and complete recovery of compressive stress at failure after impact damage. After this recovery of mechanical properties was successfully accomplished, the two sets of orthogonal channels in the material (horizontal and vertical) were each filled with a component of the two-part epoxy healing system, resin and hardener; after impact damage and a subsequent four-point bending test, it was determined that only half of the samples achieved self-healing. For the healed samples, it was clearly demonstrated that rupture of the two types of vessel

under impact allowed for adequate mixing of the two components to initiate the cure reaction and successfully restore the mechanical properties of the material. In the samples that did not recover their strength, however, it was determined that there was failure of the vessels to properly rupture under impact damage; either resin or hardener was released in these cases, but not both components.

1.6.3. Hydrogen bonding

Stimuli-responsive polymers, which can assemble and disassemble through selective, dynamic, and reversible bonds, have emerged recently as an important family of materials in which repeated healing is possible. Hydrogen bonding is one of the common mechanisms used in bulk self-healing materials and exists ubiquitously in living systems and most natural building blocks, such as carbohydrates, amino acids, and nucleic acids.

The most highly developed approach to generating supramolecular polymers harnesses multiple, co-operative hydrogen bonding interactions to assemble monomeric units into polymeric structures. Studies in this field have focused on the properties of supramolecular hydrogen bonded polymers in dilute solution (typically $<<10\%$ w/v). Under these conditions, the degree of polymerization (DP) for the system, and thus physical properties of the solution are related to the concentration ([M]) of the monomers and their respective binding constants (K_a), as defined by eqn: DP$= (K_a[\text{M}])^{0.5}$. The well-established relationship between degree of polymerization in solution and binding constant has driven the design of multiple hydrogen bonding motifs. Several heterocyclic groups which are capable of complementary recognition via multiple hydrogen bonds have been developed and explored successfully. In particular, the ureido-pyrimidinone (UPy) end-group has become the pre-eminent motif in a broad range of supramolecular polymers. This approach to supramolecular polymer design has led to the development of low to medium molecular weight materials (typically <5000 g mol^{-1}) that possess mechanical properties such as storage modulus (G'$=10^6$ Pa) and zero sheer melt viscosity ($\eta_0=2*10^6$ Pa s) similar to those of high molecular weight covalent polymers. Unlike conventional covalent polymers, the degree of polymerisation of a supramolecular polymer may be altered in situ by application of a suitable stimulus, such as increased temperature, that changes the association constant of the components. Removal of the stimulus subsequently restores the original properties of the material. Such materials are readily soluble in a range of solvents, which aids processing,

and they form tough, elastomeric films on removal of the solvent. The ease of introduction of the UPy moiety to end-cap amultitude of telechelic oligomers has resulted in the production of a visually healable, thermoreversible, supramolecular polymeric material that is now manufactured by Suprapolix BV®. In principle, under appropriate conditions, many supramolecular polymers should be able to heal micron-scale cracks by rearrangement of the supramolecular interactions to bridge the fracture void. In 2007 Leibler and co-workers produced a supramolecular system that exploits multiple hydrogen bonding elements, from inexpensive materials through a scalable methodology, to produce a weakly hydrogen bonded material that was designed to undergo several break and heal cycles. In 2012, Guan and co-workers produced an exquisitely designed healable supramolecular polymer utilizing multiple weak hydrogen bonding interactions in conjunction with spontaneous nano-scale ordering driven by phase separation – a brush-type polymer consisting of a polystyrene backbone (D.P. ≈114) with approximately 11 polyacrylic acid-amide side chains with D.P. ≈ 186. In the solid state, immiscibility of the polystyrene and polar side groups drives the self-assembly of the polymer into a core–shell type structure. This generates an elastomeric solid possessing a two-phase nanostructure in which "hard" polystyrene domains are connected through a continuous phases of low Tg, hydrogen bonded polyacrylic acid side-chains. Healing studies were carried out by cutting pristine samples into two pieces and gently pressing (by hand) the separated faces together. Healing efficiency increased with healing time (92% after 24 hours in contact). A wide variety of hydrogen bonding motifs have been designed, optimized and incorporated into polymeric materials which are able to undergo healing at ambient or elevated temperatures. However, these are generally low modulus elastomers and thus not suitable for applications which require high strength and stiffness[85]. More recently, self-healing hydrogel systems based on non-covalent interactions, or the self-healing supramolecular hydrogel systems have attracted the interest of many scientists. The development of hydrogels possessing both excellent self-healing and mechanical properties in hydrogel science due to their tight relationship with the many potential application scopes is of great significance. Herein, a novel class of polyurethane (PU) hydrogels with intermolecular quadruple hydrogen-bonding interactions were designed and fabricated. The obtained PU hydrogels can autonomously repair occurring incisions or cracks within 10 min at ambient temperature without the need for any stimulus, and more than 60% of the self-healing process can be achieved within 5 min, thereby exhibiting their

outstanding self-healing ability. They also exhibit excellent elasticity, robustness and toughness under both tensile and compressive stress. The presence of UPy units in PU macromolecular chains is a decisive factor endowing the PU hydrogels with these characteristics[86].

1.6.4. Metal-ligand coordination

Besides hydrogen bonding, another supramolecular interaction that has been investigated for its use in healable materials is that of metal-ligand coordination. In 2007, Kersey et al.[87] reported the inclusion of metal-ligand complexes within a polymer system. They initially sought to develop a polymer system comprised of an irreversible covalent network as well as some form of reversible interaction that was capable of load bearing in way that would contribute to the overall mechanical properties of the material. In this way, the reversible component would relieve stress from the permanent network, break preferentially under significant load, and would then re-form once that stress was removed to restore strength to the material. A material was created from a covalently bound polymer network that contained pyridine pendant groups, which formed a metal-ligand coordination complex with a bifunctional Pd(II) or Pt(II) compound. After first demonstrating the association between the metal and ligand, these stress-bearing groups were incorporated into a hybrid polymer gel composed of a pyridine functionalized methacrylate cross-linked network. The mechanical properties of the polymer network itself and of the network containing metal complexes were measured, indeed showing an increase in strength with the addition of the metal-ligand coordination complexes, though with a storage modulus only in the range of 10^5 Pa. Such a system containing reversible interactions that dissociate and re-associate with applied stress could be useful as a mechanically stimulated healable material in the future, and this study is the first step towards that end.

2. MATERIALS AND METHODS

2.1. Microencapsulation

In this work, microcapsules were synthetized using interfacial polymerization where the meeting of reactant monomers at the interface results in the formation of a shell and an active compound, such as a color indicator, that can be dissolved in a hydrophobic carrier, such as an oil, can be encapsulated into oil-core microcapsules.

This process is characterized by two main steps: emulsion formation and microcapsule wall formation. Figure 2.1 shows a schematic representation of the steps involved in forming oil-core microcapsules: the emulsion is formed by adding the oil phase (with pre-polymer, shown in purple) to the water phase (with surfactant, shown in light blue) and mixing; the last step is the formation of the microcapsule wall (shown in dark purple) by interfacial polymerization. Polymerization occurs exclusively in continuous phase and on the continuous phase side of the interphase formed by two immiscible phases, resulting in a polymer microcapsule containing a liquid core (Figure 2.2).

Water + surfactant   Oily phase addition   Organic phase/water   Microcapsules after
                                                 emulsion   water washing
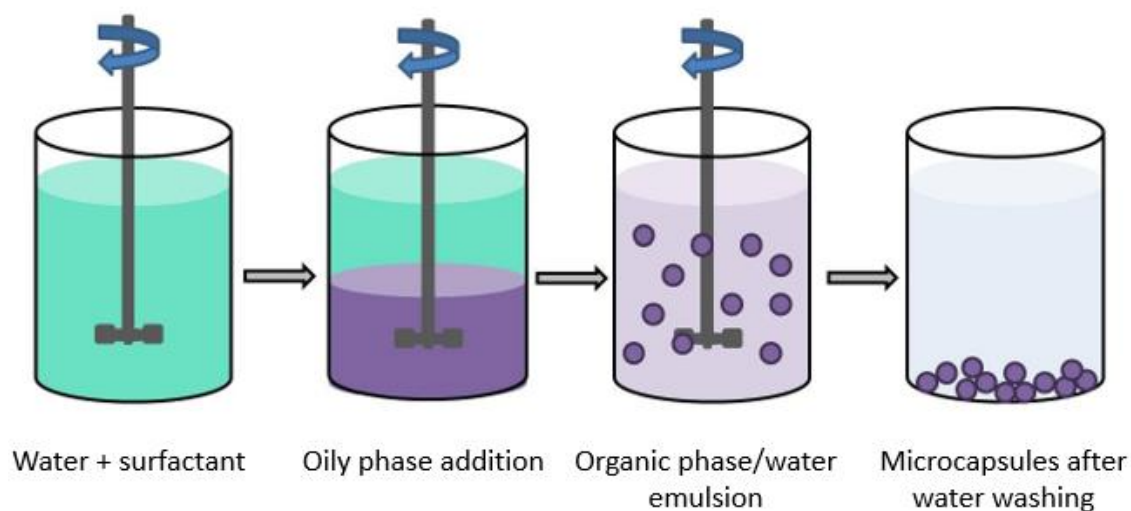
Figure 2.1: Schematic representation of the steps involved in the interfacial polymerization of an oil-in water emulsion for making oil-core microcapsules. Oil is shown in purple and water in light blue. The microcapsule wall is shown in dark purple.
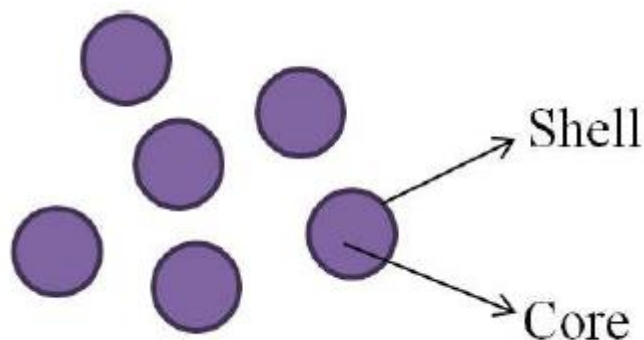
Figure 2.2: schematic representation of microcapsules

In the present work, polyurea (PUrea) microcapsules with different shell compositions were successfully fabricated via interfacial polymerizationin in O/W emulsion using a polyisocianate prepolymer and two types of UV-screening amines: 2-Amino-5-chlorobenzophenone (ACBP) and 4-4'Diaminobenzophenone (DABP). Different kinds of dyes dispersed in sunflower oil, as core materials, were embodied in these microcapsules for use in damage-sensing applications. DABP based polyurea microcapsules were also utilized for incorporation of a variety of UV-curing polymeric resins for self-healing materials applications.

2.2. Materials

2.2.1. Shell materials

Polyurea is an attractive material for coating applications: it forms in situ by the rapid reaction of isocyanates with polyamines, and its mechanical properties can be controlled over a broad range by varying the chemical structure and molecular weight of the components and the relative amounts of isocyanate and amine (i.e., the stoichiometry). Polyureas exhibit a phase separated structure similar to that of segmented polyurethanes, with rigid isocyanate domains (hard phase) embedded within a matrix of flexible chains (soft phase). Extensive intermolecular hydrogen bonding of polyurea typically leads to high mechanical toughness.
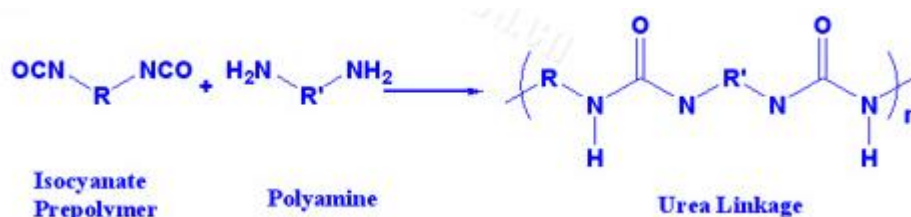
Figure 2.3: Structures of the isocyanate, diamine oligomer and the resulting polyurea chain.

Experimentally, the polyurea shell material of microcapsules was obtained by reaction of DesmodurL-75 and 2-Amino-5-chlorobenzophenone or 4-4' Diaminobenzophenone.

Desmodur L-75

Desmodur L-75 (Figure 2.4) is an aromatic polyisocyanate prepolymer based on toluene diisocyanate isomers (TDIs) in ethyl acetate with an NCO content of 13.3 ± 0.4 wt %, viscosity of 1600 ± 400 mPa s @ 23 °C, and equivalent weight of 315 g/equiv; it was a gift from Bayer Materials Science (Germany).
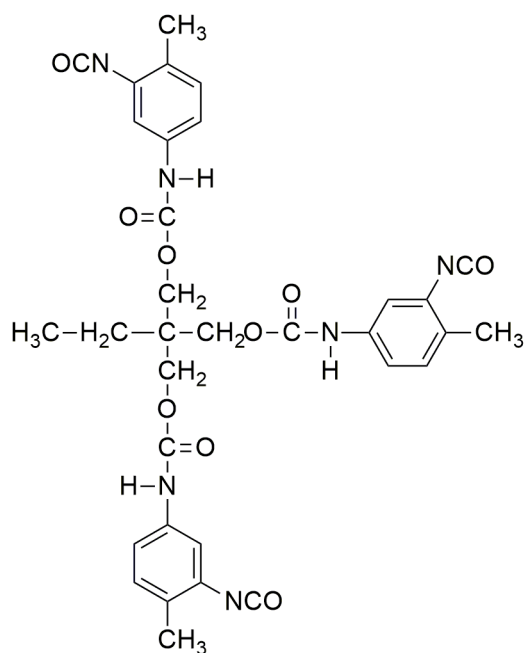
Figure 2.4: Representation of TDI prepolymer.

2-Amino-5-chlorobenzophenone and 4-4' Diaminobenzophenone

Amines are particular organic compounds, which contain basic nitrogen atom with a lone pair. These compounds are derivatives of ammonia obtained by substitution of at least one hydrogen atom with alkyl or aryl groups. Specifically, most of amines are prepared from ammonia by alkylation with alcohols. Amines are involved in many chemical syntheses due to their high nucleophilicity and basicity. For our synthesis process, amines were purchased from Sigma-Aldrich® and used as received.2-Amino-5-chlorobenzophenone, an aromatic ketones (diphenyl ketone), is an important compound in organic photochemistry and perfumery as well as in organic synthesis. It is a yellow crystalline substance; insoluble in water; melting point 49 °C; boiling point 305-306 °C. It has a molecular weight of 231.6776 g/mol and a density of 1.274 g/cm^3. 4-4' Diaminobenzophenone has molecular weight of

212.25 g/mol, density of 1.233 g/cm3, melting point 247 °C and boiling point 453°C. Benzophenones can act as optical filters or deactivate substrate molecules that have been excited by light for the protection polymers and organic substances. They are used as sunscreen agents to reduce damage by blocking UV-A, B. Figure 2.5 shows the chemical structure of these compounds.
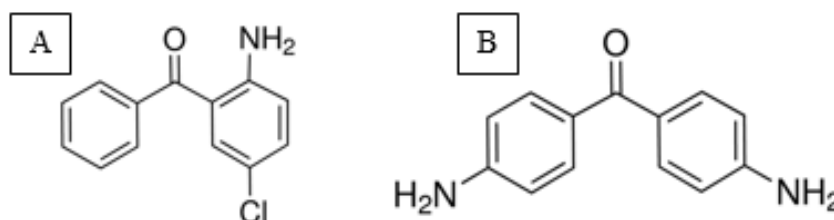
Figure 2.5: Representation of (a) 2-Amino-5-chlorobenzophenone (Sigma-Aldrich®) and (b) 4-4'
Diaminobenzophenone (Sigma-Aldrich®)

2.2.2. Core materials: damage sensing microcapsules

Sunflower oil

Sunflower oil (Figure 2.6) was kindly provided by Benasedo (Italy), it the non-volatile oil compressed from sunflower (Helianthus annuus) seeds. Sunflower oil is liquid at room temperature. The refined oil is clear and slightly amber-colored with a slightly fatty odor. Sunflower oil is mainly a triglyceride, composed by:

Saturated acid: 11%

Monounsaturated acid: 23%

Polyunsaturated acid: 65%

A typical constituent is shown in figure 2.7.
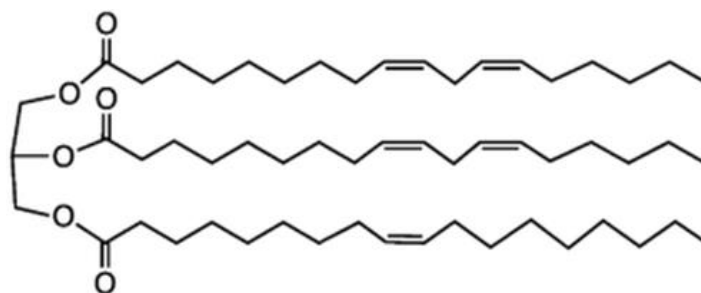
Figure 2.6: Representation of sunflower oil

Photocromic dye: Spiropyran

"Photochromism is a reversible transformation of chemical species, induced in one or both directions by electromagnetic radiation, between two states having observable light absorptions in different regions."[88]. Spiropyrans are one of the most popular classes of photochromic compounds that change their optical and structural properties in response to external inputs such as light, protons and metal ions, making them ideal molecules for the fabrication of multifunctional stimuli-responsive materials. The photochromic properties of spirobenzopyrans were first discovered by Fischer and Hirshberg[89] in 1952 where they observed that the irradiation of several solutions of spirobenzopyrans with UV-light (not exceeding 450 nm) produced color modifications that could be reversed by exposing the same solutions to yellow light (containing no radiation below 500 nm). The photochromism of spiropyran (SP) is due to the photo-cleavage of the C-O spiro bond upon irradiation with UV light. This cleavage allows a conformational rearrangement between a closed, colorless SP form and an opened, colorful merocyanine (MC) form with an important absorption band in the visible spectral region (Figure 2.7). In contrast, the exposure of the MC to visible light produces the reversion to its closed SP form; therefore, it is possible to modulate its conformation using light irradiation. These two forms are characterized by an important change of charge and dipole moment.

Closed Form (SP)   Open Form (MC)
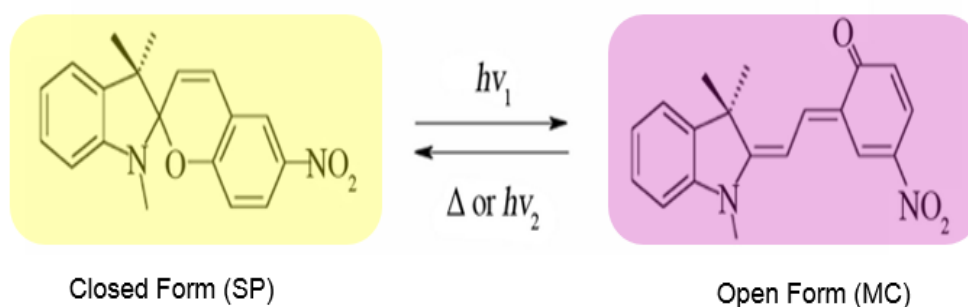
Figure 2.7: Chemical structure of Spiropyran (Colorless Closed form) and Merocyanine (Colorful Open form).

UV-sensitive photocromic dye 1′,3′-DIIDRO-1′,3′,3′-TRIMETIL-6-NITROSPIRO[2H-1-BENZOPIRANO-2,2′-(2H)-INDOLO] (SP-dye) was encapsulated previously dissolved in sunflower oil which acts as carrier. This dye was used to obtain an UV-light-sensitive mechanoresponsive smart coating by simple addition of microcapsules. After scratching the coating, the UV-screening microcapsules break and the UV-sensitive core material is

released and diffuses into the polymer matrix. Upon exposure to UV-A light, a rapid color change in the region where the damage was made is observed, because of the photoinduced transition of spiropyran to the plane merocyanine form.

Fluorescent dyes

Fluorescence generally occurs when a fluorescent molecule (fluorophore) resonantly absorbs electromagnetic radiation that promotes it to an excited electronic state. Subsequent radiative relaxation of the excited states results in emission of light, where some of the excitation energy is lost through heat or vibration, and part is emitted at longer wavelengths, compared to the excitation radiation. Unlike in phosphorescence, where light is emitted only while the radiation stimulus is present. For a given fluorophore, the fluorescence intensity is directly proportional to the intensity of the radiation received. Different materials may exhibit different colors and intensities of fluorescence, while they look identical when observed in day-light conditions. Fluorophores typically contain several combined aromatic groups, or plane or cyclic molecules with several π bonds. Fluorophores can be identified and quantified on the basis of their excitation and emission properties. The absorbed wavelengths, energy transfer efficiency, and time before emission depend on both the fluorophore structure and its chemical environment, as the molecule in its excited state interacts with surrounding molecules. Wavelengths of maximum absorption ($\approx$ excitation) and emission are the typical terms used to refer to a given fluorophore, but the whole spectrum may be important to consider. The excitation wavelength spectrum may be a very narrow or broader band, or it may be all beyond a cutoff level. The emission spectrum is usually sharper than the excitation spectrum, and it is of a longer wavelength and correspondingly lower energy. Excitation energies range from ultraviolet through the visible spectrum, and emission energies may continue from visible light into the near infrared region.

Main characteristics of fluorophores are:

- **Maximum excitation and emission wavelength** (expressed in nanometers (nm)): corresponds to the peak in the excitation and emission spectra (usually one peak each),
- **Extinction Coefficient** (or molar absorption, in $Mol^{-1}cm^{-1}$): links the quantity of absorbed light, at a given wavelength, to the concentration of fluorophore in solution.

- **Quantum yield** : efficiency of the energy transferred from incident light to emitted fluorescence (= number of emitted photons per absorbed photons)
- **Lifetime** (in picoseconds): duration of the excited state of a fluorophore before returning to its ground state. It refers to the time taken for a population of excited fluorophores to decay to 1/e (≈0.368) of the original amount.
- **Stokes shift**: difference between the max excitation and max emission wavelengths.

All fluorescent dyes used in this work are illustrated in the following Table 2.1: Properties of luminescent dyes:, where λ_{ex} is the maximum absorption wavelength and λ_{em} maximum emission wavelength. Their main chemical properties and molecular structure are represented. The last row of this table reports the characteristics of a phosphorescent dye, which was also adopted in this study during some preliminary analysis.
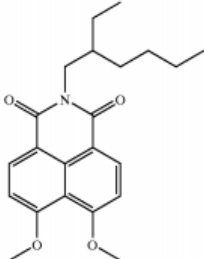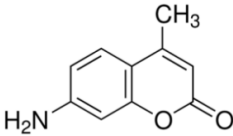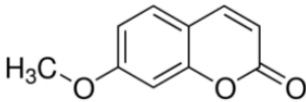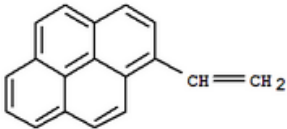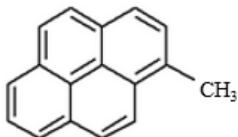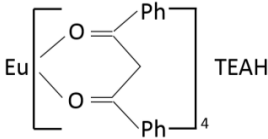
Name (Symbol)	Molecular structures
4,5-dimethoxy-N-(2-ethylhexyl) naphthalimide (Lumogen) Molecular weight = g/mol Density = 0,22 g/cm^3 Melting range = 175 - 178 °C Optical data: λ_{ex} 340 nm; λ_{em} 486 nm in chloroform	
7-Amino-4-Methylcumarin (C120) Molecular weight = 175.18 g/mol Density = 1.28 g/cm3 Melting range = 223-226 °C Optical data:: λ_{ex} 365 nm; λ_{em} 440 nm in ethanol	
7-Methoxycoumarin (7MC) Molecular weight = 176.17 g/mol Melting range = 115-121 °C	
1-Ethenylpyrene (EPy) Molecular weight = 228.2 g/mol Density =1.214 g/cm^3	
1-Methylpyrene (MPy) Molecular weight = 216.28 g/mol Density = 1.27 g/cm^3 Melting range = 72-74 °C Optical data: λ_{ex} 340 nm; λ_{em} 486 nm in chloroform	
Eu Complex (FN408) Molecular weight = 1146 g/mol Optical data: λ_{ex} 346 nm; λ_{em} 617 nm	

Table 2.1: Properties of luminescent dyes:, where λ_{ex} is the maximum absorption wavelength and λ_{em} maximum emission wavelength.

2.2.3. Core materials: self-healing microcapsule

Photopolymerizable resins

Photopolymerization, which uses light rather than heat to initiate polymerization, is a facile technique used to fabricate adhesives, protective coatings, thin films, photoresists, dental restoratives, and other materials. One attractive feature of photopolymerization is the high level of spatial and temporal control afforded by it.

A photochemical reaction is directed by the absorption of an electromagnetic radiation with a wavelength λ. This radiation excites a reacting molecule called photo-initiator. This extra component is used in the reaction because the crosslinker molecules are not sensitive to light and cannot be initiated on their own. Photo-initiators are decomposed by absorbing the UV light and form radicals or ions able to initiate the chain reaction. They manage the first step of the photo-reaction and control the reaction rate. To be efficient, a photo-initiator must have a high absorption in the emitting domain of the lamp. In order to transfer this energy, initiating molecules need an exact amount of energy to go to a higher level of energy, then, we say the molecule is excited. This is why these molecules are sensitive to some wavelength only. The excited molecule then decays into reactive species or transfers energy by radiative or non-radiative mechanisms. Therefore, the pot life of photopolymerizable formulations is very long and allows for handling or processing of the polymerizable resins in ways that other coating systems, such as epoxy gel coats, do not. Additionally, the reactivity of monomers used in photopolymerization is very high at room temperature and results in extraordinary manufacturing line speeds without the need of thermal treatment to ensure tack-free surfaces and high levels of monomer conversion. The monomers and resins used in photopolymerization most often have an average functionality greater than two. As a result, cross-linked polymers that are thermally stable and chemically resistant, two characteristics required by many photopolymerization applications, are produced.

The systems chosen as core materials for self-healing microcapsules fabrication were acrylate and epoxy crosslinkers curing respectively with a radical and cationic mechanism.

<u>Free-Radical Systems:</u>

The most common polymerization mechanism used in photopolymerization is free-radical chain polymerization. Free-radical photopolymerizations are generally very fast (cure achieved < 10 seconds) and reach very high conversions (conversion > 70-90% depending

on the system. There are a variety of effective photoinitiating systems for free-radical photopolymerization, as well as many types of monomers that are polymerizeable via free radical mechanisms. Some of the important monomer classes include: acrylates, methacrylates, acrylamides, methacrylamides, vinyl esters, and thiol-ene systems, where "ene" refers to a non-specific carbon-carbon double bond. When the UV light hit the molecule, the excited state is promoted. The excited molecule then releases the energy by hemolytic cleavage of the single bond between the two carbons, resulting in reactive radical species that initiate polymerization. An example of photodecomposition of Darocure 1173 photoinitiator is shown in Figure 2.8.
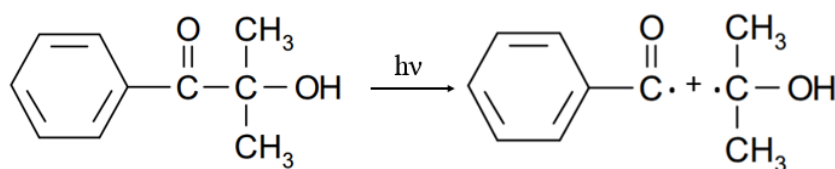
Figure 2.8: Formation of the free radical from the decomposition of radical photoinitiator molecule (Darocure 1173).

The two newly formed radicals initiate polymerization of the monomers through a chain reaction mechanism. During the propagation step of this process, the carbon-carbon double bonds of the monomers are quickly consumed generating an interconnected network of monomers linked by carbon-carbon single bonds, a polymer. Immediately after excitation, the molecular weight of the polymer grows with the successive additions of excess monomer units. A series of termination processes though slow down the polymerization until no more new carbon-carbon single bonds can be formed. For free radical mechanisms, most of polymer networks are created from unsaturated resins like acrylate or methacrylate resins. In presence of oxygen, radicals rather get involved into an oxidation reaction than the curing reaction once they have been initiated. Then the rate of curing is reduced and a longer time of exposure is required. Properties are also lowered on surface. Making a layer of nitrogen gas is the most efficient technique found to solve this problem.

For the photochemical initiation of the acrylate crosslinking, a commercially available photo initiator based on 2-Hydroxy-2- methylpropiophenone (trade name: Darocure 1173®), showed in Figure 2.8, was used. According to the manufacture's suggestion, 3 wt% was added to the polymer. This photo initiator was chosen due to its good solubility in all systems, the good processability (liquid form) and the UV absorption properties (main absorption peacks: 265 to 280, 320 to 366 nm) in the range of the emissions wavelength of

the utilized irradiation source. Above all, Darocure 1173 is used as a highly reactive and non-yellowing photo initiator in UV lacquers. Free radical polymerizable systems adopted in the present study as core materials for self-healing microcapsules fabrication, are acrylate monomers. They are: ethoxylated trimethylolpropane triacrylate (SR499 from Sartomer Co, TMPTA428 and TMPTA612 from Sigma-Aldrich®); dipentaerythritol pentaacrylate, SR399 obtained from Sartomer Co. Chemical structures and important physical properties of these monomers are presented in Table 2.2.

Physical properties	Molecular Structure
SR499 Functionality = 3 Molecular weight = 492 g/mol Density = 1.11 g/mL Viscosity =520@25°C	
TMPTA428 Functionality = 3 Molecular weight = 428 g/mol Density = 1.11 g/mL Viscosity = **TMPTA612** Functionality = 3 Molecular weight = 612 g/mol Density = 1.11 g/mL Viscosity =	
SR399 Functionality = 4 Molecular weight = 524 g/mol Density = 1.155 g/mL Viscosity = 600@25°C	

Table 2.2: The chemical structures and important physical properties of reactive monomers.

Cationic Systems:

The cationic ring-opening polymerization (CROP) of cyclic ethers, particularly epoxides, is another important reaction in photopolymerization. In some cases, cationic photopolymerizations of select monomers can meet or exceed the polymerization rates of (meth)acrylate species. However, in general, cationic photopolymerizations are slower than free-radical photopolymerizations. In contrast to free-radical reactions, the CROP mechanism is unaffected by molecular oxygen. Epoxide formulations containing a photo-acid generator (PAG) are readily polymerized at room temperature in air. Although oxygen does not affect CROP, water, another ubiquitous chemical species, has a significant impact. Water and other hydroxyl-containing species are chain transfer agents that alter both the rate of polymerization and the crosslink density or number average degree of polymerization. Control of humidity is difficult in a production environment, which makes use of moisture-sensitive systems problematic in that the properties of the polymers are not necessarily readily reproducible due to variances in the humidity levels in production facilities.

For a cationic reaction, the initiation step is carried out by creating a carbocation from which the polymer chain is made. In our case, we used stable cations to make the initiation. When they are exposed to UV light, Lewis acids (here SbF6-), which are part of the initiator molecule, turn into carbocations (H$^+$X$^-$). Epoxy resins are common thermosets and have many applications like coating, laminates, semiconductor devices, matrix material in composites. The cationic mechanism consists of creating the network by ring opening of an epoxide cycle (Figure 2.9).
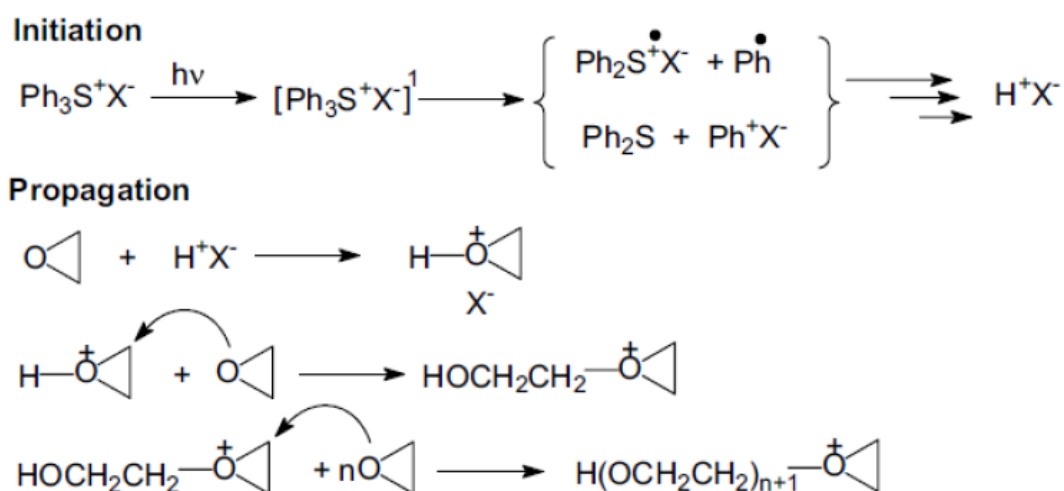
Figure 2.9: Initiation and propagation mechanisms of the cationic network.

Triarylsulfonium hexafluoroantimonate salts was used as a photo-initiator (Figure 2.10). It has been formulated to absorb and initiate in a wide domain of wavelength.Its molecular weight is 1632 g/mol.
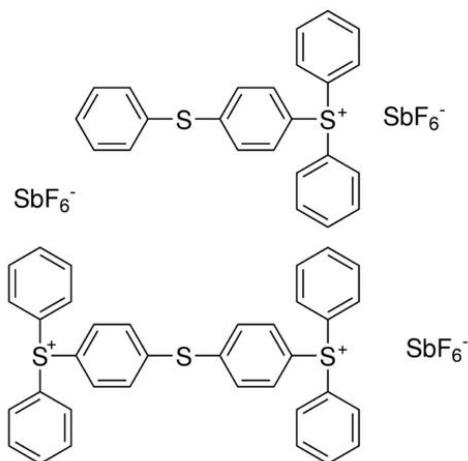
Figure 2.10: Representation of Triarylsulfonium hexafluoroantimonate salts (Sigma-Aldrich®)

The epoxy resin used is a 3,4-epoxycyclohexylmethyl 3,4-epoxycyclohexane carboxylate (EEC, Sigma-Aldrich®) with a molecular weight of 252.31 g.mol^{-1}, shown in Figure 2.11. The presence of two cycloaliphatic groups in the molecule makes it very reactive. When a carbocation is generated at the initiation, it reacts with the oxirane group and the epoxy function is opened. The crosslinker molecules can then connect to each other.
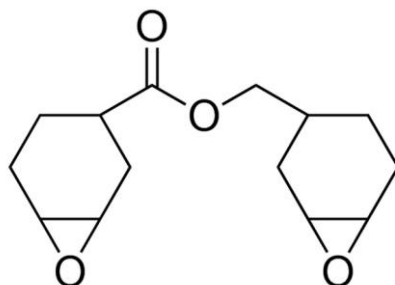
Figure 2.11: Representation of 3,4-epoxycyclohexylmethyl 3,4-epoxycyclohexane carboxylate (Sigma-Aldrich®).

2.2.4. Synthesis of microcapsules

2.2.4.1.   *Damage sensing microcapsules*

Emulsification was done at room temperature in a batch reactor 500-mL flanged glass reactor with a diameter of 90 mm, where 120 mL of deionized water and 13.5 g of GA as surfactant were mixed. At room temperature, 120 mL of deionized water and 13.5 g of GA as surfactant were mixed in a 500-mL flanged reactor (90 mm in diameter,). The reactor walls were fitted with a jacket for an external recirculation temperature system (Figure 2.12a). The solution was agitated at 500 rpm for 3 h by a mechanical stirrer, driving a six-bladed propeller (63 mm diameter, see Figure 2.12b) before beginning encapsulation. Such a system optimizes the shear and then the drop breakage.
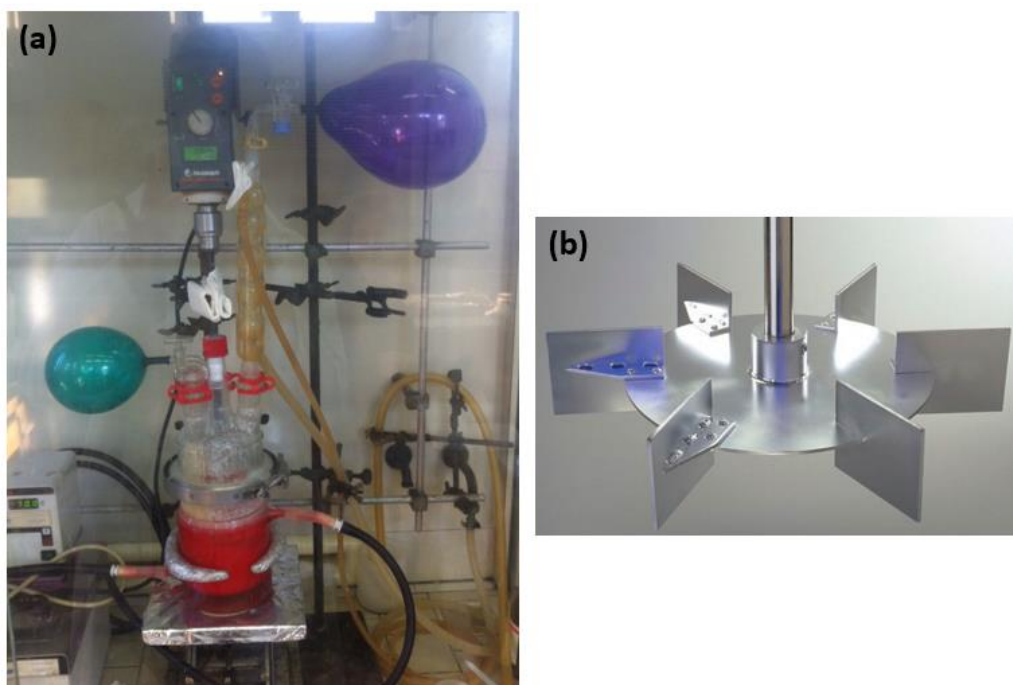
Figure 2.12: (a) photograph of reactor system used for encapsulation process; (b) photograph of flanged reactor

Desmodur L-75 prepolymer (9.0 g) was separately diluted into 8 mL of dry CB and kept under nitrogen. In another flask, 0.36g of dye (SP or fluorescent type) was mixed into 40 mL of sunflower oil for 1 h until a homogeneous mixture was obtained. In a third flask, the amine was dissolved in its solvent: ACBP (3.53 g) in 15 mL of chlorobenzene (CB) and DABP (1.517g) in 4 mL of N,N-Dimethylformamide (DMF). Successively, the flasks of Desmodur L-75 and dye/oil were slowly poured into the GA solution. The resulting mixture was then heated at 50 °C, and the amine solution was slowly added to the stirred emulsion. The reactor was heated at 70 °C. The reaction proceeded under continuous stirring for 1 h and 30 minutes after which the reaction mixture was allowed to cool to room temperature.

The microcapsules were filtered the next day using a Buchner funnel, were washed with water, and were dried under vacuum at 40°C for 24 h before sieving. The schematic outline of the procedure is given in the Figure 2.13. A summary of the recipes used is provided in Table 2.3.
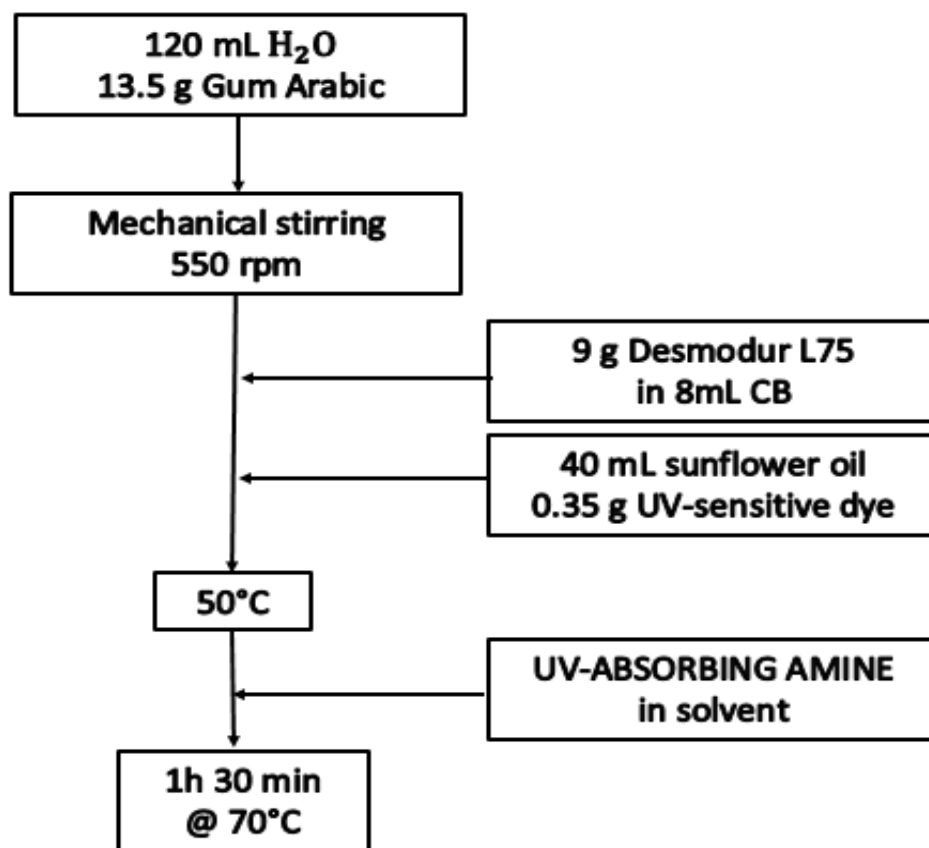
Figure 2.13: Procedure for the preparation of damage sensing microcapsules.

	Reacting monomers						Oily phase		
	DL75(g)	CB (mL)	Amine	(g)	Solvent	(mL)	Oil (mL)	Dye	(g)
S1	9	8	ACBP	3.53	CB	15	40	SP-dye	0.36
S2	9	8	DABP	1.517	DMF	4	40	SP-dye	0.36
S3	9	8	DABP	1.517	DMF	4	40	Fluo	0.36

Table 2.3: Quantities of chemicals used to prepare damage sensing microcapsules. ACBP: 2-Amino-5-chlorobenzophenone; DABP: 4-4' Diaminobenzophenone; DL75:DesmodurL75; CB: Chlorobenzene; DMF: N,N-Dimethylformamide.

Self-Healing microcapsules

The microcapsules were prepared via interfacial polymerization by experimental condition as shown in Table 2.4. The same procedure adopted for microcapsules containing UV-sensitive dye was used to fabricate self-healing systems. UV-curable polymeric compounds and photoinitiator were facilely encapsulated in UV-screening polyurea shell, which was formed by the interfacial polymerization of DABP amine and polyisocyanate prepolymer in an oil-in-water emulsion. Figure 2.14 illustrates a schematic procedure of the encapsulation process for these materials.
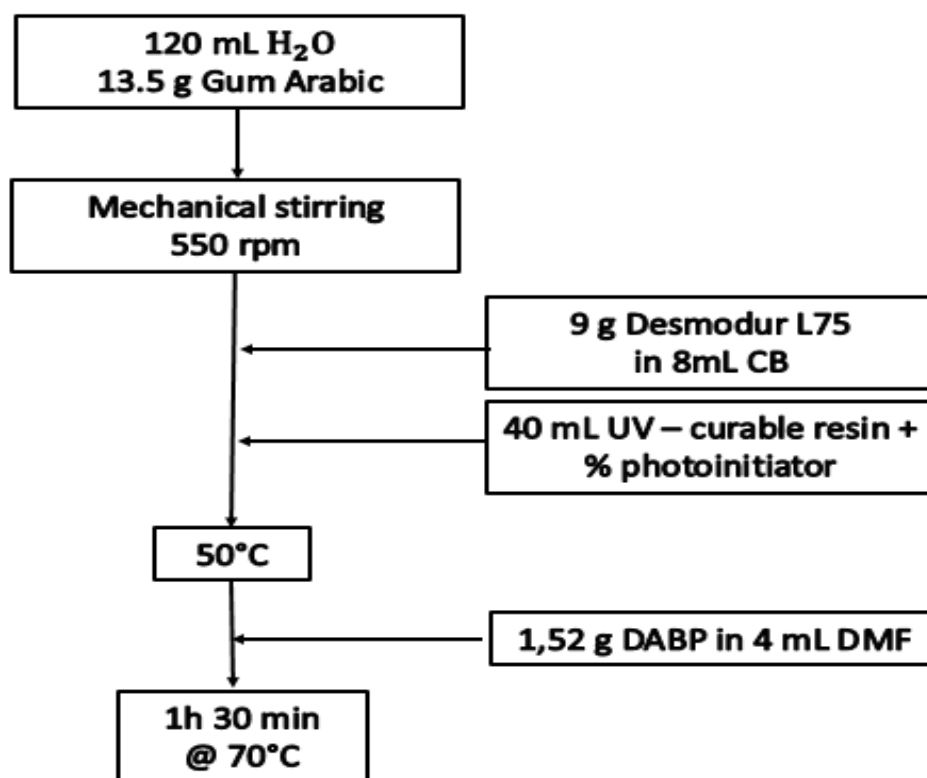
Figure 2.14: Procedure for the preparation of self-healing microcapsules.

	Reacting monomers						Oily phase			
	DL75(g)	CB (mL)	Amine	(g)	Solvent	(mL)	Healing agent	(mL)	Initiator	(%wt)
H1	9	8	DABP	1.517	DMF	4	SR499 TPETA428	40	Daroc	3
H2	9	8	DABP	1.517	DMF	4	SR399	40	Daroc.	3
H3	9	8	DABP	1.517	DMF	4	ECC	40	Antim.	2

Table 2.4: : Quantities of chemicals used to prepare self-healing microcapsules. ACBP: 2-Amino-5-chlorobenzophenone; DABP: 4-4' Diaminobenzophenone; DL75:DesmodurL75; CB: Chlorobenzene; DMF: N,N-Dimethylformamide; Dar: Darocure1173; Ant: Triarylsulfonium hexafluoroantimonate salt.

2.2.5. Polyurea films preparation

Polyurea films were formed using the same reacting monomers adopted in the microencapsulation processes. First, a solution of DesmodurL75 (3g) and CB (2ml) was mechanically stirred at room temperature. After few minutes, the required amount of amine (1.18 g of ACBP in 3 ml of CB or 0.5g of DABP in 1ml of DMF) was added into the beaker. When the mixture become homogeneous, the agitation was stopped and the formulation was applied on the surface of a grass slide. Curing was carried out at 70°C for 1h and 30 minutes. Figure 2.15 shows a photograph of synthetized polyurea films and their appearance when exposed to UV radiation.

Figure 2.15: synthetized polyurea films (a) ACBP amine based (b) DABP amine based under UV-irradiation at 366nm.

2.2.6. Composite Matrix Preparation of Smart Sensitive Materials with UV-Absorbing Microcapsules.

A polyethylene glycol methacrylate photopolymer was chosen as carrier to prepare the smart microencapsulated coating. The coating mixture had the following composition: 90.5 wt.-% tetraethylenglycol dimethacrylate, $\overline{M_W} = 330$ g·mol^{-1} (TEGDMA), 6 wt.% PEG monomethacrylate $\overline{M_W} = 360$ g·mol^{-1} (PEGMA), 3.5 wt.-% 2-hydroxy-2-methylpropiophenone (Darocur 1173, photoinitiator). The reagents were mixed in a dark glass vial in the desired ratio and stirred at room temperature for 5 min before use. Microcapsules filled with SP-dye (15 wt % on the methacrylate oligomers) were dispersed into the polymerization mixture. The liquid formulation was cast into a glass or carbon substrates and the photopolymerization was carried out under nitrogen, using a UV irradiation chamber, model G. R. E. 500 W by Helios Italquartz, equipped with a mercury vapor lamp, Zp type 500 W (with a UV emittance from 254 nm to visible wavelengths range).

Microcapsules with DABP based polyurea shell and containing SP or fluorescent dye were incorporated in a waterborne fluorinated polyurethane dispersion. FLUOROLINK® P56 (Solvay) was used for this purpose. Fluorolink P56 is a water dispersion of an anionic polyurethane based on perfluoropolyether (PFPE) backbone, which composition is 25 % PFPE derivative, 73 % water, < 2 % solvent. It has been developed in particular to impart oil- and water repellence and stain release properties to the treated surfaces[90]. Microcapsules were incorporated into the formulation (15 wt% with respect to the PEPE weight in the wet formulation) and stirred until obtaining uniform dispersion. Subsequently, the coating formulation was applied on a dark plates. Samples were left to dry at room temperature (25 °C) overnight.

ACRIPOL ZA 02 (from EP Vernici) was used to fabricate coatings with microcapsules containing fluorescent dyes. It is a glossy acrylic/polyurethane clearcoat, with good hardness, adhesion and elasticity. It is suitable for protection of brass, silver, aluminium, steel etc. and can be also used as as clear coat on metalized matt base coat for double coat finishings. As indicated by the supplier, the catalyst QA 2028 was added to allow for crosslinking.

2.3.Methods of characterization

2.3.1. Thermal analysis

Differential Scanning Calorimetry (DSC)

One of the main thermal analysis techniques utilized to characterize polymeric materials is Differential Scanning Calorimetry (DSC). In DSC analyses, a particular instrument called calorimeter records changes of specific heat (C_p) of a sample versus temperature. In a thermal cycle, C_p of a sample is also directly correlated to enthalpy variation.

$$Cp = \frac{\partial H}{\partial T}$$

On the basis of these correlations, DSC measures heat flow variations between a reference and the sample of interest[92]. To be more specific, calorimeter is composed by a heat flux plate and two crucibles of aluminum, one containing a few milligrams of materials to be investigated and the other which is empty and serves as reference. During a thermal cycle, the two crucibles will have different temperature due to the presence of sample in one of them. In this way we can measure the difference in temperature between the two crucibles and thus also the heat absorbed by the material during the thermal cycle and its specific heat. The difference of heat absorbed from the two crucibles is correlated with transitions of the specimen and are visualized as endothermic or exothermic peaks on a DSC spectra (Figure 2.16). For this reason, DSC is a powerful tool in the analysis of polymeric materials because it permits to identify the presence of transition temperatures (in particular glass transition for polymers) but also crystallization and melting of polymers. Sometimes it can also be utilized to estimate reaction kinetics and activation energies. In this thesis work, DSC analyses were carried out by means of a DSC/823e-Mettler Toledo: calorimeter is calibrated with Indium and n-hexane submitted to a thermal cycle between 0°C and 300°C at a speed of 10°C/min in nitrogen inert atmosphere.
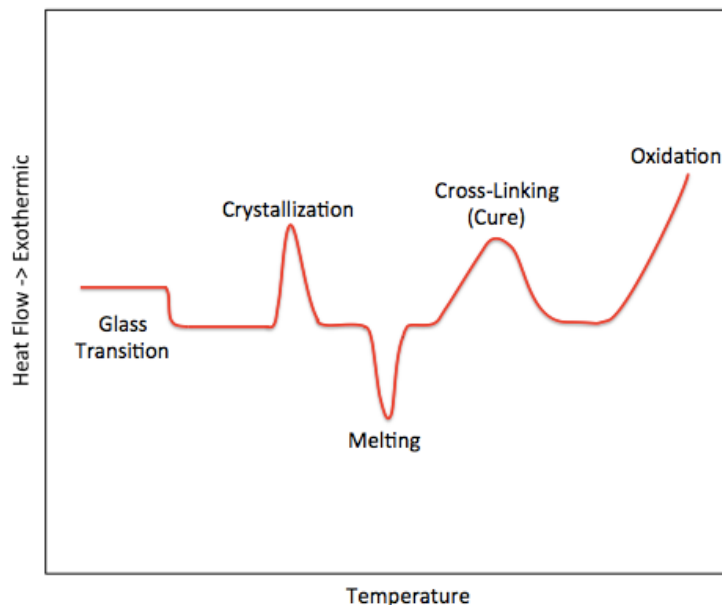
Figure 2.16: Example of a typical DSC spectrum. Peaks of characteristic phenomena are represented and described.

Photo-differential scanning calorimetry (p-DSC)

Photocalorimetry (p-DSC) has been popular because of the simplicity of the technique and the very short run times used, allowing the study of kinetics and reactivity of photoinitiated polymerization in a short space-time. The kinetic DSC profiles make it possible to compare the rate of polymerization (R_P) of a given monomer in the presence of a photoinitiation system (photoinitiator/coinitiator). The flexibility of photo-DSC allows the investigation of different variables on the photopolymerization such as; structure of monomers and photoinitiators, composition of formulations, irradiation intensity, temperature and effect of atmosphere (inert gases or air (oxygen)). Photo-DSC is a valuable experimental tool that, if used correctly, gives valuable results. However, this technique is very sensitive to a number of experimental variables and sample preparation[90].

The subject of this work was to use photo-DSC to study kinetics of photopolymerization of UV-curing resins chosen as core materials for self-healing microcapsules fabrication.

The photo-DSC analysis was carried out on DSC/823e-Mettler Toledo equipment, the same instrument used for DSC analysis, adapted for photochemical measurements. The UV light was generated by a medium-pressure mercury lamp at an intensity of 40 mW/cm^2, and the samples were exposed to this light for 2 minutes under a nitrogen flow of 50 mL/minute at a prescribed temperature of 25°C (isothermal mode). The samples were placed into an open aluminium DSC pan, and the weight of the samples was adjusted to be in the range of 2 mg.

Thermogravimetric analysis (TGA)

Another fundamental thermal investigation technique is thermogravimetric analysis, also known as TGA. TGA is an analytical method in which instrument continuously records variation of mass of a specimen in function of temperature and time in a controlled atmosphere. The results of an analysis are shown in a graph with temperature or time on X axis and absolute or percentage mass variation on Y-axis. This type of graph is usually called *curve of thermal decomposition* and give information about thermal stability of specimen and its components[93]. From a technical point of view, an instrument for TGA should be extremely precise in measuring three quantities: mass change, temperature and temperature change. Experimental apparatus is composed by a thermal precision balance, a hoven, a pipeline for gases to guarantee, when requested, an inert or reactive atmosphere and a computer to have instrument feedback and to generally control the system. To be more specific, balances utilized in TGA usually have an operative range between 5-20 mg while typical ovens can go from room temperature up to 1500°C with a heat rate between 5 to 100°C for minute. In order to obtain the required precision, temperature change are measured by means on a precise thermocouple while mass changes are measured by means of a photodiode. Indeed, variation in weight of the specimen induces a variation in current produced by photodiode. This change of current is amplified, transduced and measured and then a thermogravimetric graph is built (example in Figure 2.17).
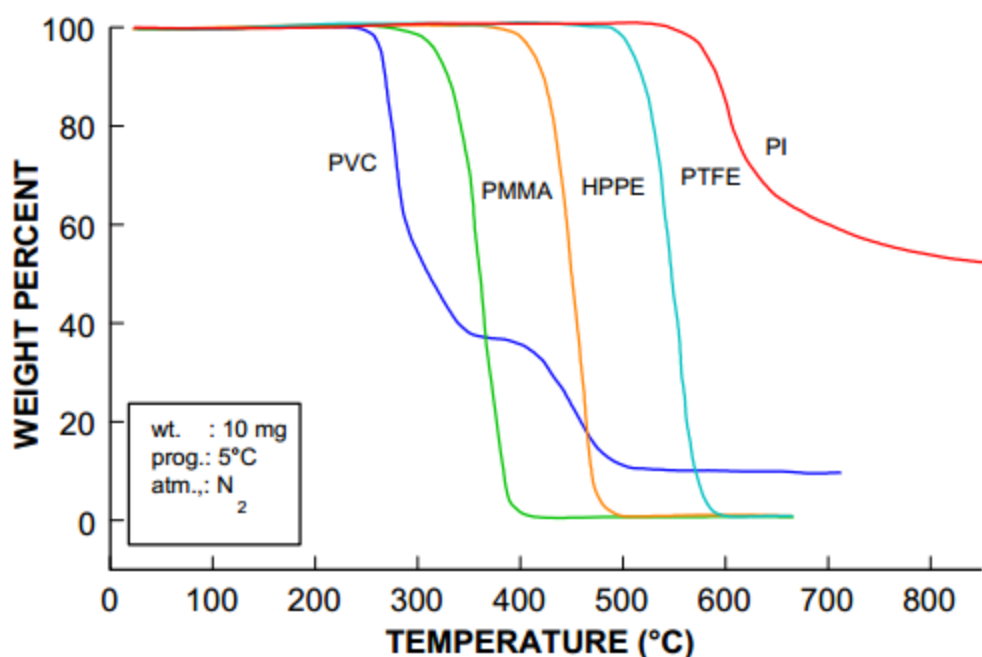
Figure 2.17: Example of TGA spectra of common polymeric materials.

TGA analyses are performed to obtain information about degradation temperature, degradation kinetic and also on evaporation temperature and kinetic of solvents or other compounds. TGA analyses presented in this thesis work were carried out by means of XSTAR TG/DTA 6300 (Seiko Instruments Inc.) with a heat rate of 20°C/min in a temperature range between 0 and 600°C.

2.3.2. FTIR spectroscopy

Infrared spectroscopy is an analytical technique, broadly utilized in chemistry and material science, for investigation on chemical composition and nature of structural bonds of a sample material. Upon absorption of an infrared photon, a molecule passes from the vibrational ground state to an excited vibrational state. Furthermore, every covalent bond and functional group present inside a molecule possesses its own natural vibrational frequency and absorbs external IR radiation only at a determined characteristic frequency. On the basis of these physical principles, it is possible to perform a spectroscopic analysis of a molecule irradiating it by means of photons with wavelength in IR range (800 nm to 1mm). As a result, we obtain a IR spectrum: typically, on the axis of abscissae frequency scale, expressed as wavenumbers (number of wave for centimeter), is listed while on the axis of ordinates percentage of transmitted or absorbed waves is represented. If a material is completely transparent to IR radiation, a horizontal line parallel to X-axis will be visualized. But, if any absorption phenomenon is present, the spectrum will be composed by peaks of different height, each one corresponding to a specific vibrational transition. For this reason, every molecule possess a peculiar IR spectrum related to peculiar functional groups composing the molecule and so IR spectroscopy can be efficiently utilized to qualitatively investigate chemical composition of sample[94]. Considering a linear molecule formed by N atoms, 3N-5 vibrational modes are possible, depending on orientation along the 3 Cartesian axes (x,y,z); for a nonlinear molecule those modes become 3N-6. Specifically, the total number of degrees of freedom for a non-linear molecule is 3N-6 because 3 translational modes and 3 rotational modes are blocked. While, for a linear molecule, the total will be 3N-5 because just 3 translational and 2 rotational modes are fixed. Molecular vibrations can be divided in two different classes: stretching vibrations, which consist in a change in length of the bond and deformation vibrations (bending), which consist in a modification of bond angles. Moreover, stretching could be symmetric if the two atoms move at the same time or asymmetric if movement of the atoms is out of phase. Bending could be symmetric or asymmetric and can

take place on the same plane of bond angle or out of the plane. So, four bending modes can be defined: *scissoring, rocking, twisting* and *wagging*. (Figure 2.18)
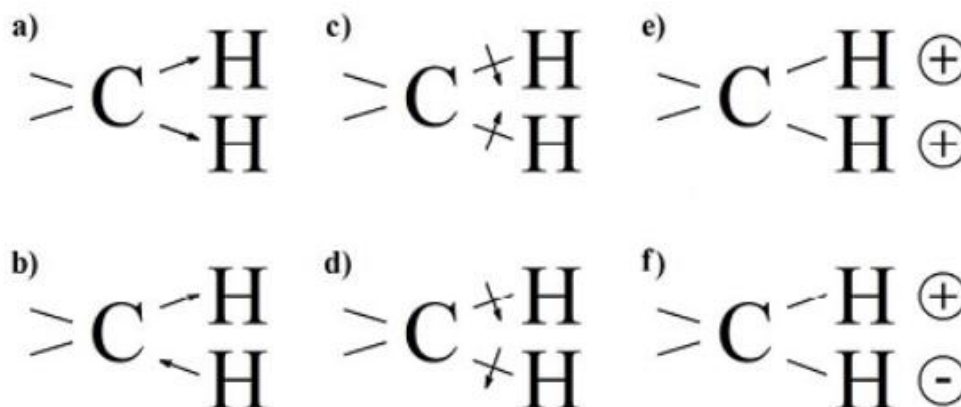
Figure 2.18: Schematic representation of molecular vibrational modes. (A) Symmetrical stretching (B) Asymmetrical stretching (C) Scissoring (D) Rocking (E) Wagging (F) Twisting.

Considering these vibrational modes, IR spectrum can be divided in 3 main zones:

1. Functional groups zone, which frequencies are between 4000 and 1300 cm-1. Peaks present in this zone are due both to stretching and bending of common organic functional groups (i.e. N-H, O-H, C-H, C=C, C=O, N=O, etc.), which have a molar mass lower than 20 g mol-1. In details, bonds with hydrogen involved can be found at very high frequencies due to very low mass of H atoms.

2. *Fingerprint* region is located between 1300 and 650 cm-1. In this region, group frequencies associated to movement of the entire molecular body show up. Peaks in this region are very peculiar for every single molecule and so spectra can be considered exactly as "fingerprint". On the other hand, spectra in this region are very difficult to interpret because these vibrations couple very strongly to each other and particular bands can hardly be attributed to a single molecular group. Typically, if two spectra show the same behavior in this region, than they are assigned to the same substance.

3. Far IR zone is located between 650 and 200 cm-1 and here there are bands due to stretching of heavy atoms, body vibration and aromatic C-H out of plane bending vibrations. In particular, peaks in these zones are considered in order to check if any aromatic compound is present inside the molecule.

From a technical point of view, IR analyses have been carried out using a complex device called Fourier Transform Infrared Spectrometer. FTIR spectroscopy is based on the idea of interference of radiations between two beams to yield an interferogram. FTIR instrumentation is based on the model of Michelson interferometer and it is constituted by

an IR source (Nerst glowers or heated wires), an interferometer and a detector (Thermal or photon-sensitive), as schematized in Figure 2.19.
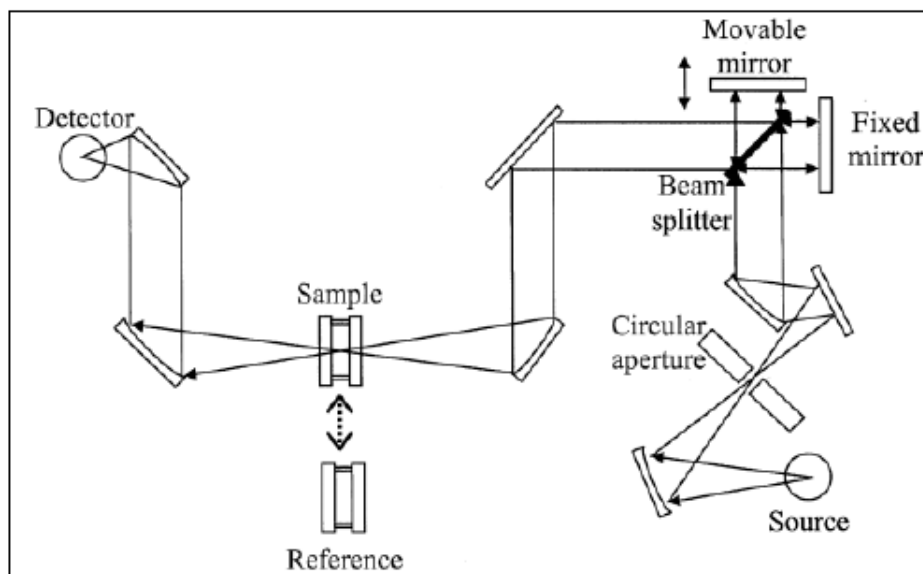
Figure 2.19: Schematic representation of FTIR spectrometer.

In this thesis work, spectra were collected by means of a Nicolet 760-FTIR nexusvspectrometer. In details, samples were put between two KBr pads and analysed in transmission mode. The spectra were collected with 64 scans between 400 and 4000 cm-1 with a resolution of 4 cm-1. Analogous set up has been utilized in collection of background data.

2.3.3. Optical microscopy

The optical microscopy is an analytical technique, which allows visual observation and magnification of sample morphology. Observations are carried out using optical microscope. This type of microscope uses visible light (photons with wavelength between 380 e 760 nm) and an optical lens system to obtain magnified images of very small specimens with a maximum zoom of about 500x. Two different optical configurations can be utilized: *bright field*, in which sample illumination is transmitted and contrast in the sample is caused by absorbance of some of the transmitted light in dense areas of the sample, and *dark field* in which contrast in the sample is caused by diffraction through the specimen. Optical microscopy is widely utilized due to its simplicity and high speed of analysis. On the other hand, this investigation technique has its biggest limit in relatively poor optical resolution (around 200 nm with conventional lenses); anyway, for the purpose of present thesis work, optical microscopy represents a valid and useful resource.

In the present thesis work, visual analyses were carried out using an Olympus BX-60 optical microscope, represented in Figure 2.20.

Figure 2.20: Olympus BX-60 optical microscope utilized to carry out visual analyses on samples.

Microscopy was used in this to determine the average diameter of the microcapsules from data sets of at least 250 measurements by means an image analysis program. In the same way, the particle size-weight distribution was obtained by sieving the synthesized product using different mesh sizes.

2.3.4. Scanning Electron Microscopy (SEM)

To obtain more accurate characterization of the sample scanning electron microscopy (SEM), EVO 50_ Extended Pressure (ZEISS) was employed (Figure 2.21).

SEM consists of an electron column that creates a beam of electrons; a sample chamber, where the electron beam interacts with the sample; detectors, that monitor a variety of signals resulting from the beam-sample interaction; and a viewing system that constructs an image from the signal. An electron gun at the top of the column generates the electron beam. In the gun, an electrostatic field directs electrons, emitted from a very small region on the surface of an electrode, through a small spot called the crossover. The gun then accelerates the electrons down the column toward the sample with energies typically ranging from a few hundred to tens of thousands of electron volts. The electrons emerge from the gun as a

divergent beam. A series of magnetic lenses and apertures in the column reconverges and focuses the beam into a demagnified image of the crossover. Near the bottom of the column a set of scan coils deflects the beam in a scanning pattern over the sample surface. The final lens focuses the beam into the smallest possible spot on the sample surface. The beam exits from the column into the sample chamber. The chamber incorporates a stage for manipulating the sample, a door for inserting and removing the sample and access ports for mounting various signal detectors and other accessories. As the beam electrons penetrate the sample, they give up energy, which is emitted from the sample in a variety of ways. There are two major ways of emission: Secondary Electrons (SE) are sample atom electrons that have been ejected by interactions with the primary electrons of the beam. They generally have very low energy (by convention less than fifty electron volts). Because of their low energy they can escape only from a very shallow region at the sample surface. As a result they offer the best imaging resolution. Contrast in a secondary electron image comes primarily from sample topography. More of the volume of interaction is close to the sample surface, and therefore more secondary electrons can escape, for a point at the top of a peak than for a point at the bottom of a valley. Peaks are bright. Valleys are dark. This makes the interpretation of secondary images very intuitive. They look just like the corresponding visual image would look. Backscattered Electrons (BSE) are primarily beam electrons that have been scattered back out of the sample by elastic collisions with the nuclei of sample atoms. They have high energy, ranging (by convention) from fifty electron volts up to the accelerating voltage of the beam. Their higher energy results in a larger specific volume of interaction and degrades the resolution of backscattered electron images. Contrast in backscattered images comes primarily from point to point differences in the average atomic number of the sample. High atomic number nuclei backscatter more electrons and create bright areas in the image. Backscattered images are not as easy to interpret, but properly interpreted, can provide important information about sample composition. Each emission mode is potentially a signal from which to create an image.

The SEM's primary limitations, as a general imaging and analytical technique, were the restrictions it imposed on samples by requiring a high vacuum sample environment. The samples had to be clean, dry and electrically conductive. Nonconductive specimen had to be coated with a conductive film to avoid specimen charging. The ESEM was developed in the mid-eighties. Its primary advantages lie in permitting the microscopist to vary the sample

environment through a range of pressures, temperatures and gas compositions. The Environmental SEM retains all of the performance advantages of a conventional SEM, but removes the high vacuum constraint on the sample environment. Wet, oily, dirty, non-conductive samples may be examined in their natural state without modification or preparation. The ESEM offers high resolution secondary electron imaging in a gaseous environment of practically any composition, at pressures as high as 50 Torr, and temperatures as high as 1500 °C.

Figure 2.21: ZEISS EVO® 50 EP instrument used for SEM images acquisition.

2.3.5. UV-VIS analysis

UV-VIS spectroscopy is an absorption spectroscopic technique in the ultraviolet-visible spectral region (190-780 nm) commonly used in analytical chemistry. UV-Visible light absorption causes an electronic transition from an energetic ground state to an excited state. So, in a UV-Vis spectroscopy, samples are irradiated with UV-Vis photons in order to determine when samples absorb light and with which intensity. The output of a UV-Vis spectrophotometer is a plot of the absorbance or transmittance as a function of the incident wavelength. Specifically, peaks in the spectra represents electronic transitions between different energy levels. A UV-VIS spectrometer consist of a light source, a monochromator, a chopper to generate two beams as well as to recombine them, a sample and a reference

compartment and a detector[95]. In Figure 2.22, a block diagram of a typical double beam spectrometer is reported.
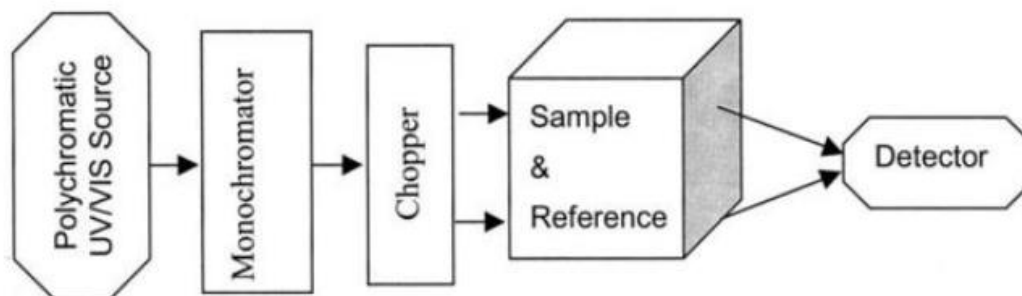
Figure 2.22: Schematic representation of a UV-VIS spectrometer.

Typical light sources used to obtain UV-VIS wavelength are incandescent tungsten lamps, halogen lamps, deuterium lamps and xenon arc lamps. Deuterium lamps are used only in ultraviolet region between 180 nm to 350 nm, while tungsten filament and halogen lamps are used in visible field between 400 nm and 900 nm. However if light source covering the entire UV-Vis range is required, xenon arc lamps can be used whose emission is from 175 nm to 1000 nm. Monochromators are a fundamental part of UV-VIS spectrometer because they allow isolating a defined wavelength from all the other wavelengths. Typical monochromators are composed by a system of concave lenses and by an optical prism. By exploiting the dependence of the index of refraction on wavelength, separation of defined wavelengths can be achieved. Modifying the disposition of optical lenses and slits, it become possible to select which wavelengths are allowed to pass. During the analyses, samples and reference are put in particular rectangular compartments known as Cuvettes. Cuvettes must be transparent at wavelengths used in spectroscopic analyses. For this reason, in visible spectroscopy (380-750 nm), glass or plastic cuvettes are used, while, for UV analyses (175-350 nm), fused quartz cuvettes are required. Most common detectors are photosensible devices based on photoelettric effect; typically a photomultiplier tube, a photodiode, a photodiode array or a charge-coupled device (CCD) are used in UV-VIS spectrometers. In this work, UV-Visible spectroscopy analysis were performed by means of a Jasco V-570 UV-VIS-Near spectrophotometer in a range between 300 and 700 nm with a scan speed of 100 nm/min and a bandwidth of 5 nm.

2.3.6. Rheological analyses

A rheometer is an instrument exploited to measure in which way a liquid or viscous material flows in response to an applied stress. By means of a rheometer, two typologies of measurements can be carried out: steady flow measurements and oscillating measurements. Oscillating measurements allows for the study of viscoelastic behavior of sample on different temporal scales and can be also used to understand degree of crosslinking during a polymerization process[96]. In our tests, we used a cone plate rotational type rheometer (Figure 2.23). The liquid is placed on horizontal plate and a shallow cone placed into it. The angle between the surface of the cone and the plate is of the order of 1 degree, i.e. it is a very shallow cone. Typically the plate is rotated and the force on the cone measured. A diagram with shear rate and shear stress is obtained and so viscosity and other rheological properties can be calculated.
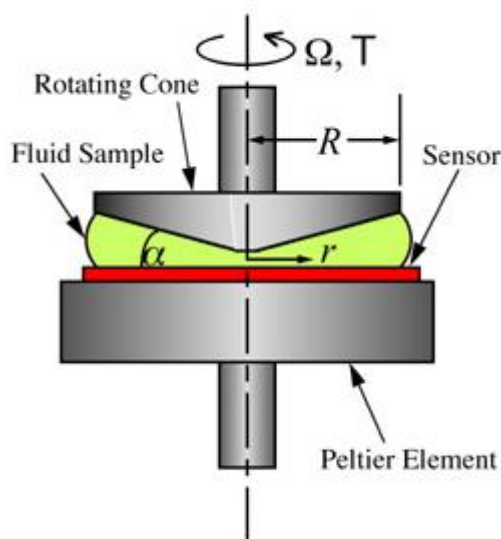
Figure 2.23: Scheme of a core plate rotational rheometer.

To perform rheological analyses, a Rheometrics DSR200 (Dynamic stress rheometer) with cone plate geometry (Figure 2.24) was utilized. It is characterized by a cone diameter of 25 cm and a gap of 0.051mm and sample temperature was 25°C.The flow curves were obtained by measuring the shear rate at applied stress between $1-10^3$Pa.

Figure 2.24: Rheometrics DSR200 instrument utilized to carry out rheological analyses.

3. RESULTS AND DISCUSSION

3.1. DAMAGE SENSING

Self-sensing capability of changing color in polymeric coatings could be used to detect microcracks and damages which may result in the component failure, thus allowing to extend the lifetime of a material through appropriate assessment, modification, and improvement of the damaged part. Several nondestructive structural health monitoring techniques are currently available, but normally they cannot be applied in situ, since they require removal of the component from the system to carry out the analysis. Therefore, it appears very interesting to develop sensitive detection methods that can be easily applied directly on the assembled system and that can be readily accessible also by nonspecialized personnel.

This work aims at developing a general versatile approach that allows one to convert a conventional polymeric coating into a UV-light sensitive, mechanoresponsive smart coating by simply introducing within the formulation our newly prepared UV-screening microcapsules.

To test the applicability of this new approach, these new UV-screening microcapsules were embedded into a polymer to form a new mechanoresponsive system. The UV-light-induced visual response of the coating could be activated by imparting a mechanical damage capable of breaking the microcapsules, thus releasing the UV-responsive dye. Upon release of the dye from the protective UV-screening shell and its diffusion through the polymer matrix, simple UV-A light irradiation allows identification of the mechanical damage by visualizing a clear color change in the damaged area. This method makes it easy to detect damaged zones without the use of color developers or expensive catalysts.

In damage sensing applications, it is important for the microcapsules to be thermally stable and robust enough to enable their survival in a variety of environmental and processing conditions. In addition, it is important to prevent capsule core from leaching into the surrounding matrix before a damage event, which could cause an incorrect information. But it is also critical that the liquid within the microcapsules is efficiently delivered into the crack planes after damage in order to provide a visual observation of the material condition. So, resulting microcapsules were characterized to satisfy all these purposes. This chapter describes synthesis and characterizations carried out on UV-absorbing microcapsules and their application in damage-sensing coatings. The microcapsule synthesis procedure used in

this work is based on the interfacial polymerization method, which is schematically illustrated in Figure 3.1.
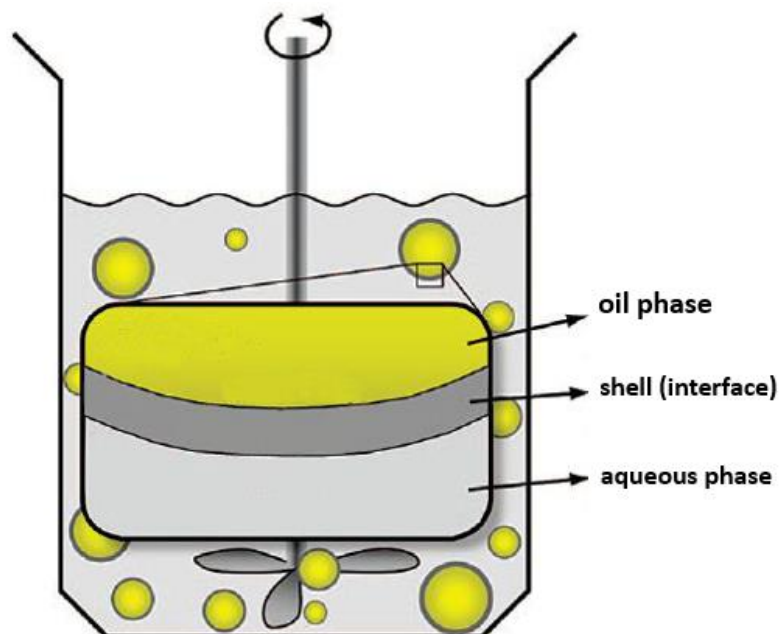
Figure 3.1: Schematic diagram of capsule shell wall formation under mechanical agitation.

In this techniques, two immiscible liquids are agitated so as to generate a stable emulsion. The reactants are dissolved in the two liquids and their reaction occurring at the interphase leads to the shell formation. Our emulsion is an oil in water emulsion

Oil will be encapsulated and its ability to diffuse in the polymeric matrix is fundamental for the final application. For damage visualization two different kinds of dyes have been used: a photocromic dye (SP-dye) which change color under UV radiation and fluorescent chemical compounds that can re-emit light upon UV light excitation (fluorescent-dye). Different parameters have to be taken into account when selecting the appropriate dye (solubility, concentration in oil, final screening effect of MC). Different microcapsules shells have also been tested, using two benzophenone-based amines in order to obtain the polyurea membrane. Benzophenone derivatives are widely known for their ability to absorb the UV light. The selected molecules, ACBP and DABP, differ in the quantity of amine substituent present in the molecule: the ACBP is monosubstituted whilst the DABP has two amine functional groups. The different typologies of microcapsules synthetized and the corresponding adopted nomenclature are summarized in Table 3.1.

Sample	S1	S2	S3
Core	Sunflower oil	Sunflower oil	Sunflower oil
Dye	SP-dye	SP-dye	Fluorescent
Shell	ACBP	DABP	DABP

Table 3.1: Chemicals used for microencapsulation

3.2. SYNTHESIS OF MICROCAPSULES FOR DAMAGE SENSING

3.2.1. UV-Absorbed Microcapsules Filled with SP-Dye

The oil-in-water (O/W) emulsion is prepared by, firstly dispersing a surfactant agent, the arabic gum, in water. The polyisocianate prepolymer (TDI) and a sunflower oil solution containing the UV-sensitive dye were stirred vigorously in water. By adding a benzophenone-based amine to O/W emulsion, the reaction between polyisocianate and amine can occur, leading to formation of the polymeric microcapsule shell based on polyurea linkage.

1',3'-dihydro-1',3',3'-trimethyl-6-nitrospiro[2H-1-benzopyran-2,2'-(2H)-indole] has been used as photocromic dye (SP-dye) in these microcapsules. In order it to dissolve rapidly into sunflower oil, the SP-dye was pre-dissolved in few ml of chloroform. Two different final concentration of SP-dye in sunflower oil were used. (0.7% - 1.4%) Conversely, for dye concentrations of 1 wt% and lower, an efficient UV-screening effect was observed.

Exciting a spiropyran species in the near-ultraviolet (UV) to the first electronic singlet excited state leads to a ring-opening, involving cleavage of the C-O bond that connects the chromene and indoline parts, and results in the formation of merocyanine (MC) species. This produces a clear color change from yellow-earth to red. (Figure 3.1)
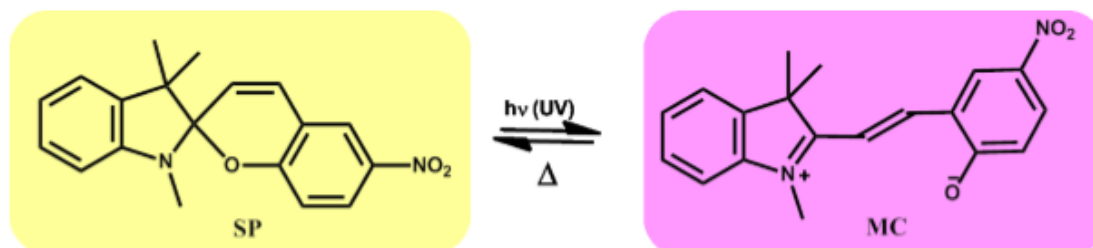
Figure 3.2: Conversion photochemical reaction of spiropyran (SP) into merocyanine (MC)

Therefore, we tested two different encapsulation recipes to maximize the capsules screening property and results obtained have been compared. The amount of chemicals used in different recipes, previously labelled (in Table 3.1) S1 and S2 are shown in Table 3.2.

	Oily phase		Reacting monomers			
Sample	Sunflower oil (mL)	SP-dye (g)	TDI (g)	ACBP (g)	DABP (g)	NH$_2$\NCO
S1	40	0.35	9	3.53	-	1:1
S2	40	0.35	9	-	1.5	2:1

Table 3.2: Quantities of chemicals used in the recipes used to prepare microcapsules

3.2.2. UV-Absorbing Microcapsules Filled With Fluorescent Dyes

According to the same procedure described in the previous section, here the UV-screening polyurea shell was obtained by the reaction of 4-4'Amminobenzophenone (DABP) and the polyisocyanate prepolymer (TDI). They form a polymer which has a good screening property under UV radiation, in a more extended wavelengths range than that of the pulyurea obtained by reaction of TDI and ACBP.

Here polyurea microcapsules were synthesized by interfacial polymerization using several fluorescent dyes dispersed in the oily phase. After a preliminary study on fluorescent behavior of a wide range of fluorophores, only some of them have been adopted for microencapsulation reaction. The list of microcapules obtained is shown in Table 3.3.

Sample	CORE CARRIER	DYE	Conc. Dye\core (g/L)
S3-L	Sunflower oil	LUMOGEN F Violet	0,1
S3-C	Sunflower oil	Coumarine120	0,1
S3-MPy	Sunflower oil	1-MethylPyrene	0,1
S3-EPy	Sunflower oil	1-EthenylPyrene	0,1

Table 3.3: Experimental Condition for Syntesis of Microcapsules containing Fluorescent Dye

3.2.2.1.   UV-VIS absorption spectra

UV-vis spectra were collected at room temperature in the wavelength range 300-500 nm, using the UV-vis spectrophotomer (Thermo Scientific) described in the previous chapter. A liquid cell of 1 cm path length with quarz window was used.

In order to study the change in colour of the photochromic dye ant the key role played by ACBP and DABP as a UV-absorbing species, UV-vis spectra of SP-dye, TDI prepolymer, ACBP and DABP were measured. It is evident from the spectra (Figure 3.3a) that TDI prepolymer has no absorption in the wavelength range analysed, while absorption peak centred at 383 nm and 335 nm are detected for ACBP and DABP respectively. The UV-vis spectrum of the dye (Figure 3.3b) confirms that SP-dye has almost no absorption in the visible regiopn before UV light exposure and a peak in the visible region (ca. 550nm) after UV light exposure.
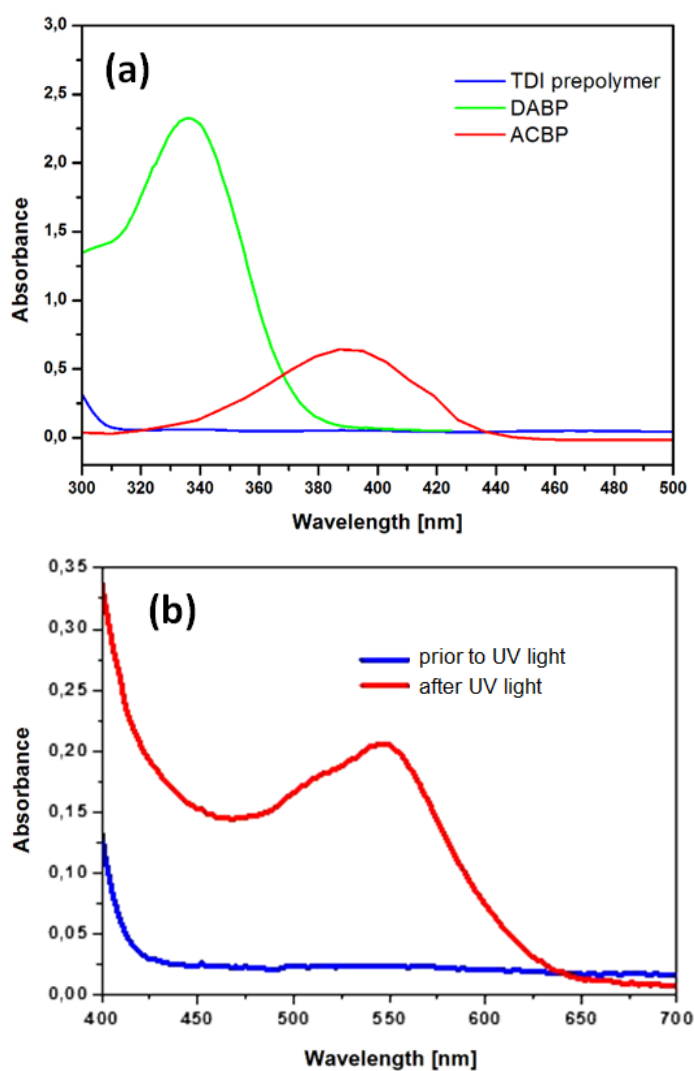
Figure 3.3: (a) UV−vis absorption spectra of ACBP, DABP and TDI-based polyisocyanate prepolymer; (b) UV−vis spectrum of dye employed in this work prior to and after UV-light exposure.

A first series of spectra were collected by dissolving the dyes in dicholomethane. The dichloromethane was used for its ability to dissolve efficiently all the compounds and for its very low cutoff wavelength (245 nm) below which it absorbs too strongly for sample measurements to be performed. For comparison UV-vis spectra of dyes in oil were also performed. Solvents all exhibit a cut-off wavelength in the UV range. Dyes in oil spectra were taken in the range 300-500 nm because of the oil high cutoff wavelength (300nm).

The concentration normally affects the band intensity only. At high concentrations, however, molecular interactions may cause changes in the shape and position of the absorbance band. These changes in turn affect the linearity of the concentration versus absorbance relationship and may lead to inaccurate qualitative results. For this reason all spectra were collected at concentrations lower than the ones used in the microencapsulation processes.

As luminescent species the following organic dyes were used: Lumogen F Violet, 7-Amino-4Methylcumarin (C120), 7-Metoxycumarin (7MC), Europium complex (FN403), 1-Ethenylpyre (EPy), 1-MethylPyrene (MPy). An overview of all dyes used for UV-VIS analysis is given in Table 3.4.
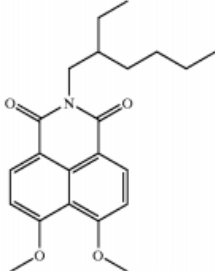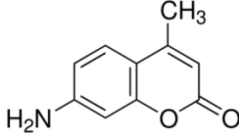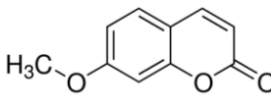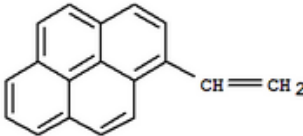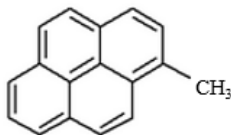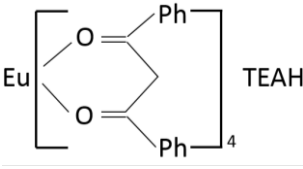
Dyes		
Simbol	**Name**	**Molecular structures**
Lumogen	4,5-dimethoxy-N-(2-ethylhexyl) naphthalimide	
C120	7-Amino-4-Methylcumarin	
7MC	7-Methoxycoumarin	
EPy	1-Ethenylpyrene	
MPy	1-Methylpyrene	
FN408	Eu Complex	

Table 3.4: List of dyes used in this study.

To have a general idea on the peaks positions of all dyes the UV–vis spectra of dyes solutions in DCM and the positions of absorption maxima experimentally detected are collected in Table 3.5.
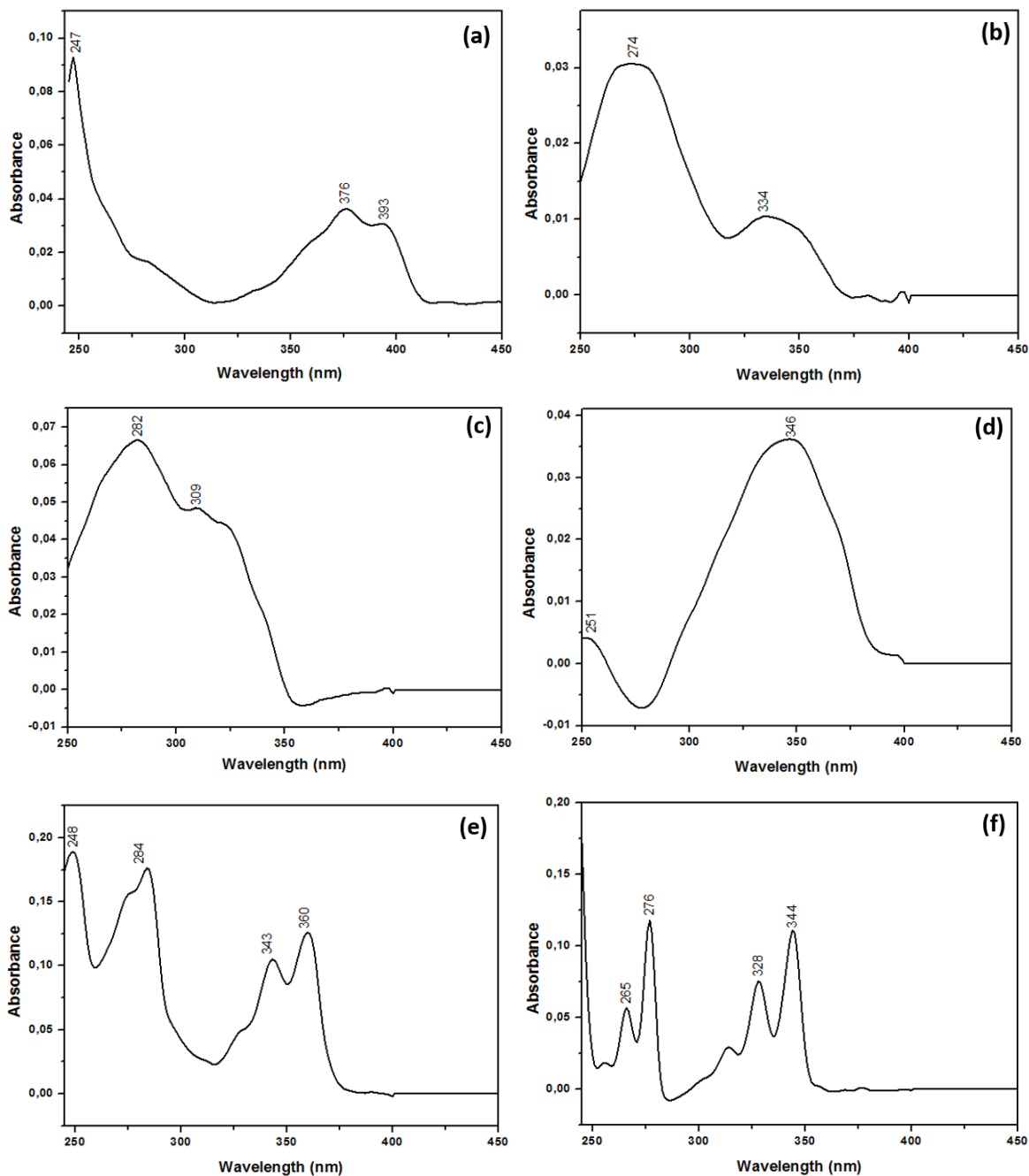
Figure 3.4: Comparison of UV-VIS spectra of all dyes in DCM at cocentration of 0.1mg/L. (a) Lumogen F Violet; (b) 7-Amino-4Methylcumarin (C120); (c) 7-Metoxycumarin; (d) Eu complex (FN408); (e) 1-Ethenylpyre; (f) 1-MethylPyrene.

Compound	$\lambda_{abs,max}$ (nm)
Lumogen	247 – 376 - 393
C120	270
7MC	283
FN403	348
EPy	249 – 284 – 343 - 360
MPy	266 - 277 - 328 - 344

Table 3.5: Packs position of fluorescent dyes in DCM at concentration of 0.1 g/L

All dyes dissolved in oil, which is the carrier used in the microencapsulation process, were also analyzed at different concentrations. For all compounds the same procedure has been adopted: a certain amount of fluorophore was dissolved in the adequate quantity of sunflower oil to create a stock solution, typically the highest concentration. Then, a small volume of oil, analytically weighted, was added to gradually reduce the concentration.

In all cases, the intensities of absorption band decreases with decreasing concentration of the solutions whilst the absorbance peak position remains unaltered for all dyes, except for C120. As can be clearly seen from the UV-VIS spectra (Figure 3.5b) C120 exhibits considerable quenching by sunflower oil solvent, there is also a blue shift in going from less (0.008 g/L) to more (0.04 g/L) concentrate solution. These factors indicate that this organic compound does not completely dissolve in oil. The absorption spectra of Lumogen F Violet (Figure 3.5a) at concentrations between 0.01 and 1 g/L has two maxima in the UV region at approximately 374 and 390. Similarly EtenylPyrene (Figure 3.5c) in the concentration range: 0.02-0.06 g/L, have two peaks at 343 and360 nm. MethylPyrene (Figure 3.5d) only shows a single peak in the UV region at 345 nm, with concentration ranging within the 0.01-0.05 g/L range. FN403 and 7MC spectra are not reported because they are completely insoluble in oil. All these relevant spectral data are summarized in Table 3.6 together with an image of the corresponding solutions under UV light.
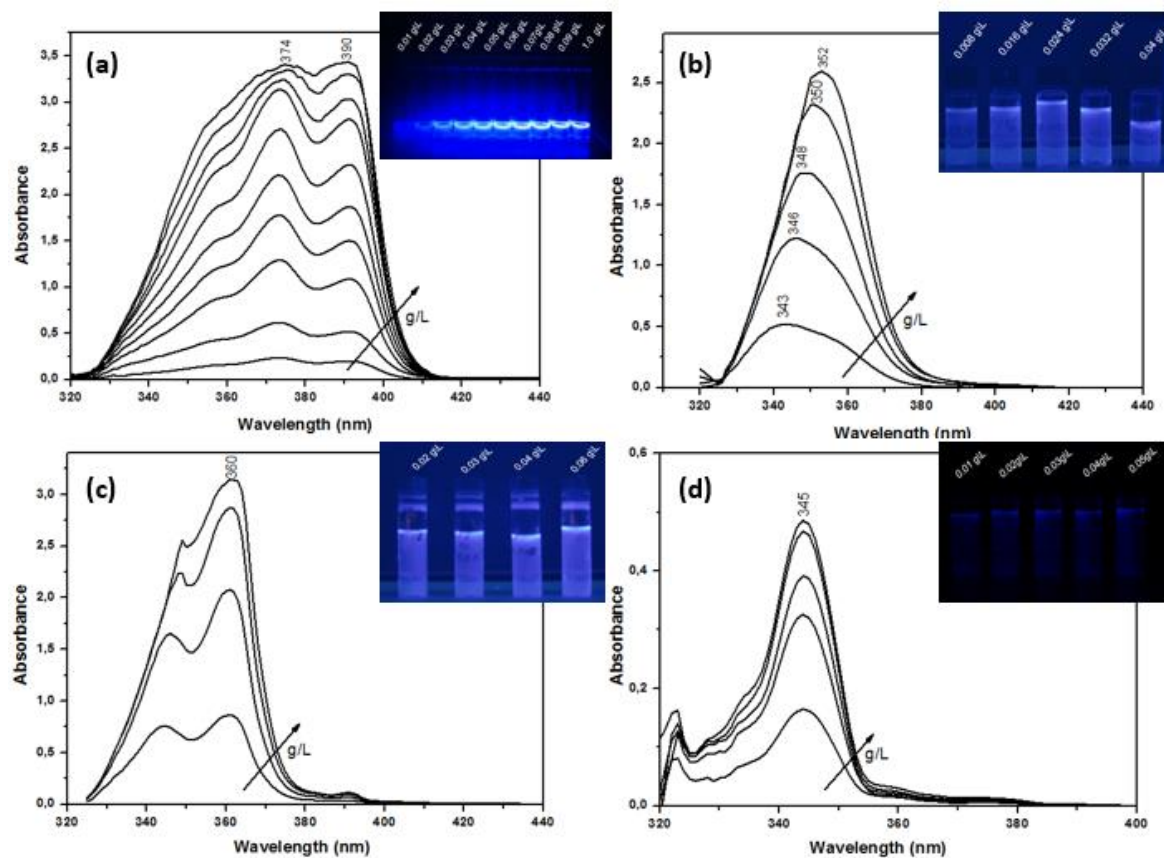
Figure 3.5: Comparison of UV-VIS spectra of dyes in sunflower oil at different compositions. (a) Lumogen in Oil 0.1-1g/L; (b) 7-Amino-4Methylcumarin (C120) in oil 0.008-0-04 g/L; (c)) 1-Ethenylpyre in Oil 0.02-0.0.06g/L; (d) 1-MethylPyrene in Oil 0.01-0.05 g/L.

Compound	$\lambda_{abs,max}$ (nm)
Lumogen	374,390
C120	343-362
EPy	344,360
MPy	345

Table 3.6: Peaks position of fluorescent dyes in OIL.

To investigate the UV-screening property of the microcapsules shell, Ultraviolet-Visible absorption measurement was performed on a thin film of polyurea, obtained by reaction of DABP and TDI prepolymer in the same stoichiometric quantities used in the microencapsulation processes. The polyurea spectrum was compared with those obtain from dyes dissolved in oil (Figure 3.6).
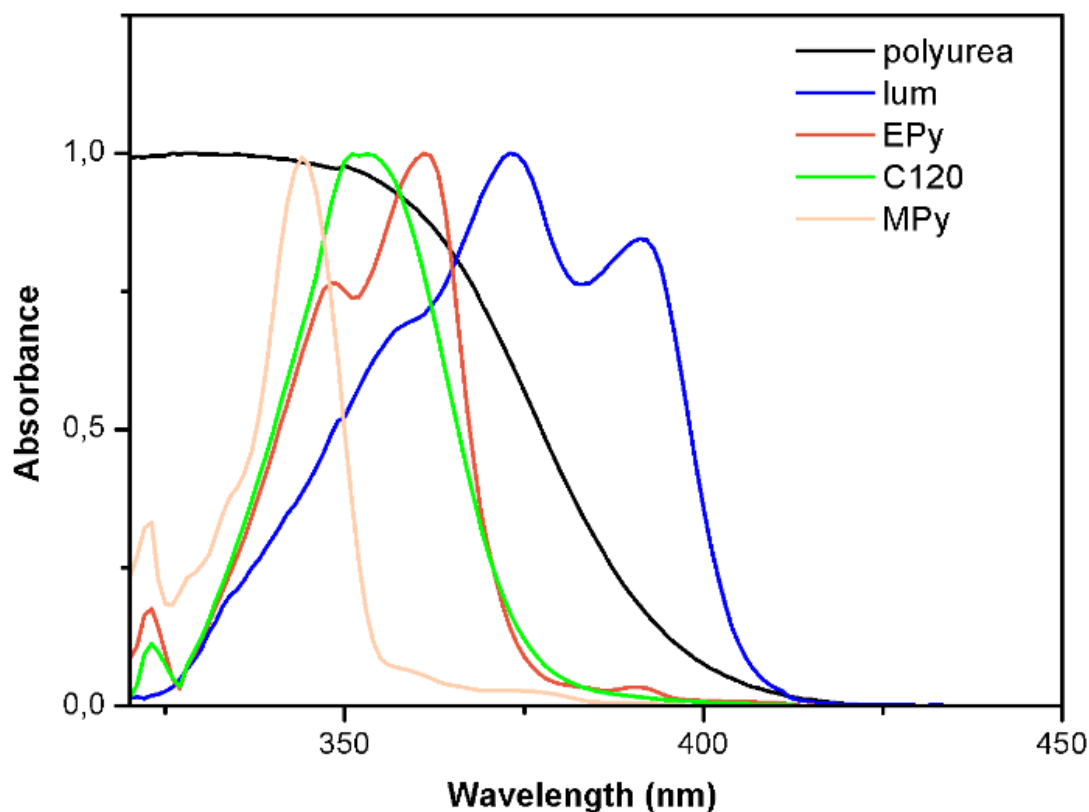
Figure 3.6: Normalized plots of Polyurea film and dyes dissolved in oil

The graph, in which the maximum absorbance of all spectra is normalized to the unit value, clearly shows that the dyes peaks fall within the polyurea range of absorbance. In fact, the polyurea sample absorbed the radiation up to 420 nm where there is a finite overlap with the Lumogen absorption. In this way the theoretical polyurea screening effect was assessed for all dyes.

Finally all dyes were observed under an UV-hand-held lamp at UV-A (366 nm) wavelength irradiation in order to visualize their fluorescence. The dyes were observed in their powder form and dissolved in sunflower oil (0,1 g/L). From Figure 3.7 it is possible to see that Lumogen, C120 and EPy fluorescence is clearly visible in both cases, MPy has a lower intensity than the Lumogen, C120 and EPy, whilst FN403 and 7MC lose their luminescence when dissolved in oil.

Powders

Dyes in oil 0.1 g\L
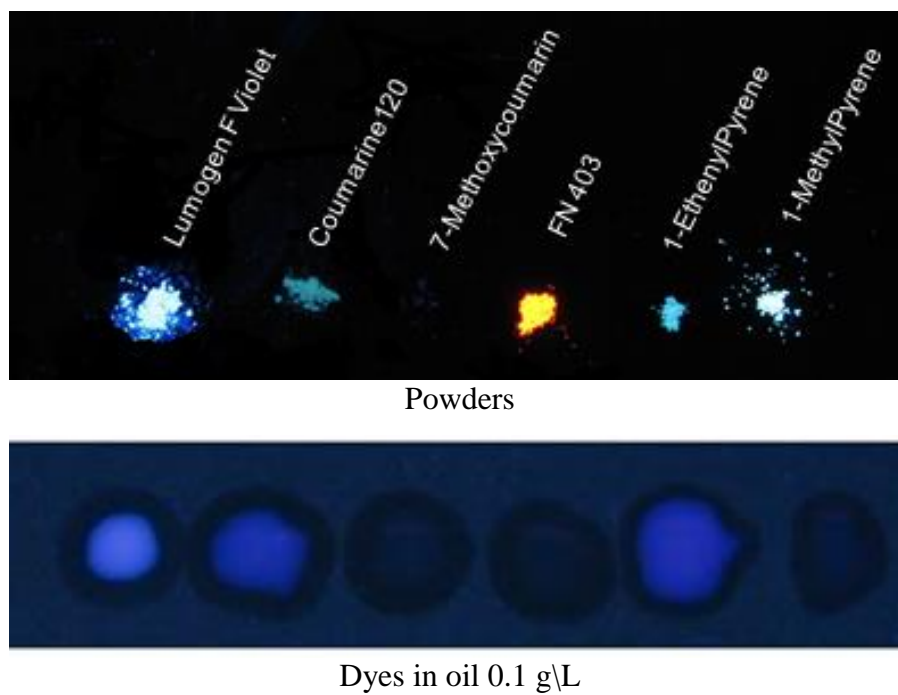
Figure 3.7: luminescent dyes in powder form and dissolved in oil irradiated at 366nm.

3.3. CHARACTERIZATION OF MICROCAPSULES

The presence of different dyes does not influence the chemical and physical characteristics of microcapsules, meaning that the morphological characteristics are the same for all samples (S1,S2,S3).

3.3.1. OM and SEM images (Diameters and thicknesses)

A preliminary investigation of microcapsules synthesized was performed using the Optical Microscope (OM) to observe morphology and size distribution of the prepared microcapsules. During the microcapsules synthesis, precisely 30 and 60 minutes after the reagent addition, and straight after the end of the process (at 90min), a drop of reaction mass was withdrawn with a Pasteur pipette, spread over an examination glass and observed under the microscope with a magnification of 50x. Then, from the OM pictures collected, the mean diameters were evaluated at different reaction time using a image analysis program (see Figure 3.8).

It should be noted that the average diameter of microcapsules slightly increases as the polymerization reaction proceed, but also that just after 30 minutes there is a significant amount of particles with diameter in the order of hundreds of microns.
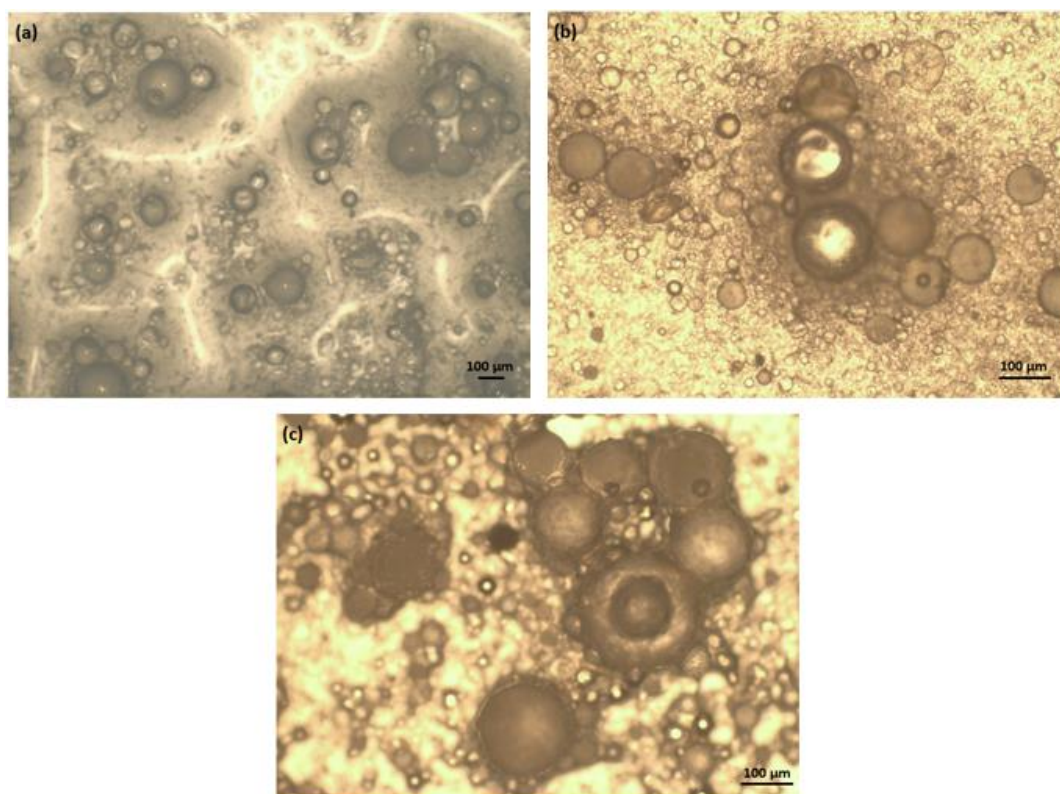
Figure 3.8: MO images of microcapsules during the reaction (a) at 30 and 50x magnification, (b) 60 and (c) 90 minutes 100x at magnification.

The synthesis aim was to produce intact microcapsules with diameters less than 150 µm that can be efficiently separated from nanoparticles and form a free-flowing powder upon drying. Inevitably, due to its intrinsic characteristics, the process produces a size distribution of microcapsules (50-400 µm). Polymer nanoparticles are also formed as by-product due to the benzophenone amine polymerization reaction in the bulk solution as opposed to the surface of oil droplets. For this reason, it was necessary to sieve the dried microcapsules in order to only select the particles which fell within the dimension range of interest (75-150 µm). Such a range was considered ideal for producing microcapsules based coating of 200 µm dry film thickness. For the microcapsules sieving steel sieves with 53, 100 and 200 mesh sizes were used. Figure 3.9 depicts OM images of dry microcapsules after sieving. As shown in the images spherical microcapsules with a quite smooth outer surface were obtained, moreover no broken microcapsules were observed despite the vigorous agitation and the sieving process. This is also confirmed by SEM images of microcapsules in Figure 3.10 (a) and (c). The spherical shape is a positive factor for improving the dispersion into the coating matrix.
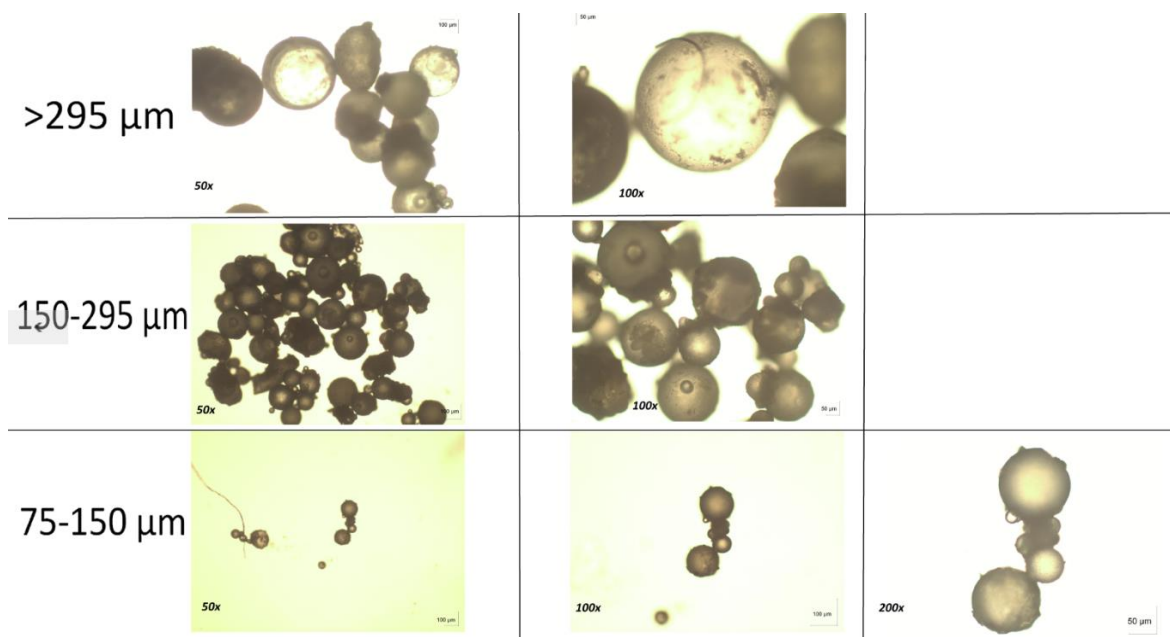
Figure 3.9: OM images of microcapsules filled with sunflower oil after sieving.
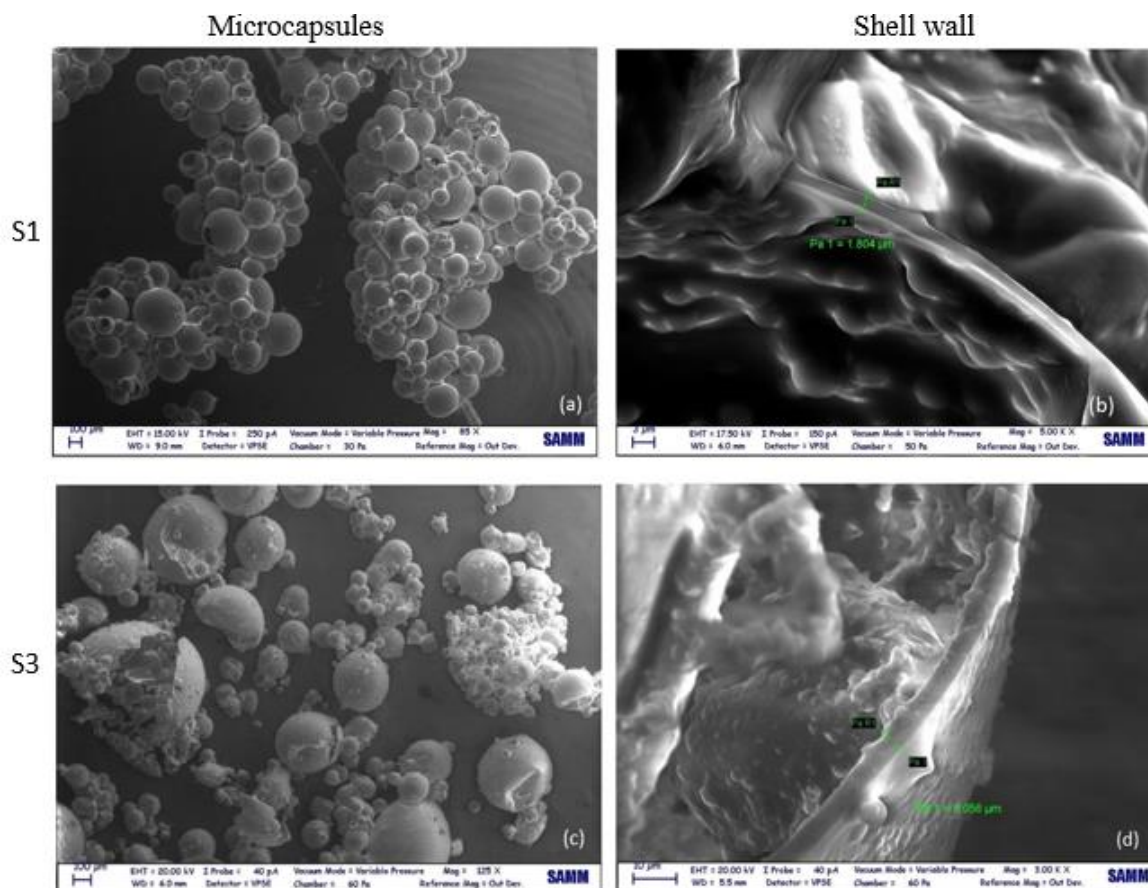
Figure 3.10: SEM images of (a)and (c) crusced microcapsules; (b) and (d) shell wall profile.

For shell thickness measurements microcapsules were crushed with a pestel in a mortar and scanning electron (SEM) microscopy was used. As shown in Figure 3.10 the presence of sunflower oil can be observed on both shell wall sides, likely due to the liquid core release from the microcapsules purposely broken before SEM analysis. This represent a further confirmation of successful encapsulation of core material. A very uniform shell wall thickness is observed; a 2 μm shell thickness (Figure 3.10b) was measured for capsules obtained with ACBP whilst 5 μm were measured (Figure 3.10d) for capsules obtained with DABP. Such shell thicknesses prevent the leakage of core material and the diffusion of surrounding media toward the inside of the microcapsules; moreover the shell provides high enough mechanical strength so as to avoid the microcapsules breakage during processing of after inclusion into the polymeric carrier.

In the development of smart materials through microencapsulation, a proper control of the capsule diameter is a key issue because the diameter greatly influences the performance, and in some conditions, only the capsules with a given range of diameters are suitable. The microcapsules diameter is influenced by a combination of several factors including the

geometry of the mixing device, viscosity of the reaction media, surfactant concentration, agitation rate, temperature and surface tension. However, the average diameter of microcapsules was primarily controlled by the agitation rate after all other parameters were optimized.

Mean diameter and standard deviations were determined from data sets of at least 250 measurements obtained from OM images of dry microcapsules. The size distribution of the S3 microcapsules produced using DABP is shown in Figure 3.11. It can be seen that most of the capsules clusters are below 300 nm; only a few microcapsules are between 300 and 400 µm, and none of them is above 400 nm. This variation in size is caused by the variation in the oil droplets formed during emulsification. The average capsule size was calculated to be 132 µm (see Table 3.2).

Using the same procedure, 148 and 104 µm mean diameter are obtained for S1 and S2 microcapsules respectively and a size distribution similar to that of S3 microcapsules.

Sample	D_{mean} [µm]	SD[µm]	D_{max} [µm]	D_{min} [µm]
S1	148	43	252	73
S2	104	51	293	53
S3	132	85	395	28

Table 3.2: Average Diameter and Size Distribution of Microcapsules Synthesized by Different Experimental Conditions
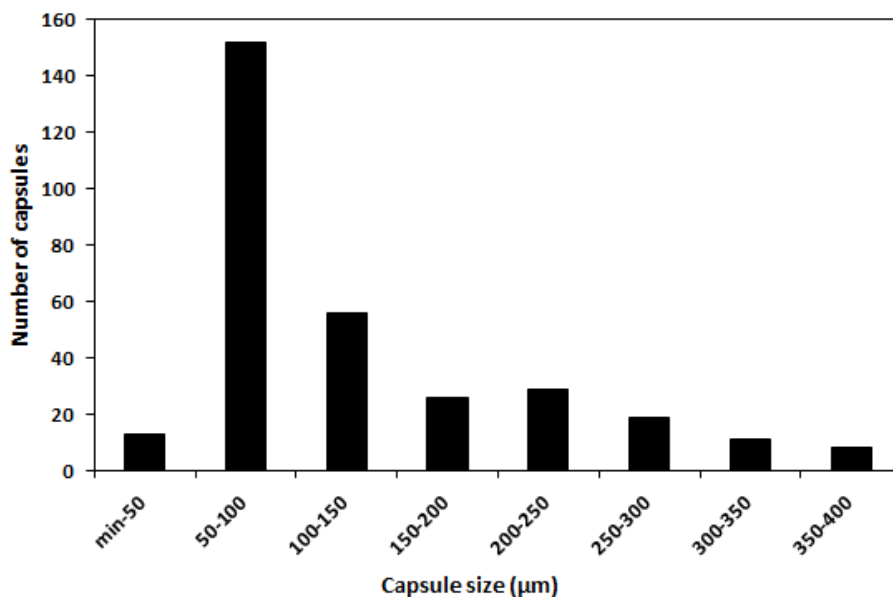
Figure 3.11: Size distribution of microcapsules S3

3.3.2. Determination of core content and encapsulation efficiency

To evaluate the encapsulation process different types of yield can be defined.

- Reaction efficiency: amount of reaction product obtained with respect to the starting amount of reagents.

$$\eta_r = \frac{m_{caps}}{m_{reagent\ start} - m_{by-products}}$$

where m_{caps} is the mass of collected dry microcapsules; $m_{reagent\ start}$ is the total mass of initial substances added (Desmodur L75, 4-4'diaminibenzophenone and sunflower oil); $m_{by-products}$ is the mass of reaction by-products and it is completely omitted in our calculation (only polyaddition reaction are involved).

For this reason, considering the equation before, the reaction efficiency is calculated just as the microcapsules weight over the reagent weight.

- Core Fraction: can be defined as the ratio of the weight of core experimentally calculated by extraction process.

- Encapsulation efficiency: is the capability of encapsulation of the organic phase (sunflower oil) into the capsules. The amount of oil not encapsulated is a loss of product which has to be removed by rinses.

They are determined by extracting method based on selective dissolution principle. First, a certain mass of synthesized microcapsules (m_i) are crashed adequately in mortar using pestle

and transferred in a beaker with an abundant quantity of solvent (petroleum ether). The beaker is immediately cover with parafilm to avoid the solvent evaporation. After standing 24h at room temperature, the mixture is carefully filtered and the beaker is completely rinsed with PE to collect the residual shell material. The final mass of residual material is measured and noted as m_s. The mass of core material (sunflower oil) is measured after the completely solvent evaporation of the liquid filtered and noted as m_c. Then the core content of prepared microcapsules and encapsulation efficiency can be calculated:

Core content of capsules $X_c = \frac{m_c}{m_i}$

Encapsulation efficiency $\eta_{encaps} = \frac{m_c * m_{caps}}{m_{ic}}$

Sample	$\eta_r(\%)$	$\eta_{encaps}(\%)$	$X_c(\%)$
S1	85	85	74
S2/S3	84	74	72

Table 3.3: Reaction efficiencies, encapsulation efficiencies and core fractions of damage sensing microcapsules.

3.3.3. Thermal properties and composition analysis

The thermal properties of microcapsules were investigated using TGA and DSC thermal analysis.

DSC experiment of PUrea film (Figure 3.12 a) were performed for films obtained by the reaction of TDI prepolymer and both ACBP and DABP. The DSC curves show an endothermic peaks around 230°C for the ACBP-polyurea and 250°C for the DABP-polyurea. The DABP DSC curve also shows a glass transition temperature at 57°C. DSC plots of microcapsules (Figure 3.12b) show an endothermic peak which indicates a degradation behaviour starting from about 230°C for all samples. This will be confirmed further by TGA analysis.
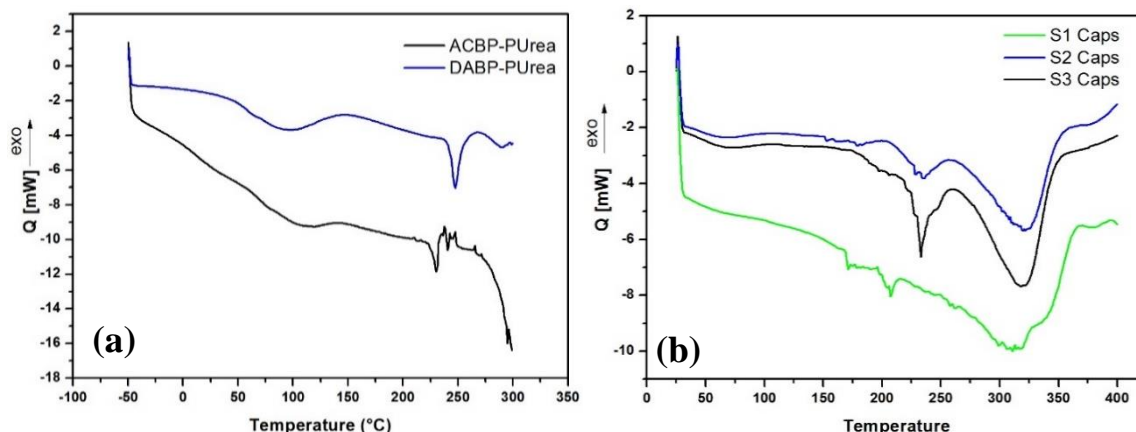
Figure 3.12: DSC thermograms of (a) Polyurea films obtaine by reaction of TDI and ACBP or DABP ; (b) prepared microcapsule with ACBP based shell(S1 Caps) and with DABP based shell (S2,S3 Caps) .

The thermal degradation characteristics of pure sunflower oil, polyurea shell and synthetized microcapsules containing oil and SP-dye (samples S1 and S2) were also analyzed using TGA (Figure 3.13).

TGA of the oil sample in air atmosphere shows its thermal stability at high temperatures, as its curve is completely flat up to 250°C. However a three-stage decomposition is also observed, resulting from decomposition of polyunsaturated (250-300°C), monounsaturated (380-480°C), and saturated (480-600°C) fatty acids. The maximum weight loss, corresponding to an amount of 45%, occurs in the range of 300-380°C; the weight loss is 47% between 380-470°C and 8% at higher temperatures. This data clearly suggests that weight loss during first, second and third step equals to percentage composition of polyunsaturated fatty acid, monounsaturated fatty acid and saturated fatty acid, respectively. The TGA curve and its corresponding derivative mass loss curves of polyurea shell materials obtained with ACBP are shown in Figure 3.13(a, b) . The sample exhibites two degradation stages located at 270 and 337 ˚C. The mass losses for the first and second stages were 25% and 50%, respectively. Polyureas have a microphase-separated segmented block copolymer morphology that consists of hard segment domains dispersed in a soft segment matrix. The hard domains are extensively hydrogen-bonded and serve as reversible physical cross-links, thus providing good mechanical properties, especially toughness. So the first mass loss can be attributed to the degradation of the hard segment because of the relatively low thermal stability of the urea group. The second mass loss is due to soft segment decomposition. Figure 3.13(c,d) shows the TGA curve and its corresponding derivative mass loss of DABP based polyurea. Three degradation steps can be recognized, where the first one, (about 34% mass loss), corresponds to the degradation of solvent used for the film formation. The

96

maximum rate of mass loss occurs at 309 °C. This degradation step, which has been shifted to lower temperature compared to ACBP based polyurea, is due to the degradation of the hard segment and results in the formation of isocyanate and diamine. The second degradation step, which takes place in the temperature range 372–500 °C and has a maximal rate of mass loss at 435 °C, may be attributed to the degradation of the soft segment. In the TGA plots of microcapsules the first weight loss (about 2%) is observed around 150°C for S1 (Figure 3.13c) and S3 (Figure 3.13e) samples, this means that our capsules are stable until this temperature. Evidently, the thermal stability of these microcapsules is reasonably high. This factor is crucial in high temperature functional coating applications. Comparing the curves, it can be seen that the thermal stability of PUrea microcapsules encapsulating sunflower oil has the onset of their degradation at 150 ˚C, 20°C higher than that of pure polyurea samples.

This technique might be also used to calculate the core fraction of the microcapsules, evaluating the weight loss as function of temperature. In the sunflower oil plot the three-stage decomposition observed in the range of temperature 250-600°C overlaps with the degradation of the shell material. For this reason, we cannot used TGA to determine the quantity of oil encapsulated.

Figure 3.13: (a) TGA weight loss curves of synthesized microcapsules (S1), capsule shell wall, and core material. (b) Derivatives of TGA data of the S1 capsule, the capsule shell wall, and the core material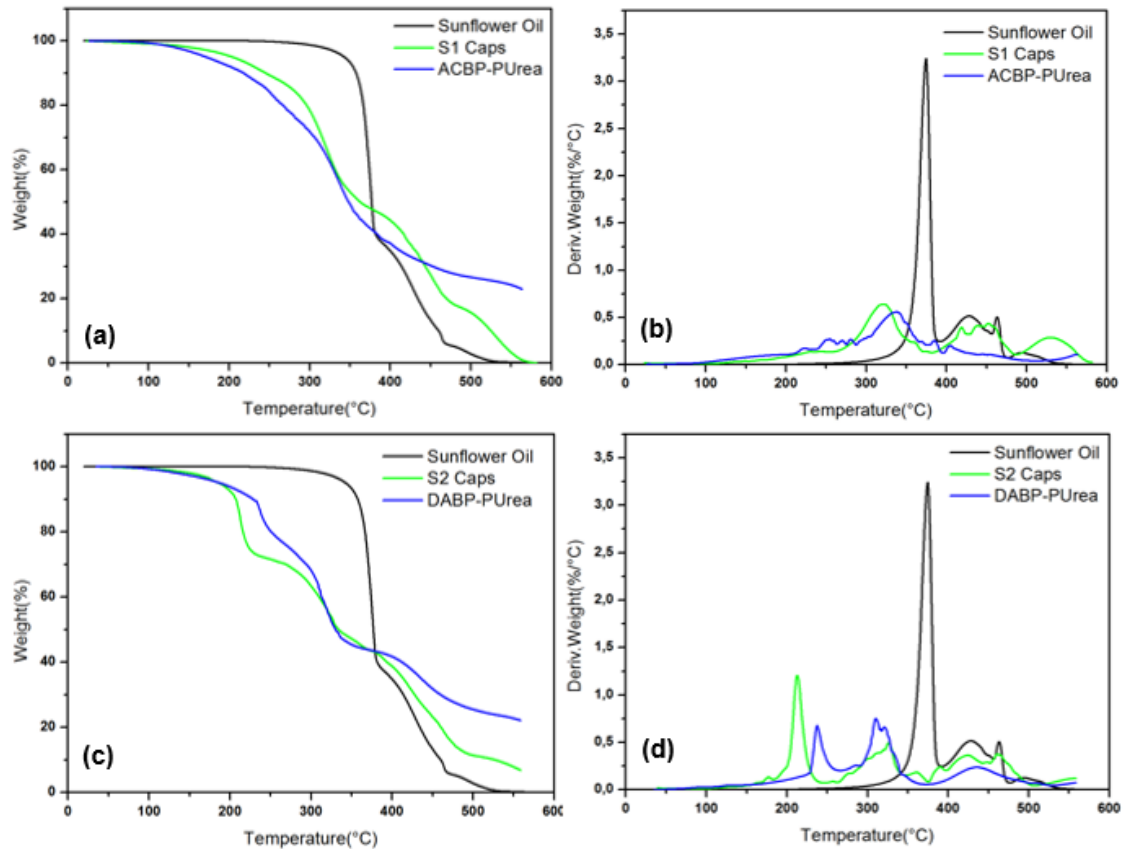. (c) TGA weight loss curves of synthesized microcapsules (S2), capsule shell wall and core material. (d) Derivatives of TGA data of the S2 capsule, the capsule shell wall and the core material. All experiments were conducted at a heating rate of 20 °C min⁻¹ in an air environment

3.3.4. Chemical characterization by spectroscopic technique

The chemical characterization of microcapsules constituents was analyzed by Fourier Transform infrared (FTIR) spectroscopy. FTIR spectra of liquids (core, TDI prepolymer, sunflower oil) were collected on NaCl plates, while FTIR spectra of solids (microcapsules, shell wall) were collected by dispersing the material in KBr powder to form a solid disc. FT-IR spectra of the synthesized microcapsules

IR spectra were collected in order to evaluate the reaction between the TDI prepolymer and the DAB and therefore verify the formation of polyurea capsule shell. FTIR tests of pure sunflower oil and extracted core material were also performed to evaluate the success of encapsulation.

The formation of shell material, namely the reaction of the NH_2 groups of DABF with the NCO group of Desmodur L75, was confirmed by the disappearance of the N=C=O stretching signal (2270 cm^{-1}) in the FTIR spectrum of the as-prepared microcapsules shell (Figure 3.14). FTIR spectrum of PUrea film showed characteristic bands of urea groups at 3318 cm^{-1} (N-H stretching). Peaks corresponding to C=O were observed at 1736 cm^{-1} (non-hydrogen bonded) and 1648 cm^{-1} (hydrogen bonded). Bending vibrations of N-H bond at 1536 cm^{-1} and 1222 cm^{-1}, characteristic of C-N group stretching, are also present in this spectrum. All these peaks can be observed in the shell spectrum, also provide strong evidence for the formation of PUrea polymer as wall of microcapsules[97].

The FTIR of the extracted core material is shown in Figure 3.15, together with that of sunflower oil. The FITIR spectra of oil and core material appear to be nearly overlapping. In particular, the peaks in the aliphatic C-H_2/C-H stretching region ($2700\text{-}3100 \text{ cm}^{-1}$), the C=O stretching peak at 1750 cm^{-1}, and the peaks at 1460 cm^{-1} and 1165 cm^{-1} present in the FITIR spectrum of sunflower oil are also found in the FITIR spectrum of the extracted core. On the other hand, the signal peaks of TDI prepolymer at 1739 cm^{-1} was not present in the core material. This clearly indicates that sunflower oil, and not TDI, was successfully encapsulated.
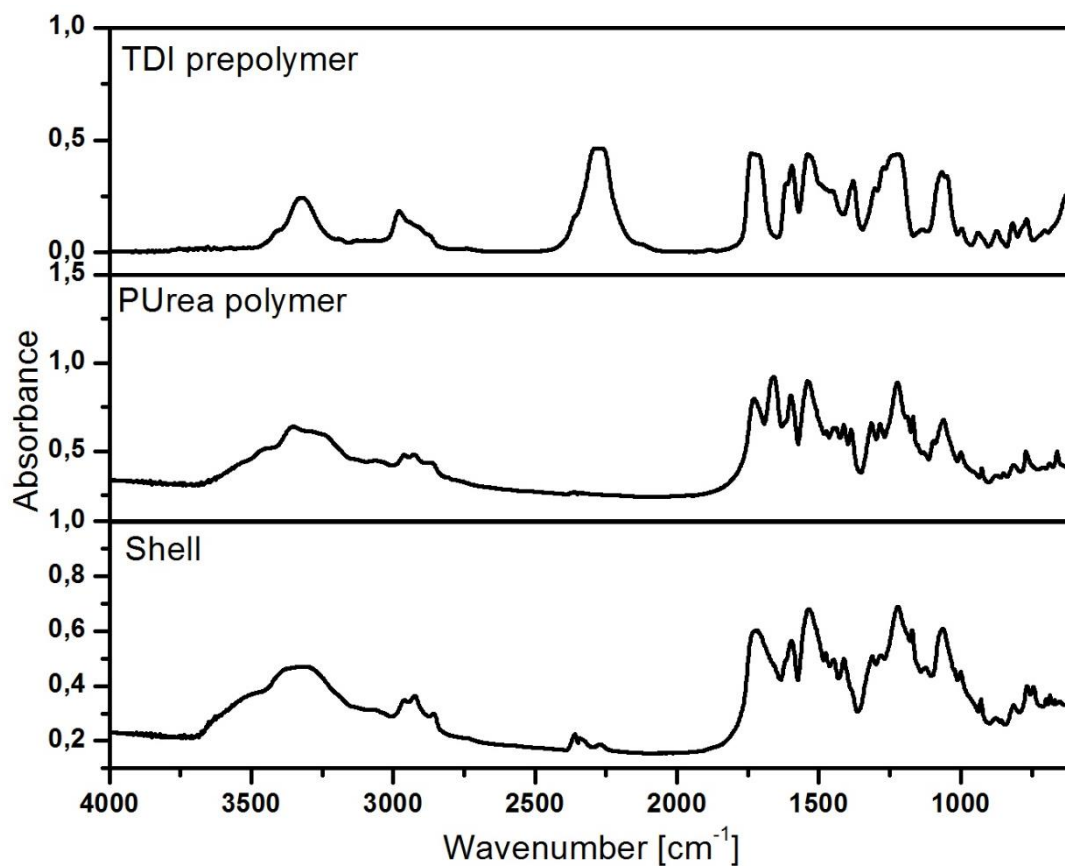
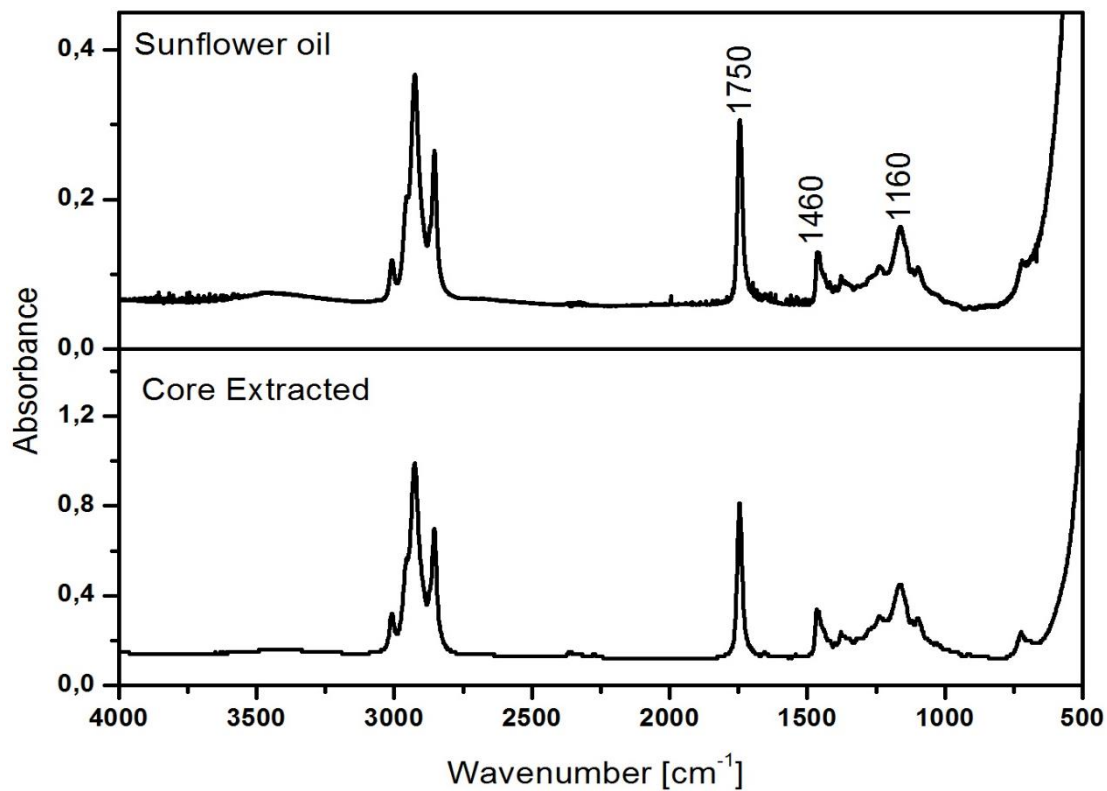**Figure 3.14: FTIR spectra of core materials, polyurea, microcapsule.**

Figure 3.15: FTIR spectra of sunflower oil and core material of microcapsule.

100

3.3.5. Leaching test

In practical applications, microcapsules have to be robust enough to survive under severe processing or application conditions, such as the presence of solvent, moisture, exothermal reaction or acid/alkaline environments. However, the preparation of robust microcapsules with superior resistant properties, especially regarding solvent attacks, is still greatly challenging. In the coating field, indeed, the chemical resistance to solvent of microcapsules is a key issue. For damage sensing applications the preparation and final use of microcapsules may entail the prolonged interaction of solvent media, which act as diluting agents in practical coating systems; the solvent diffuse into the core domain and may transfer the core materials out of the microcapsules, this significantly affecting the damage visualization properties of the system.

In this section, the chemical resistance of the synthetized polyurea microcapsules is investigated by prolonged immersion in methanol (MeOH) and butyl acetate (BuOAc). These two solvents were selected because they belong to two distinct classes of solvents, namely alcohols and esters. In particular, BuOAC is one of the most commonly used solvents for application in the field of industrial coatings. On the other hand, MeOH was selected because of its different polarity and low molecular weight that favor diffusion through the porous microcapsules shell and subsequent core extraction. Moreover, the absorbance spectrum of these two solvents does not overlay with the optical response of SP-dye.

The capability of microcapsules to retain the encapsulated material and consequently their chemical resistance in solvents was evaluated using UV-vis spectroscopy. S1 and S2 samples have been chosen for this analysis due the different chemical composition of their shell material. The same procedure has been adopted for all analyses: 1,5 mg of microcapsules were immersed in 10 ml of solvent, then the UV-vis spectra of the solvent medium were recorded at fixed time intervals namely 1, 5, 15, 30, 45, 60 minutes.

According to the encapsulation efficiency data calculated in section 3.3.2, the core fraction was assumed to be 70% for both samples. This value gives an indication of the maximum amount of core material that can be released from the microcapsules upon immersion in the solvent. As a result, by knowing the amount of the encapsulated core material, the theoretical maximum concentration of SP in the selected solvent can be evaluated (corresponding to its complete release into the solvent).

1wt% SP-dye solution in sunflower oil (same concentration of SP-dye in oil as that used for the preparation of microcapsules) was prepared and dissolved in the selected solvents so as to obtain a reference solution characterized by a final concentration of dye in solvent equal to the maximum theoretical concentration achievable in case of complete core release from the microcapsules under test.

The UV-VIS spectrum of such solution was collected from 250 to 700nm. Such UV-VIS spectrum is presented in Figure 3.16a. As shown in the plot, two distinct peaks can be observed at 266 nm and 366 nm. In this study, the peak at 266 nm was used for monitoring the core release rate upon solvent extraction, as this peak can be directly related to the absorbance of the spiropyran species. The absorbance intensity of the signal ascribed to the SP-dye was used as reference work intensity. As a result, the release rate was evaluated by plotting the ratio of absorbance of the solvent where the microcapsules have been immersed to the absorbance of the reference solution at increasing immersion times, according to the following formula:

Normalize Absorbance $= \frac{A_t^{266}}{A_{SP}^{266}}$

Where: A_t^{266} is the absorbance of solvent solution containing microcapsules at time t and $\lambda=266$nm and A_{SP}^{266} is the SP-dye absorbance at maximum release concentration and $\lambda=266$nm and.

It can be seen from Figure 3.16 b,c that S1 microcapsules(those with ACBP based polyurea shell and SP-dye in core material) have a low resistance in solvents. Core release of S1 in MeOH reaches a significant amount (around 50%) after 10 minutes of microcapsules immersion in this solvent. Then, at higher times the release gradually increases up to a value of 70% at immersion time of 60 minutes. For S1 in BuOAc a significant amount of core was extracted within the first minute (around 60%), it continues to increase more gradually at higher times until having a release of 100% after 60 minutes. On the other hand S2, therefore those with DABP based polyurea shell and SP-dye in core material, have an almost flat behavior with release values of 10% in MeOH and in BuOAc, indicating a no significant core release in this system. As further investigation, microcapsules were immersed in water and UV-vis analysis of solvent was performed. As expected, no dye signal was revealed in both two sample, means that S1 and S2 microcapsules will perform in the same good way into water based coatings. These results clearly demonstrate the excellent solvent resistance of S2 microcapsules, which therefore allow for their use also in common commercial coating

systems. The use of S1 capsules, instead, is more limited as they can be easily processed in waterborne matrix only. In particular, mixing S1 microcapsules with solvent based resin for longer than 2-3 minutes may cause the core leaching into the matrix resulting in a misleading interpretation in the damage visualization under UV light.
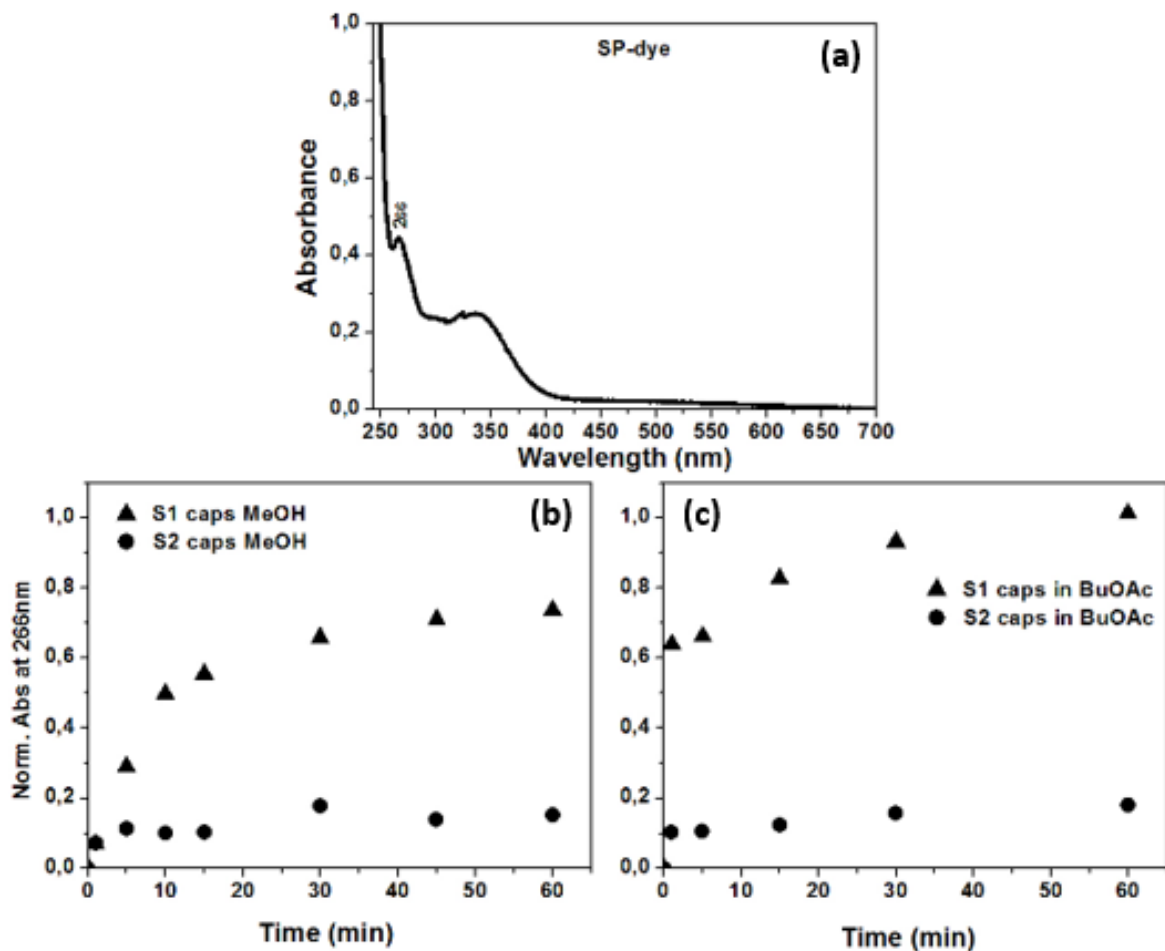

Figure 3.16: (a) UV-vis spectrum SP-dye in solvent; (b) core release profiles of caps in MeOH, (c) core release profile of caps in BuOAc.

3.4. DAMAGE VISUALIZATION

The goal of this work is to synthetize new UV-screening microcapsules containing a UV-sensitive dye and to develop novel active coatings based on the implementation of these microcontainers filled with active agent into the coating matrix. The microcapsules act as damage sensor within the composite material.

In this section the behavior of all typologies of microcapsules described and characterized previously is illustrated. Caps S1, S2 and S3 were observed under UV radiation illumination before and after a mechanical rupture. Furthermore, all UV-screening microcapsules were embedded in a polymeric matrix to demonstrate the possibility to produce a smart coating able to visually respond to a mechanical damage such as a scratch or a hit. In principle, upon application of a mechanical stress such as a scratch on the coating, the UV- screening microcapsules break and the UV-sensitive core material is released and diffuses into the polymer matrix. Upon exposure to UV-A light, a rapid color change in the region where the damage was made is observed, thus serving as a visual marker (see Figure 3.17).
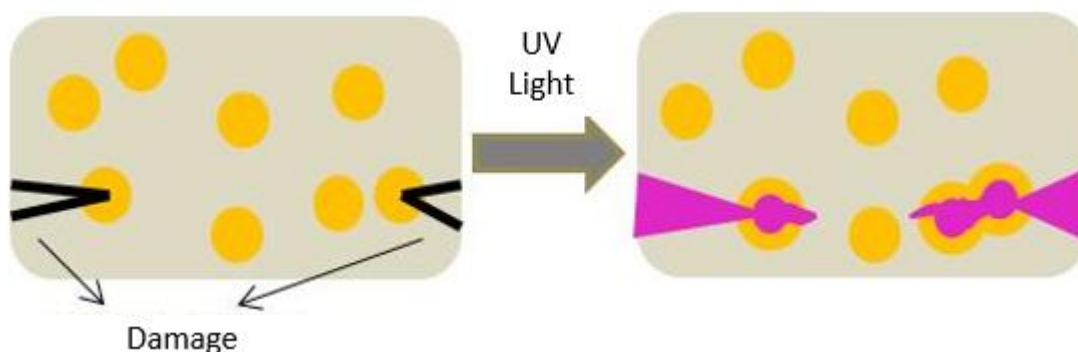
Figure 3.17: Schematic representation of the visual identification of the mechanical damage by exposure to UV-A light.

Composite materials containing microcapsules for damage visualization have been created using three different kinds of polymeric matrixes, as described in more details in the Chapter 2. Briefly, they are: Poly(ethylene glycol)methacrylate (PEGMA); P56: a water-borne polymer chosen for processing in order to minimize capsules degradation and leaching of oily core into the polymer matrix during film deposition and the commercial paint, ACRIPOL: a two-component polyurethane enamel used for its resistance to atmospheric agents, to scratches, and stability to light and very good adhesion to other materials. All these matrixes were chosen because of their inherently low Tg which leads to a soft film. This facilitates the easy introduction of a damage in the film with a razor blade and the concomitant rupture of the capsules.

Microcapsules were added under slow agitation to the resin solution and, after mixing for few minutes, the composition deposited on the substrate. Depending on its formulation, the composite coating were cured under UV light or air-dried at ambient temperature for 24h and after that a small, shallow cut was introduced with a razor blade. Then, they are observed under UV lamp to detect the damage; thought the intense fluorescence emission of dye. Sample nomenclature and microcapsule-containing coatings formulations are illustrated in the following table (Table 3.4).

Sample	Microcapsules	Matrix
SP-dye		
C1	S1	Methacrylate
C2	S2	Methacrylate
C3	S2	P56
Fluorescent dyes		
C4	S3-L	Acripol
C5	S3-L	P56
C6	S3-EPy	P56

Table 3.4: Schematic representation of Microcapsules-containing coatings for damage visualization.

In order to demonstrate the potentialities of this new UV-screening approch, firstly the newly synthisized UV-absorbing shells used to microencapsulate the SP-dye, that undergoes a color change upon exposure to UV-A light (Figure 3.18), was tested The SP-dye microcapsules were deposited onto a glass slide and irradiated with UV-A light ($\lambda = 350\ nm$). As shown in Figure 1.8a and b, no color change was observed after 10s of exposure to UV-A light, indicating that the presence of benzonphenone moiety in the microcapsule shell successfully acts as a UV-absorbing filter. These microcapsules were then broken by compression between two glass slides, thus allowing the core material to be released. Upon irradiation (10s) with UV-A light, the extracted liquid core underwent a clear color change from yellow to red (Figure 1.8c), in accordance with the photochromic response of the UV-sensitive dye. This is true for microcapsules with polyurea shell obtained both with ACBP and DABP.
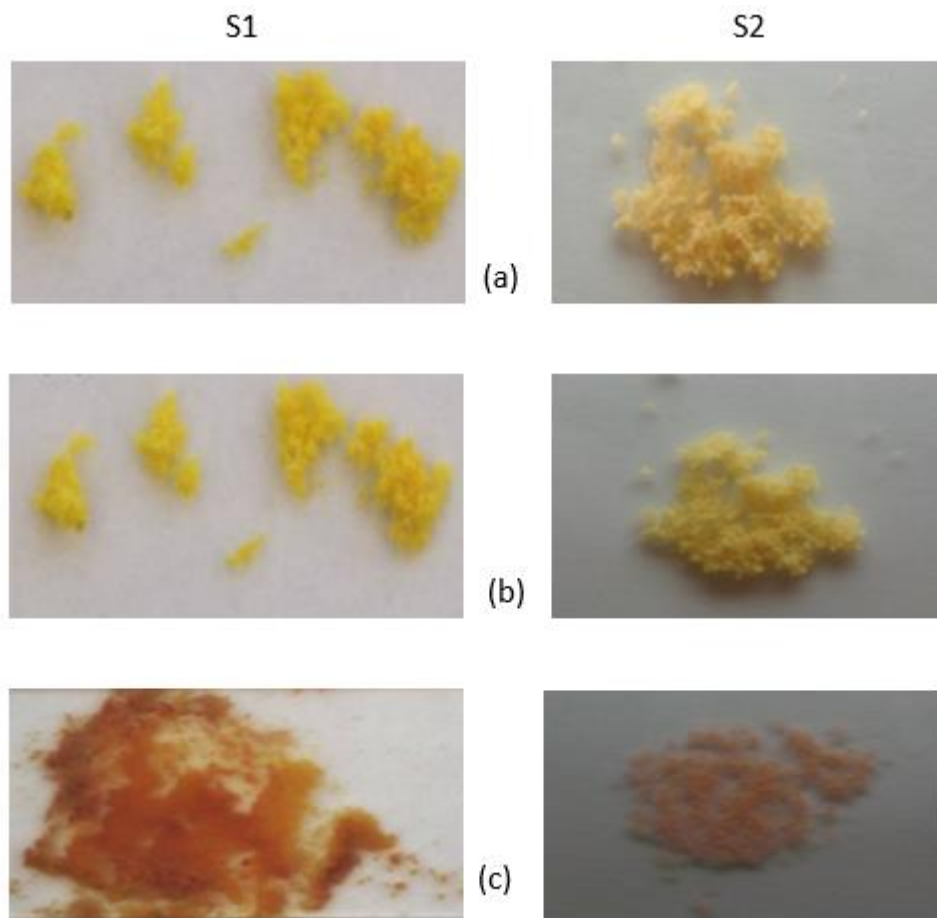
Figure 3.18: Photographs of (a) as-synthesized UV-screening microcapsules with SP-dye, (b) UV-screening microcapsules after exposure (10 s) to UV-A light, (c) UV-screening microcapsules after shell rupture and exposure (10 s) to UV-A light

For S1 and S2 microcapsules the photopolymer PEGMA (see section 2.2.6) was chosen as the polymeric carrier to prepare the smart coating. As shown in Figure 3.19a, no color modifications were observed on the as-prepared PEGMA-based film containing UV-screening microcapsules upon exposure to UV-A light, indicating that, despite being embedded in a solid polymeric matrix, the microcapsule shells are still able to retain their UV- screening properties. In addition, no rupture of the microcapsules was observed after inclusion in the polymeric matrix, thus confirming their good mechanical stability and robustness. In order to demonstrate their potential use as visual markers, the film containing UV-microcapsules was scratched with a lancet so that the microcapsules would break and the core material would be released and would diffuse into the polymeric matrix (Figure 3.19b). Such a phenomenon is possible because of the ability of the carrier material- in this case, sunflower oil- to rapidly diffuse into the mechanically induced crack with a diffusion time of ~10 s. With no UV-light shone on the coating, a uniform yellow-earth color was

observed. After exposure to UV-A light, the immediate appearance of an intense dark-red/purple stain in the scratched region was observed, as a result of the photochromic response of the released UV-sensitive dye (Figure 3.19c). This behavior further demonstrates the viability of our approach as a promising nondestructive in situ technique for easy visualization of mechanical damages.
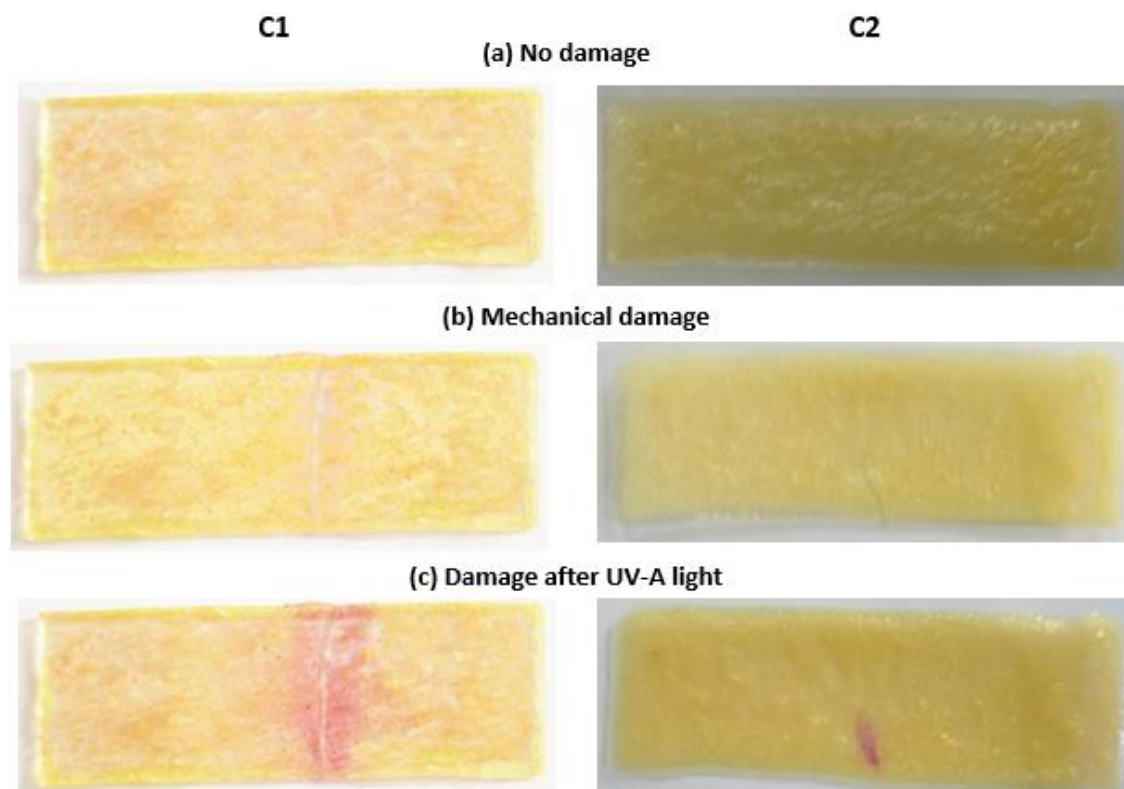
Figure 3.19: Photographs of microcapsule-containing PEGMA-based films: (a) as-prepared, (b) after being scratched, and (c) after exposure to UV-A light (λ = 350 nm, 10 s). Dimensions of PEGMA-based films (b, c, d) are 75 mm × 25 mm × 1 mm

S2 microcapsules were also incorporated into a polyurethane (P56, see section 2.2.6) matrix. A water-borne PU paint was chosen in order to minimize capsules degradation and leaching of hydrophobic core into the polymer matrix during mixing and film deposition. After curing overnight at room temperature, the film was scratched with a razor blade. Within ~10s after the damage application and the UV-A irradiation, the scratched region displayed the typical red color of the SP-dye (Figure 3.20d), similarly to what had been observed when crushing capsules and enlighted under the UV lamp (Figure 3.20). This result demonstates that the S2 microcapsules maintain the same damage detection ability of S1 but they can be used in a wider range of applications thanks to their capability to resist in solvent-based matrix.
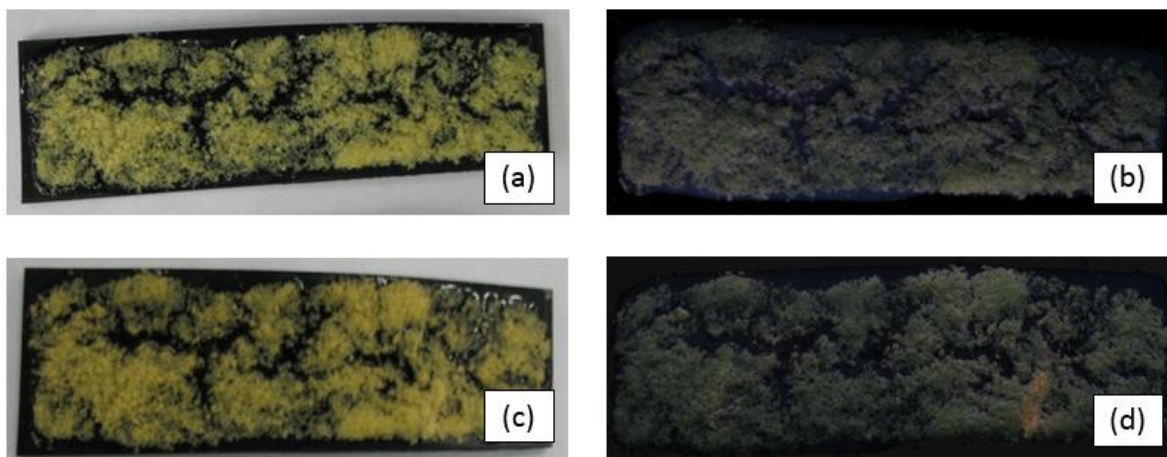
Figure 3.20: Photographs of microcapsule-containing P56-based films: (a) as-prepared , (b) as-prepared under UV-A light, (c) scratched and visible light exposure and (d) after scratched and exposure to UV-A light (λ = 350 nm, 10 s).

Once the SP-dye microcapsules functionality had been assessed, the second step consisted in verifying the applicability of the fluorescent systems. To this end S3 capsules were observed under UV-light irradiation before and after rupture. Figure 3.21 shows comparison images of synthetized microcapsules containing fluorescent dyes taken under the UV light. On the left side there are the uncrushed capsules, while on the right the same capsules were crushed releasing the core material. The presence of fluorescent molecules, dissolved into the sunflower oil, result into an easy detection of the core material released after capsules rupture and UV-light exposure. In S3-MPy the dye have a pale blue color and the difference in the fluorescence intensity between uncrushed and crashed capsules is not enough appreciable thus making this dye unsuitable in damage sensing coating. For this reason these capsules were not used for composite material fabrication. On the other hand, S3-L and S3-EPy capsules show the typical yellow color of polyurea shell when intact and an intense fluorescent color when crushed.

108
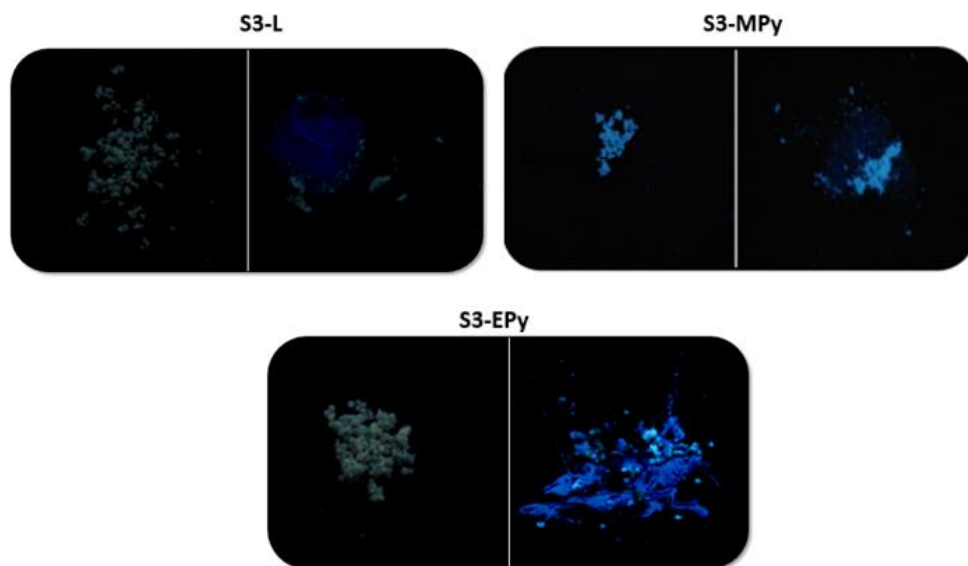
Figure 3.21: photographs of microcapsules before (left) and after (right) mechanical rupture irradiated by UV-A light.

The fluorescent dyes containing microcapsules synthesized were embedded in two types of matrixes: Acripol and P56 film. The coatings were fabricated appling the same procedure previously described for the SP-dye capsules coatings. Table 3.5 summarizes all coatings realized with microcapsules containing Lumogen and EPy as fluorescent dyes.

Sample	Microcapsules	Matrix	λ irradiation (nm)
C3	S3-L	Acripol	366
C4	S3-L	P56	366
C6	S3-EPy	P56	366
C6	S3-EPy	P56	254

Table 3.5: Nomenclature of coatings with microcapsules.

Figure 3.22 shows images of sample C3, obtained when S3-L microcapsules were embedded in a Acripol coating. Images of undamaged coating under visible and UV light is reported on the left, whilst on the right there are the images of mechanical damage coating in the same conditions. The 'X'-shaped region, obtained by a razor blade, simulates the damage area and shows a fluorescence signal at a cut when exposed to UV radiation. In this conditions also the undamaged parts appear fluorescent, this is caused by the solvent based nature of the matrix which causes extraction of oily phase of microcapsules. This represents a limitation

in the application of this kind of coating. When, S3-L microcapsules were embedded in the P56 film (sample C4), practically no fluorescence emission was observed when undamaged sample was exposed to UV-A light (Figure 3.23), due to the water borne nature of this coating. Pictures of the sample under UV radiation present the typical yellow colour of polyurea shell microcapsules for intact coating and a strong fluorescent signal located only in the damage parts. Sample C5, made of S3-EPy capsules in P56 matrix (Figure 3.24), have the same behaviour of C4.

Figure 3.22: Photographs of C3 sample under visible and UV light in undamaged and damage conditions.
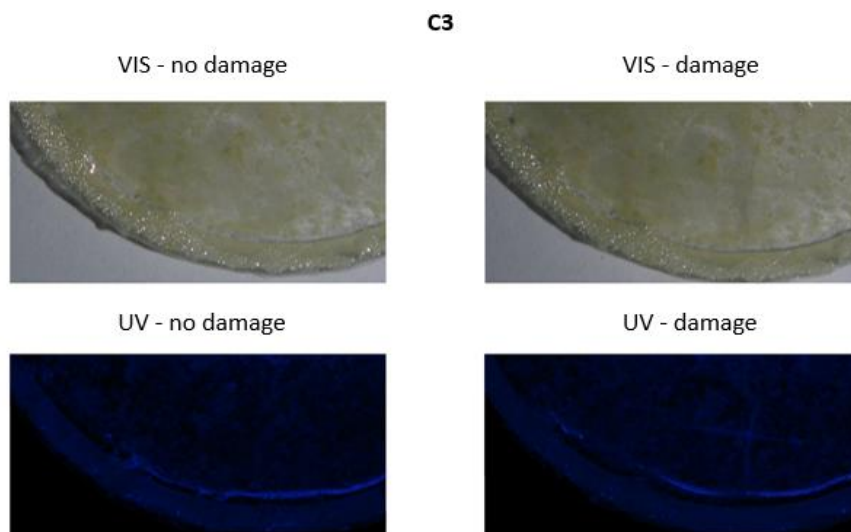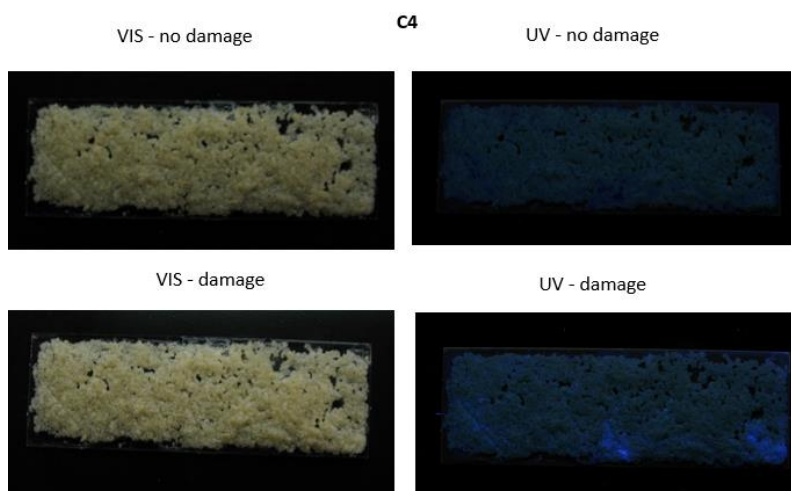

Figure 3.23: Photographs of C4 sample under visible and UV light in undamaged and damage conditions.
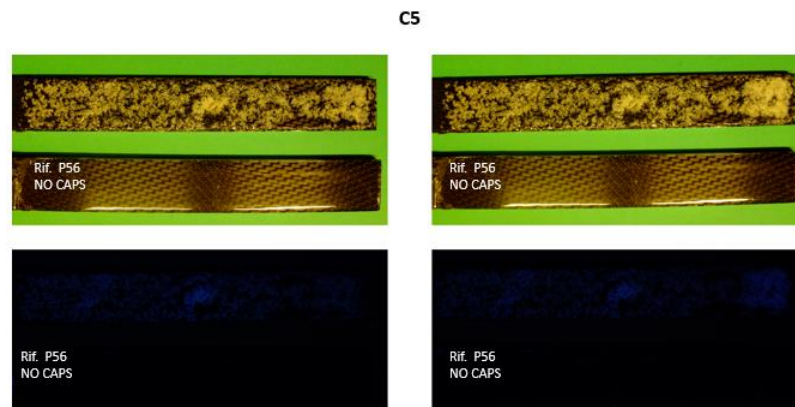
C5

Figure 3.24: Photographs of C5 sample under visible and UV light in undamaged and damage conditions.
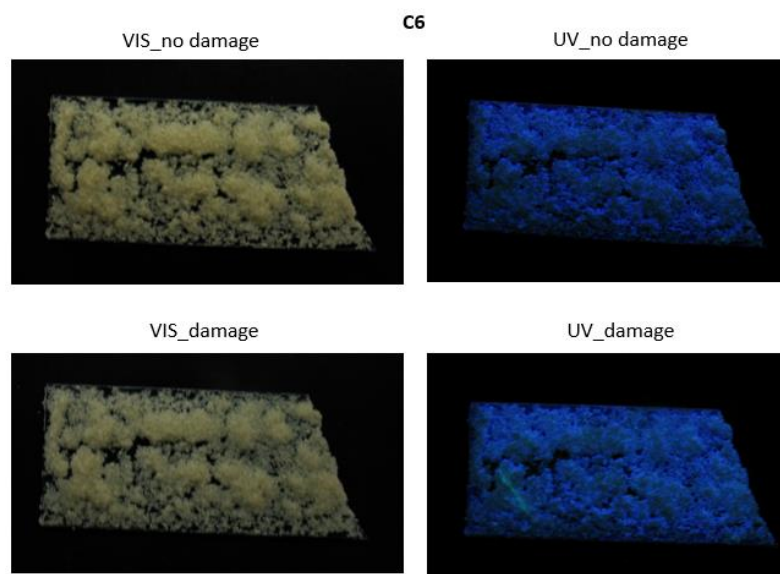
C6

Figure 3.25: Photographs of C6 sample under visible and UV light in undamaged and damage conditions.

3.5. UV INDUCED HEALING

UV-radiation curable coatings represent a class of coatings with no or little volatile organic compounds (VOCs). In addition, compared to thermally cured coatings, the use of UV-radiation curable coatings offers some advantages, such as host drying, broad formulating range, reduced energy consumption, coating of heat sensitive substrate, and low space and capital requirement for curing equipment. This technology is also very attractive from the environmental point of view since no organic solvents are required. The greatest advantage of UV coatings comes from the general properties improvement. Polymers cured by UV light usually exhibit superior mechanical, chemical and heat resistance because of their higher cross-linking density. Among the oligomers used for UV-curable coatings, polyurethane acrylate (PUA) oligomers have gained more and more attention and speedy development due to a wide range of excellent application properties, such as high impact and tensile strength, abrasion resistance and toughness combined with excellent resistance to chemicals and solvents. UV-curable coating resins basically include a prepolymer, one or several reactive diluents, a photoinitiator and other additives in minute amounts (surfactants, stabilizers, etc**.**)[98]. Self-healing coatings have been extensively studied and exploited in the last decade to protect materials, in a better way, from the effects of environmental exposure. During normal use, the coatings undergo stresses that can cause cracking, and this leads consequently to mechanical failure. Self-healing materials should be able to retain functionalities, to restore structural integrity autonomously after an eventual damage caused by a mechanical injury or by corrosion, to extend the lifetime of the material. Different triggering mechanism, that can impose self-healing processes in thermoset polymeric systems, have been proposed. These complex systems can be based on mechanical, thermal, photo, electrical or other external stimuli, capable of initiating a healing process. Presently, judging from the number of publications, self-healing systems utilizing mechanical stimulus, seem to be the most realistic approach to truly autonomous self-healing polymeric coating. The approach is based on incorporation of microcapsules, filled with reactive chemicals, into the polymer matrix.

Having been inspired by the above concepts, an efficient method for the preparation of stable UV-screening microcapsules containing photopolymerizable resins as core materials, for future use in self-repairing coatings, is investigated in this section. UV screening polyurea

obtained by reaction of TDI-based polyisocyanate and DABP was chosen as shell material due to its capacity to screening UV light as well described previously (Chapter 3.1).

Table 3.6 illustrates the chemical representation and the name, with their abbreviation in brackets, of thermosetting resins chosen as possible candidates of encapsulated core materials for UV-healing microcapsules. They are: Trimethylolpropane ethoxylate triacrylate (SR499), dipentaerythritol pentaacrylate (SR399) and 3,4Epoxycyclohexylmethyl3,4epoxycyclohexanecarboxylate (Epoxy). As largely explained previously in the Chapter 2, SR499, SR399, TMPTA428 and TMPTA692 cure according to a radical mechanism while ECC is thermoset made from cationic reaction. Moreover, these molecules need a photo-initiator to start the reaction which are Darocure 1173 for all and Triarylsulfonium hexafluoroantimonate salts for Epoxy resin only.

Sample Name	Core material	
	Name	Chemical Structure
1	Trimethylolpropane ethoxylate triacrylate (SR499) (TMPTA428) (TMPTA692)	
2	Dipentaerythritol pentaacrylate (SR399)	
3	3,4-Epoxycyclohexylmethyl-3,4-epoxycyclohexane carboxylate (EEC)	

Table 3.6: Names and structures of chemicals as possible candidates for UV-healing microcapsules preparations.

A preliminary study based on viscosity measurements and UV DSC analysis helping to understand the mayor characteristics of UV curable resins will be firstly presented. Then, structure and properties of synthetized microcapsules were characterized by all same techniques used for damage sensing capsules. The thermal properties of our microcapsules

will be checked using Thermogravimetric Analysis (TGA) and Differential Scanning Calorimetry (DSC). Infrared Spectroscopy (IR) will provide information about the chemical structure and morphology of capsule will be obtained by Optical Microscope (OM) and Scanning Electron Microscope (SEM).

3.5.1. Viscosity

The physical properties of the liquid healing agent are a key factor for a successful functionality of the final product. In particular its viscosity has to be low enough for being able to flow onto the damage region on one hand;on the other hand its diffusion into the polymer matrix must be limited, otherwise the liquid would not polymerize in cracked area. Another interesting factor to investigate is the healing efficiency of the repairing agent. This will depend upon the kinetics of the repairing process and on the polymerization extent of the healing agent. Furthermore the resulting polymer must have strong adhesion onto the substrate and high mechanical properties in order to prevent further damages. With this set of requirements in mind, the first property to be evaluated was the viscosity of different photocurable monomers.

Rheological analyses were carried out on all photopolymerizable resins and on the sunflower oil. Viscosity η was measured by means of a rheological test conducted at room temperature varying the applied stress in a typical steady shear test. The rheological curves obtained are presented in Figure 3.25and the resulting viscosity values are listed onTable 3.7. On the diagrams, represented in linear scale all materials show a Newtonian behavior; therefore, viscosity is constant and it does not dependent on the shear rate. Sunflower oil ($\eta = 0.06$ Pa*s) was taken as a reference, because it could be successfully encapsulated as described in section 3.1. All investigated monomers exhibits higher viscosity than oil, except for TMPTA428 and SR499 which values are comparable: $\eta = 0.06$ and 0.09 Pa*s respectively. TMPTA612 ($\eta = 0.14$ Pa*s) has a viscosity which is about twice the oil viscosity, whilst the EEC ($\eta = 0.4$ Pa*s) is one order of magnitude higher. Finally, SR399 ($\eta = 8.9$ Pa*s) has a viscosity greater than two orders of magnitude compared to the others. The two resin with the most similar rheological behavior to that of the oil (TMPTA428 and SR499) and the two most viscous ones (EEC and SR399) were chosen for the microencapsulation synthesis. .
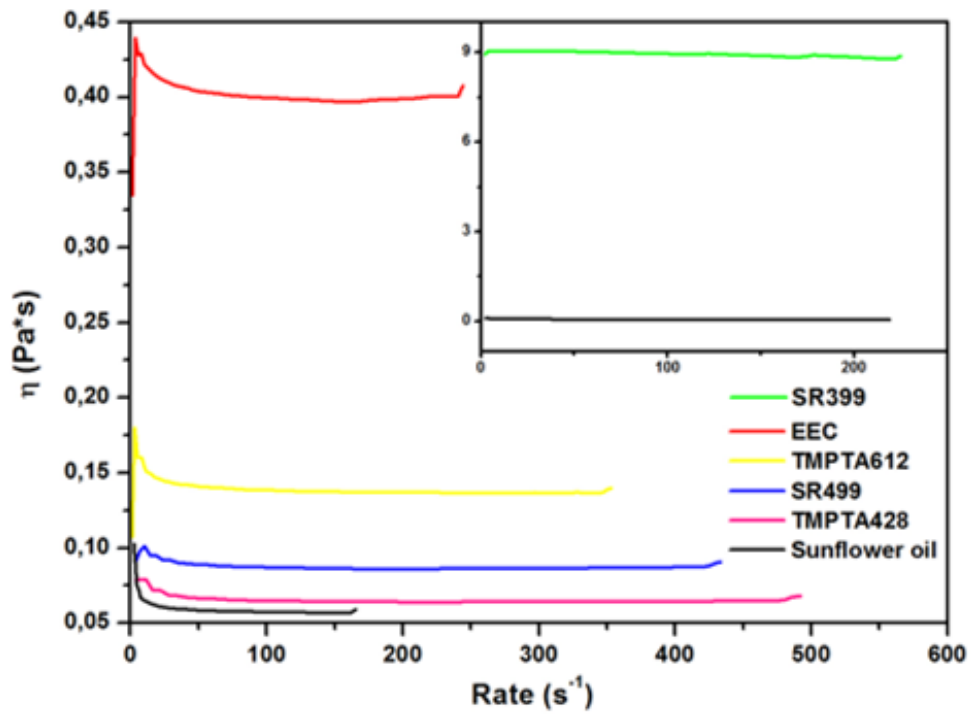
Figure 3.26: Viscosity measurement of all UV curing resins and sunflower oil.

Sample	η (Pa*s)
SR399	8.90
ECC	0.40
TMPTA612	0.14
SR499	0.09
TMPTA428	0.06
Sunflower oil	0.06

Table 3.7 Measured viscosity values of UV curing resins.

3.5.2. Photocalorimetry (Photo-DSC)

Photo-differential scanning calorimetry (p-DSC) has been the first technique able to monitor the kinetics of UV-curing processes. At a given temperature, the photocalorimetry measures the heat flux evolved by the photo-initiated exothermal reaction as a function of time. The main advantage of photocalorimetry resides in a good temperature control. On the other hand, this technique provides only a measure of the global heat flow without any information about specific chemical reaction.

For H1A, H1B, H2 and H3 samples, the corresponding pure resin (with the same amount of photoinitiator as in the microcapsules), the unbroken microcapsules and the core extracted were analyzed with this technique. It was possible to verify whether the polymerization enthalpy of the pure resin and that of extracted core are comparable. Moreover, the scans of unbroken microcapsules are performed in order to access the screening property of shell

The photo-curing behaviour of the samples, i.e. reaction rate and the extent of reaction versus time, is reported in the picture below (Figure 3.27).

The numerical values of enthalpy measured for pure resins are 329 J/g for SR499, 355 J/g for TMPTA, 254 J/g for SR399 and 65 J/g for ECC. The enthalpies of cores extracted show a reduction of one order of magnitude for all samples, except for H3. The values are 77, 48, 35, 71 J/g for H1A, H1B, H2 and H3 core materials respectively. The reason why the polymerization enthalpy of the extracted cores are much lower than that of the corresponding pure resins might be the reduced photoinitiator concentration. During the synthesis, in fact, the photoinitiator might undergo a scission creating free radicals when added in the reaction medium. This fact can cause its loss during the microencapsulation process, resulting in an incomplete curing reaction of the extracted core in the p-DSC analysis. However, this numerical difference does not affect the functionality of the core. Indeed, all extracted samples exhibit a fast polymerization (1 min time peak) after exposure to UV radiation at 366 nm wavelength. This makes all the synthetized microcapsules possible candidates in self-healing coatings applications. A further confirmation of this statement may be inferred by considering p-DSC thermograms of unbroken microcapsules. In particular, no exothermic peaks are observed in the case of pristine microcapsules, suggesting that polyurea shell effectively screen the core from UV radiation thus avoiding the reaction of the core material.
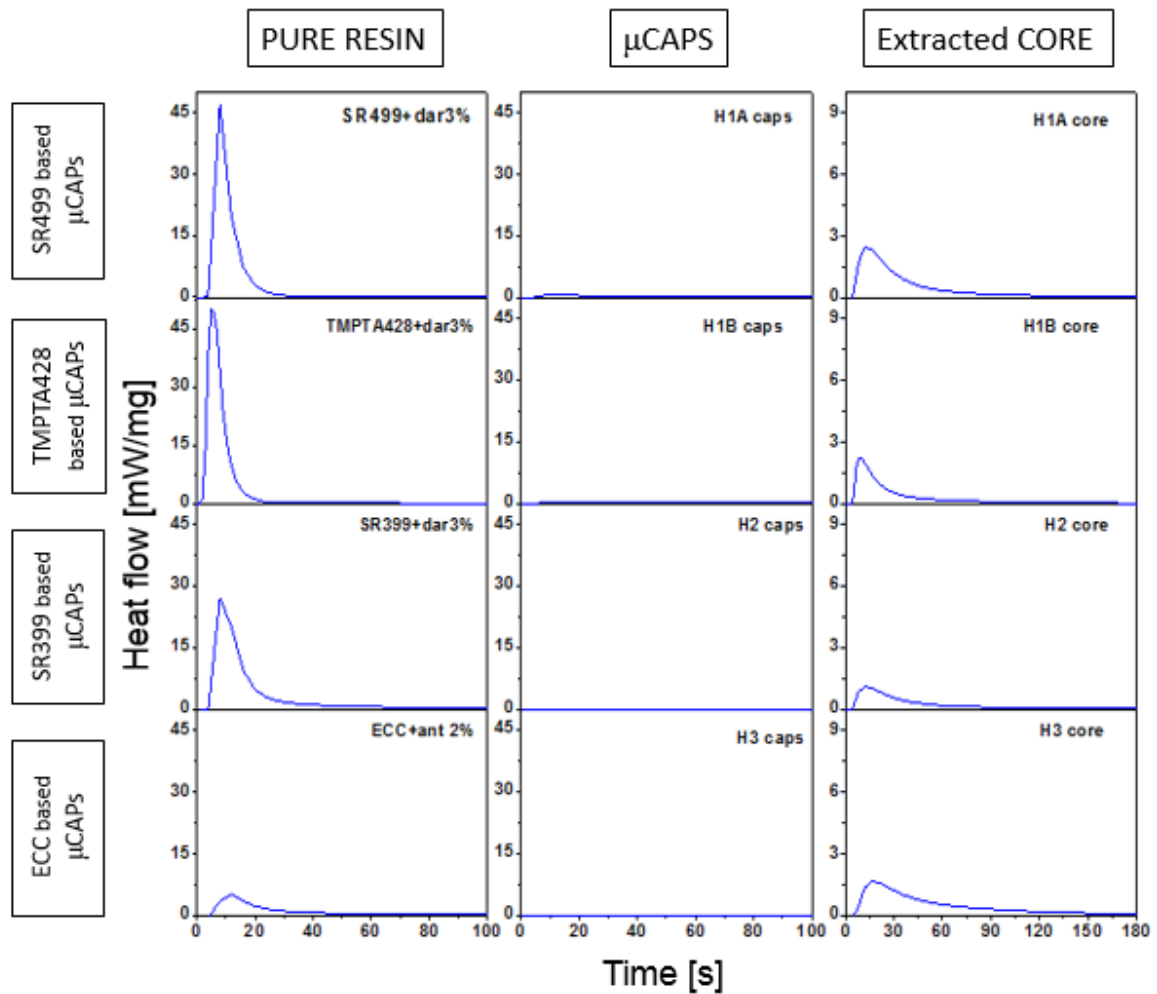
Figure 3.27: p-DSC thermograms of pure resins, synthetized microcapsules and cores extracted.

Resin Sample	Enthalpy measured by p-DSC (J/g)	Capsules	Enthalpy measured by p-DSC (J/g)
SR499 + dar 3%	329	H1A	77
TMPTA428 + dar 3%	335	H1B	48
SR399 + dar 3%	254	H2	35
ECC+ant2%	65	H3	71

Table 3.8: Data from p-DSC measurements performed on the different self-healing system.All values are affected by 5% error.

3.5.3. SYNTHESIS OF MICROCAPSULES FOR UV HEALING

Microcapsules were prepared by interfacial polymerization by oil-in-water (O/W) emulsion technique. Polyurea shell of microcapsules was obtained by reaction of TDI-prepolymer and 4-4' Diaminobenzophenone (DABP). The fabrication of microcapsules O/W emulsion has been reported in section 0.

The mechanism of the microencapsulation of UV-curable agents and its photoinitiator in a PUrea shell has been illustrated in Section 2.2.4. It is well-known that the synthesis of PUrea resin includes two steps. In the first step, one of the UV-curable monomers and the TDI-prepolymer were added into the aqueous reaction solution to form the emulsions so that the TDI would precipitate on the surface of the oily phase droplets, forming a PUrea shell reacting with the amine added in the second step. At the end of the process microcapsules loaded with an UV-curable healing system were obtained. A list of the synthetized microcapsules is reported in Table 3.9.

SAMPLE	Core	Shell
H1A	SR499	DABP
H1B	TMPTA428	DABP
H2	SR399	DABP
H3	EEC	DABP

Table 3.9: Nomencalture and chemicals of self-healing microcapsules.

3.6. CHARACTERIZATION OF MICROCAPSULES

3.6.1. OM and SEM (diameters and thicknesses)

Microcapsules were imaged using Optical Microscope (OM) and scanning electron microscopy (SEM) at various magnifications, Figure 3.28 reports most representative pictures of synthetized microcapsules and shows that all microcapsules are spherical in shape. The outer and inner surfaces of the capsules are quite smooth and the shell wall thicknesses are roughly uniform (see SEM images Figure 3.28). The microcapsules were

ruptured to measure the shell thickness, and it was found to be 2.5 μm for H1A and 3 μm for H1B (Figure 3.29). From OM imagining it is interesting to note that the microcapsules have a different optical transparency (Figure 3.28 OM), probably caused by the different materials encapsulated.
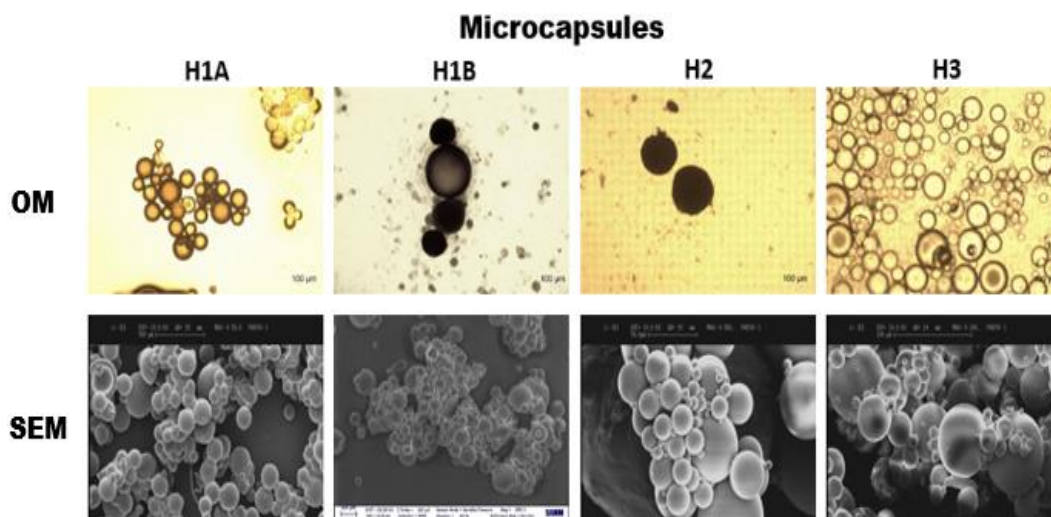
Figure 3.28: OM (up) and SEM (down) images of UV-healing microcapsules.
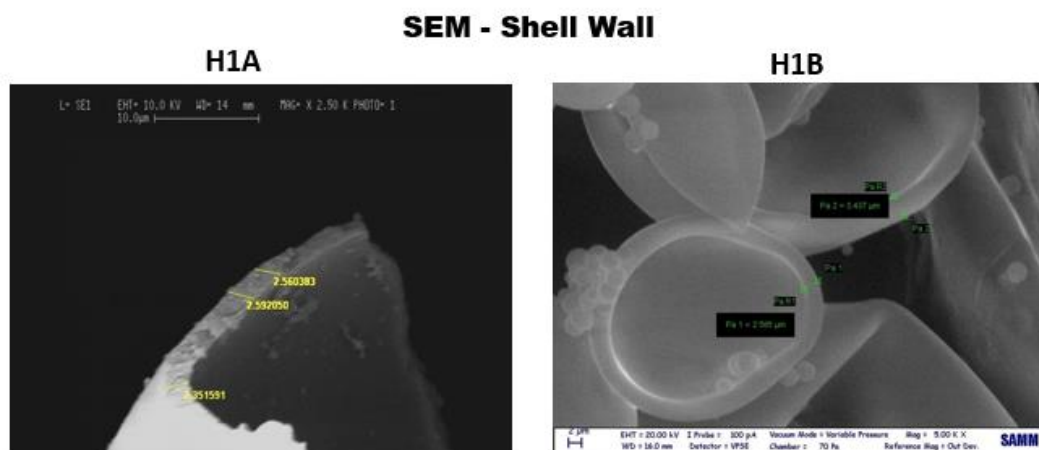
Figure 3.29: SEM images cross-section of capsule shell wall.

The average size of the microcapsules (values reported in Table 3.10) is approximately 111,100, 528 and 119 μm for H1A, H1B, H2 and H3 sample respectively, with a narrow particle size distributions as confirmed from Figure 3.30. The microcapsule size is in a wide range of 47–311 μm for H1A, 39-249 μm for H1B, 110-984 μm for H2 and 110-1218 μm for H3 (also listed in Table 3.10). The reason is that the fluid flow around the propeller is turbulent; in the region of flow away from the propeller; many larger micro eddies exist, and in the vicinity of the propeller blades, many smaller micro eddies exist, which result in a wider length scale. As can be seen from Figure 3.28, most of the particles fall in the size

range between 50-150 μm for H1A, H1B and H3 samples, this is quite satisfactory for the use in self-healing of material. While H3 is characterized by a big amount of capsules with diameter higher than 600 μm, which made them impossible to use for any coating applications.

Sample	D_{mean} [μm]	SD[μm]	D_{max} [μm]	D_{min} [μm]
H1A	111	48	311	47
H1B	100	39	249	39
H2	642	225	1218	110
H3	119	48	308	26

Table 3.10: Average Diameter and Size Distribution of Self-Healing Microcapsules Synthesized
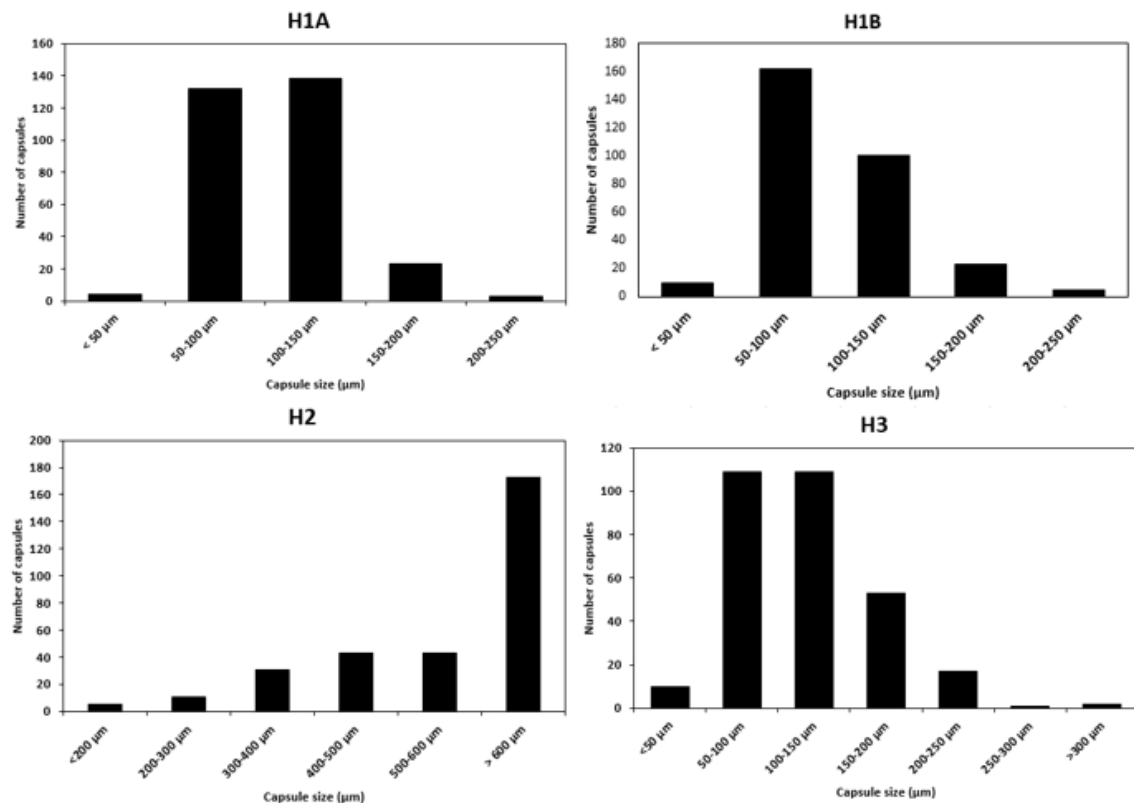

Figure 3.30: Microcapsule sizes and their distributions.

3.6.2. Yield of microcapsules and determination of core fraction.

The amount of encapsulated content in microcapsules was determined by the weighing method, using the same procedure adopted for sunflower oil based microcapsules described in Chapter 3.3.2. The process follows a solvent extraction method, that is used to separate the encapsulated species from shell, and that is based on solubility characteristics. Acetone was used as extracting solvent, owing to its good miscibility with all resins. The following equations were used to calculate the efficiencies.

Reaction efficiency
$$\eta_r = \frac{m_{caps}}{m_{reagent\ start} - m_{by-products}}$$

Encapsulation efficiency
$$\eta_{encaps} = \frac{m_c * m_{caps}}{m_{ic}}$$

Core fraction
$$X_c = \frac{m_c}{m_i}$$

Where, m_{caps} is mass of collected dry microcapsules; $m_{reagent\ start}$ is total mass of initial substances; $m_{by-products}$ is mass of reaction by-products supposed to be equal to zero; m_c is mass core extracted; m_{ic} is initial mass core and m_i is mass crushed capsules, always equal to 1g.

The reaction efficiency, the encapsulation efficiency and the core fraction (obtained by both the extraction method and TGA calculations) are reported in Table 3.11. According to the data, reaction efficiencies fall within the range 55-71%. The amount of oily phase encapsulated with respect to the total amount introduced in the reaction (η_{encaps}) is essentially the same (around 70%) for all of experiments, apart from the H3 sample where less than half of the initial value of core material (43%) was encapsulated. These are unsurprising results, to which several factors contribute. In fact, because of the different viscosity of the resins, the droplets of the dispersed phase produced in the emulsifying step have dissimilar sizes; moreover, due to their chemical nature, different losses of resin mass may occur during the synthesis as a consequence of the differences in the volatility, aqueous solubility, or reactivity of some constituents in the reaction medium. Then, the synthetic conditions (emulsion composition, reaction temperature stirring rate, etc.) should be tuned case by case to maximize the encapsulation efficiencies.

In Table 3.11 values of core fraction, obtained by the extraction method and TGA analysis, can be compared. The values obtained with two methods are in agreement for H1A and H3 samples only, demonstrating that the synthesized microcapsules in this study consist mainly of UV curing resin (core material) and of a smaller amount of DABP based UV screening

polyurea (shell material). The core fractions resulting from the TGA for H1B and H2 samples are significantly lower than those obtained by the extraction method. This discrepancy might be due to the underestimation of the core fraction using the TGA analysis; it could happen indeed that the core and shell evaporation occurred at nearly overlapping temperature interval. The extraction method however revealed that the core fraction of all samples fall within the reasonably narrow range 57-70%

Sample	$\eta_r(\%)$	$\eta_{encaps}(\%)$	X_c (%)	X_c^{TGA} (%)
H1A	71	73	70	72
H1B	68	65	65	37
H2	71	64	65.5	31
H3	55	41	57	50

Table 3.11: Reaction efficiencies, encapsulation efficiencies and core fractions of self-healing microcapsules.

3.6.3. Thermal properties and compositional analysis

The thermal properties of the photopolymerizable resins as a core material, the microcapsule shell wall, and the filled microcapsules were determined by thermogravimetric analysis (TGA). The resultant curves of weight loss and derivate of TGA data for each material are given in Figure 3.31.

The decomposition of DABP based polyurea polymer is composed of three weight loss stages corresponding to 34% at 25-268 °C, 32% the at 268–372°C and 44% at 372-600°C. The core constituents all show one step loss at different temperatures. The microcapsules samples as a consequence showed again three weight loss steps. In details, for the H1A sample, in the TGA curve there is a 28% weight loss at 266-365°C, 48% at 365-500°C and 10% at 500-563°C. For H1B microcapsules, the TGA curve shows a 14% weight loss up to 228°C, 57% at 228-436 °C, 9% at 436-488°C and 14% at higher temperatures. In the H2 TGA curve there are weight losses at 235-360°C (20%), at 360-432°C (32%),at 432-496°C (15%). Finally for the H3 sample, the TGA curve shows a 50% weight loss at 100-362°C and a 30% weight loss at 362-526°C. Determining all these weight loss intervals was useful in extrapolating the core fraction values already shown in table 3.11. Furthermore all microcapsules plots in figure 3.31 clearly demonstrate their thermal stability up to 200°C. This fundamental property ensures their processability at high temperature and makes them suitable for a wide range of applications including high temperature resistance coatings.
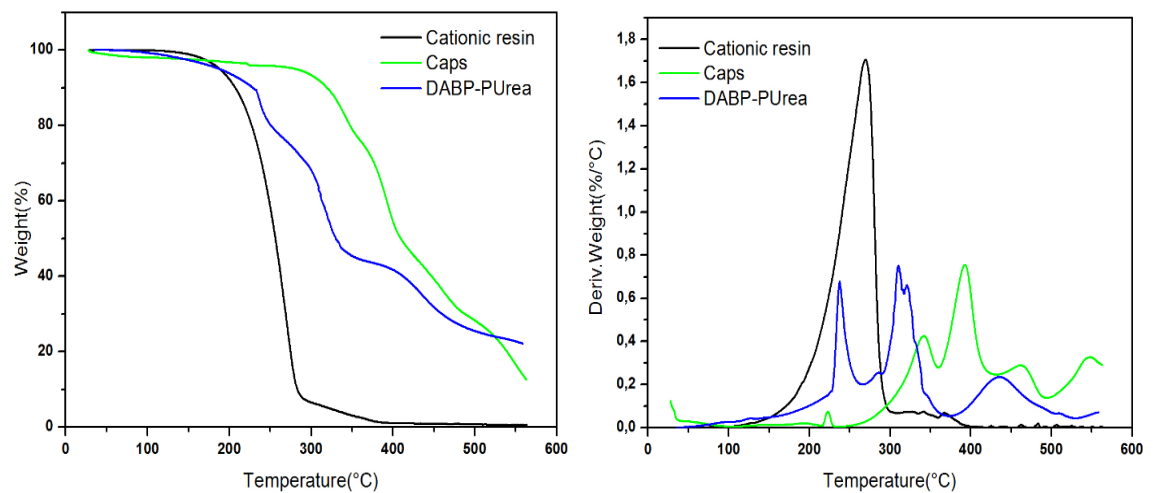
H1A
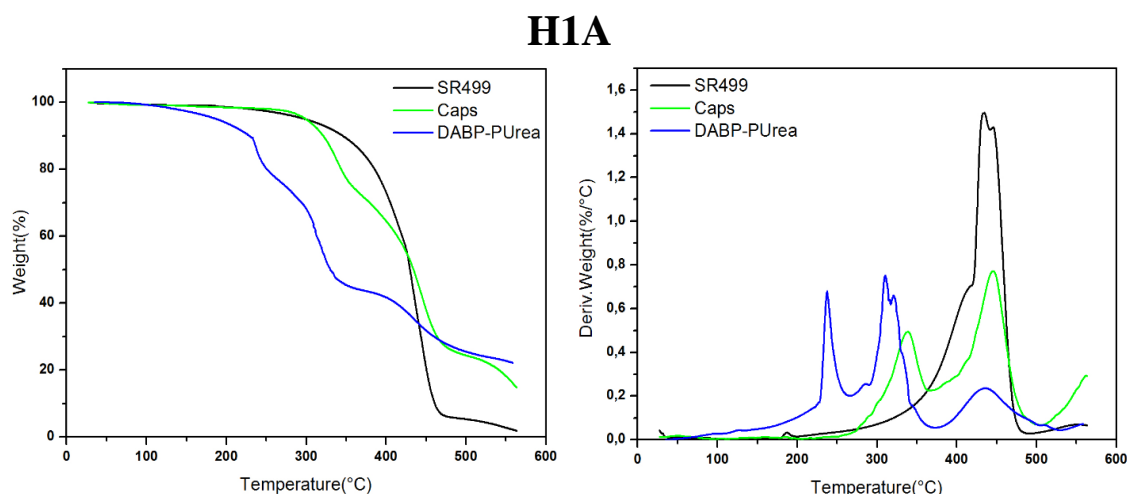
H1B
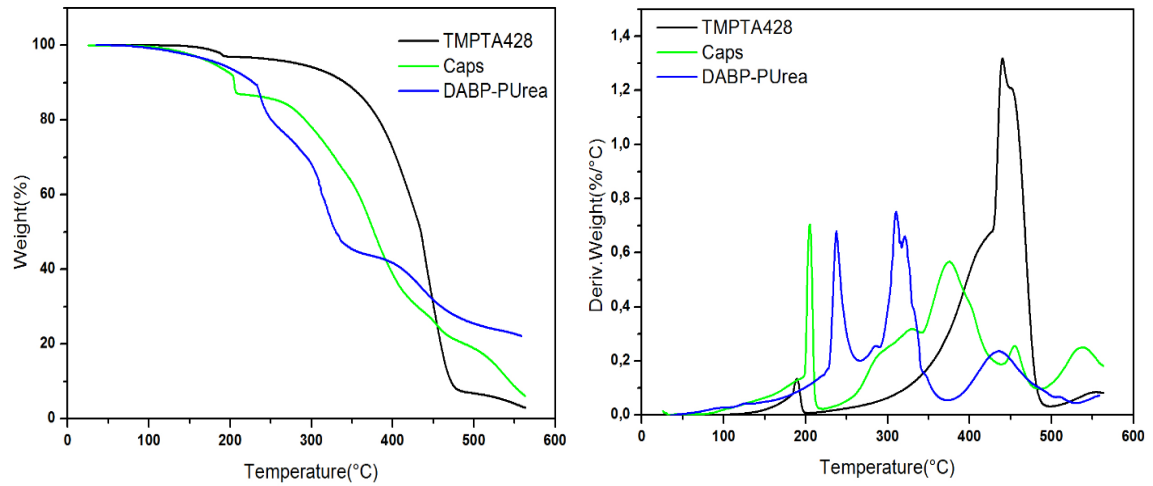
H2
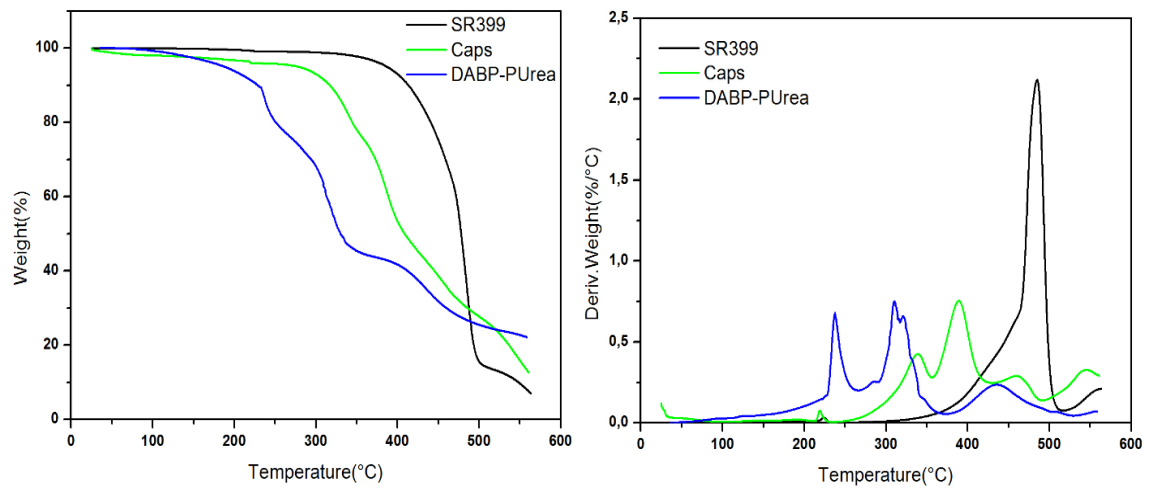
H3

Figure 3.31: TGA (left) and Weight loss curves (right) of pure resin, synthetized microcapsules and shell for all self-healing systems.

3.6.4. Chemical characterization by spectroscopic technique

FTIR spectroscopy analyses were performed on the resins with the same amount of photoinitiatorused for the encapsulation processes. Those spectra were compared with the FTIR of the core extracted from all synthetized microcapsules. The comparison of two spectra it is a fundamental tool to have a further confirmation that the core material was successfully encapsulated.

Figure 3.32 and Figure 3.33 show spectra of SR499 and TMPTA428 which are identical since the molecule is exactly the same. It is possible to see the presence of characteristic bands of this molecule, in particular at 1722 cm^{-1} (C=O stretching vibration), 983 cm^{-1} (wagging of the =CH_2 group), and 808 cm^{-1} (twisting of the =CH_2 group).

In Figure 3.34 is presented the spectrum of the cationic resin (EEC). The main absorption band of oxirane ring is located at 790 cm^{-1}. This resin shows also the bands corresponding to the stretching C-O-C of ethers (1100 cm^{-1}) and the C=O stretching (1730 cm^{-1}) of esters. These peaks are presented also in the core material of H1B sample, which indicates that this compounds have been encapsulated in microcapsules.
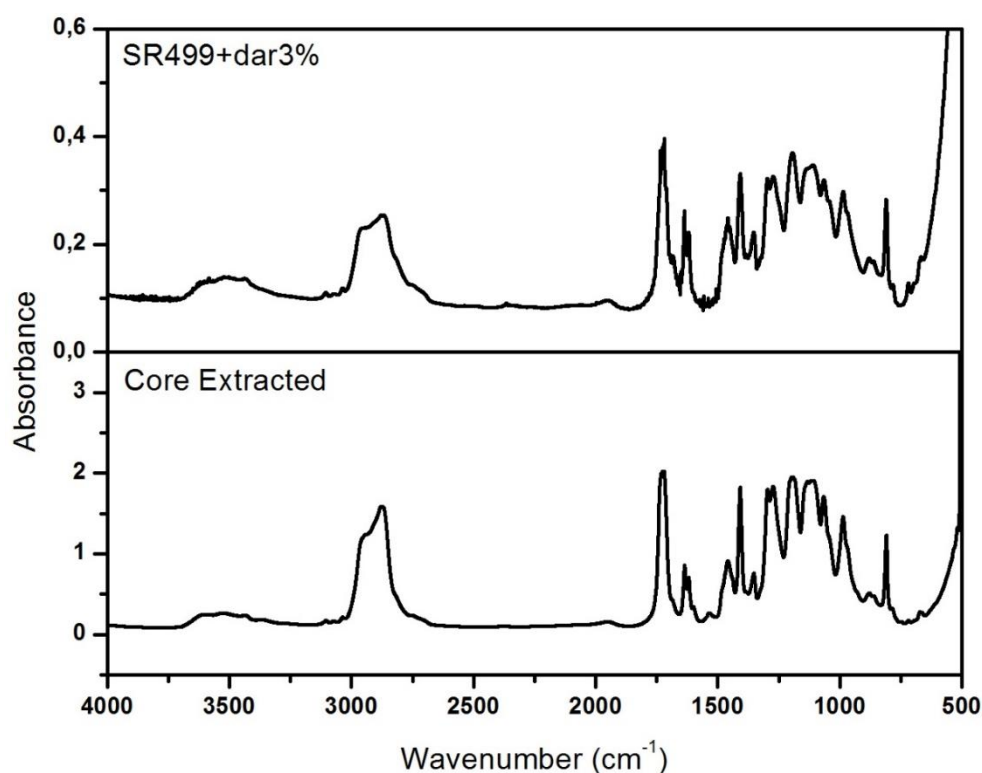

Figure 3.32: FTIR spectra SR499 and core material of microcapsule.
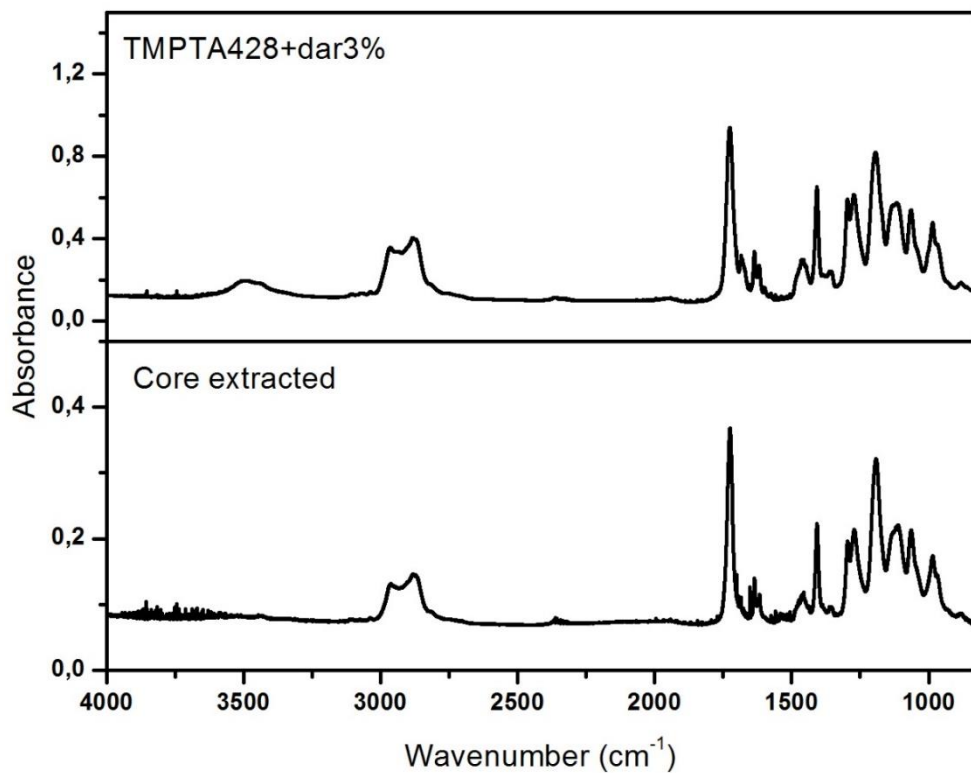
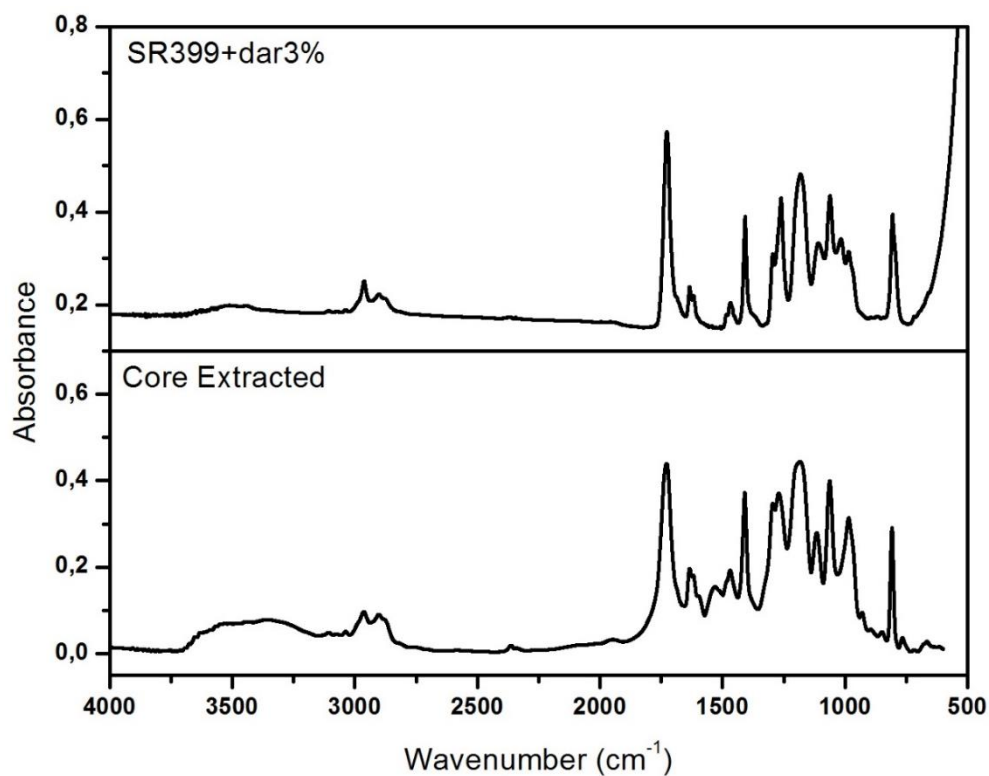**Figure 3.33: FTIR spectra TMPTA428 and core material of microcapsule.**

Figure 3.34: FTIR spectra SR399 and core material of microcapsule.
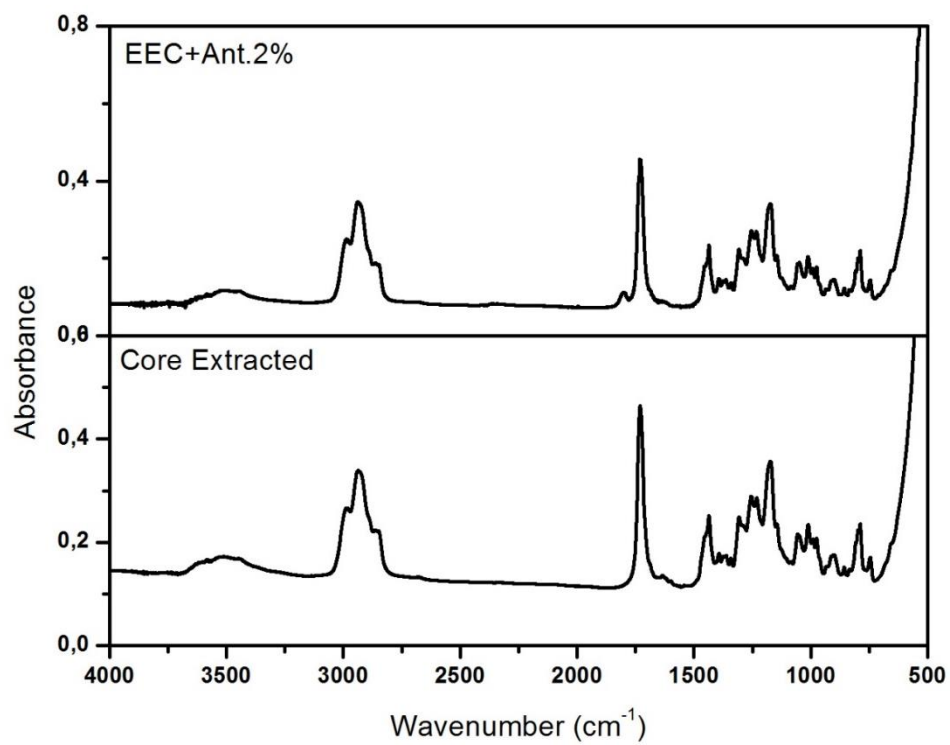
Figure 3.35: FTIR spectra ECc and core material of microcapsule.

4. CONCLUSION AND FUTURE WORKS

The design, fabrication, and construction of smart structures is one of the ultimate challenges for engineering researchers today. In this field, the development of microcapsule-based coating systems is an area of great interest. An ideal triggerable microcapsule system is easy to prepare from readily available components, exhibits good stimuli selectivity, is compatible with many triggers, and disassembles into products that are inert and gaseous. An ideal capsule would interact with its environment rather than merely be reactive, thereby unlocking new applications for triggered release. Obtaining an ideal system requires improvements in capsule materials and synthetic methods along with goals for future applications and design paradigms.

The present work reports the fabrication of novel microcapsules characterized by a UV-screening shell to be used as fillers in advanced composite materials. By reacting a TDI-based polyisocyanate with a benzophenone based amine, it is possible to obtain mechanically robust UV-absorbing shells based on polyurea. Microcapsules were designed to be used in two types of smart systems in the field of damage-sensing and self-healing.

Initial efforts were focused on the optimization of a microencapsulation process in which the core material was based on a photochromic UV-sensitive dye dissolved in sunflower oil. The influence of the composition of the shell, on microcapsules properties was firstly investigated by synthetizing microcapsules incorporating on shell based on either 2-Amino-5-chlorobenzophenone (ACBP) or 4-4' Diaminobenzophenone (DABP). Differential scanning calorimetry (DSC), thermo-gravimetric analysis (TGA), optical (OM) and scanning electronic microscopy (SEM), Infrared spectroscopy (FTIR) revealed that there are no substantial differences in terms of thermal properties, dimensions, morphology between the two types of microcapsules. Both polyurea shells have also demonstrated a good screening capability when exposed to UV radiation. However, the synthetized microcapsules demonstrated different degrees of stability depending on shell materials when in contact with solvents commonly used in commercial coatings. ACBP microcapsules showed a low resistance in solvents, with a release of a large amount of core materials within a few minutes. Instead, the release of DABP capsules turns out to be quite insignificant. The results reveal a different potential for the use of these microcapsules in functional coatings for the nondestructive in situ visual detection of mechanical damages by color change. In particular,

while ACBP based microcapsules may pose significant challenges in coating application due to the possibility of employing only solvent-free coating systems, DABP microcapsules have shown a much wider potential in terms of solvent compatibility, making this system also suitable for common solvent based paint formulations.

After optimization of the microcapsule shell properties, the laboratory study focused on the encapsulation of a different family of dyes. Microcapsules containing sunflower oil with a fluorescent molecule encapsulated within DABP polyurea shell were successfully synthesized and analyzed to develop an innovative damage sensing system. These microcapsules were incorporated into different matrixes including a waterborne polyurethane and a commercially available acrylpolyurethane. Coating formulations containing polyurea microcapsules with fluorescent dye encapsulated acted as damage sensors, showing a fluorescent signal when scratch was applied on its surface to simulate a real damage and after subsequent exposure to UV radiation. The incorporation of sensors in a protective coating, simple and accessible to non-specialized personnel, is an important improvement with respect to traditional coatings and potentially complement some of the existing technologies for assessment of structures and visual inspection of products. This system permits an easy detection of the damaged area by the use of a common UV lamp.

Finally, the possibility to incorporate photopolymerizable resins into the UV-screening polyurea shell was also demonstrated. Chemical and morphological characterizations revealed that all types of resins chosen were successfully encapsulated. Microcapsules containing UV curing resins will enable new healing chemistries for self-healing polymers that are robust and stable and are single component catalyst-free systems. Fast curing of the extracted core material under UV-light irradiation was observed, suggesting that the encapsulated resins do not lose their crosslinking capability after processing. This system shows therefore great promise in the field of advanced self-healing.

Stimuli-sensitive composites possess great potential for solving some of the most limiting problems of polymeric structural materials: microcracking and hidden damage. Microcracks are the precursors to structural failure and the ability to reveal and consequently heal them will enable structures with longer lifetimes and less maintenance. Filling microcracks will also mitigate the deleterious effects of environmentally assisted degradation such as moisture swelling and stress corrosion cracking. This work demonstrates that microencapsulation is

a versatile approach because it can be used to encapsulate a large number of materials and it is possible to incorporate microcapsules into composites or coatings.

Future investigations will focus on testing the microcapsules in compression to determine the elastic stiffness of the shell wall and the strength of the microcapsule as a function of dimensions and shell composition. A potential future application may include the possibility to encapsulate dues of different colors within microcapsules with different known molecular properties and use such system as highly sensitive pressure or stress sensors. Also different compounds, such as self-healing agents and dyes can be encapsulated obtaining systems with a synergic action of damage detection and repair capability.

BIBLIOGRAPHIC REFERENCES

[1] Gandhi, M. V. & Thompson, B. S. Smart Materials and Structures. (Chapman & Hall, London, UK,, 1992).

[2] Thompson, B. S., Gandhi, M. V. & Kasiviswanathan, S. An introduction to smart materials and structures. Mater. Des. 13, 3–9 (1992).

[3] Rogers, C. A. & Crawley, E. F. Intelligent Materials Systems and Structures (Seminar Notes): March 29-30, 1990. (1991).

[4] Bogue, R. Smart materials: a review of recent developments. Assem. Autom. 32, 3–7 (2012).

[5] Goddard, N. D. R., Kemp, R. M. J. & Lane, R. An Overview of Smart Technology. Packag. Technol. Sci. 10, 129–143 (1997).

[6] Funakubo, H. Shape Memory Alloys. (1987).

[7] Chen, H. R. Shape Memory Alloys: Manufacture, Properties and Applications. 546 (Nova Science Publishers, 2010).

[8] Rogers, A. . Distributed optical-fibre sensors for the measurement of pressure, strain and temperature. Phys. Rep. 169, 99–143 (1988).

[9] Filisko, F. E. Electrorheological materials: smart materials of the future. Chem Ind. 370–373 (1992).

[10] Moulson, A. & Herbert, J. Electroceramics: Materials, Properties, Applications. (Springer Series, 1990).

[11] Feng, W., Patel, S. H., Zunino III, J. L., Young, M.-Y. & Xanthos, M. Smart polymeric coatings—recent advances. Adv. Polym. Sci. 26, 1–13 (2007).

[12] Zwaag SV (2007). An Introduction to Material Design Principle: Damage Prevention versus Damage Management. In self Healing Materials: An alternative Approach to 20 Centuries of Materials Science, Vol. 100. The Netherland: Springer.

[13] H. Fischer / Natural Science 2 (2010) 873-901.

[14] S. Rattanachan, Y. Miyashita, Y. Mutoh Fabrication of piezoelectric laminate for smart materials and crack sensing capability Sci. Technol. Adv. Mater., 6 (2005), pp. 704–711.

[15] S.-G. Shin, H.-J. Lim, J.-H. Lee Fabrication and properties of self-diagnosis glass fiber-reinforced plastics for low loading Han'guk Chaelyo Hakhoechi, 13 (2003), pp. 732–736

[16] B. Zhang, B. Benmokrane, J.-F. Nicole, R. Masmoudi Evaluation of fiber optic sensors for structural condition monitoring Mater. Struct., 35 (2002), pp. 357–364

[17] K. Sudo, H. Watanabe, G. Nishino, Cracking detection materials, their manufacture and system and method using them, JP 2005172809 (2005).

[18] Bergman, S. D. & Wudl, F. Re-Mendable Polymers. 45–68 (2007).

[19] Wool, R. P. Self-healing materials: a review. Soft Matter 4, 400 (2008).

[20] Van Der Zwaag, S. . Self Healing Materials: An Alternative Approach to 20 Centuries of Materials Science. (Springer Series, 2007).

[21] Wu, D. Y., Meure, S. & Solomon, D. Self-healing polymeric materials: A review of recent developments. Prog. Polym. Sci. 33, 479–522 (2008).

[22] Yuan, Y. C. Self healing in polymers and polymer composites. Concepts, realization and outlook: A review. eXPRESS Polym. Lett. 2, 238–250 (2008).

[23] Spanoudakis J, Young RJ. Crack propagation in a glass particle-filled epoxy resin. J Mater Sci 1984;19:487–96

[24] Aaron P. Esser-Kahn, Susan A. Odom, Nancy R. Sottos, Scott R. White and Jeffrey S. Moore "Triggered Release from Polymer Capsules" Macromolecules 2011, 44, 5539–5553.

[25] De Geest, B. G.; Van Camp, W.; Du Prez, F. E.; De Smedt, S. C.; Demeester, J.; Hennink,W. E. Macromol. Rapid Commun. 2008, 29, 1111–1118.

[26] Pastoriza-Santos, I.; Sch€oler, B.; Caruso, F. Adv. Funct. Mater. 2001, 11, 122–128.

[27] Khapli, S.; Kim, J. R.; Montclare, J. K.; Levicky, R.; Porfiri, M.; Sofou, S. Langmuir 2009, 25, 9728–9733.

[28] Brown E. N, Sottos N. R., White S. R.: Fracture testing of a selfhealing polymer composite. Experimental Mechanics, 42, 372–379 (2002).

[29] Cho S. H., Andersson H. M., White S. R., Sottos N. R., Braun P. V.: Polydimethylsiloxane based selfhealing materials. Advanced Materials, 18, 997–1000 (2006).

[30] Huang M, Yang J. Facile microencapsulation of HDI for self-healing anticorrosion coatings. J Mater Chem 2011;21:11123–30.

[31] M. W. Keller and N. R. Sottos, "Mechanical properties of microcapsules used in a self-healing polymer," Experimental Mechanics, vol. 46, no. 6, pp. 725–733, 2006.

[32] E. N. Brown, S. R. White, and N. R. Sottos, "Microcapsule induced toughening in a self-healing polymer composite," Journal of Materials Science, vol. 39, no. 5, pp. 1703–1710, 2004.

[33] J. D. Rule, N. R. Sottos, and S. R. White, "Effect of microcapsule size on the performance of self-healing polymers," Polymer, vol. 48, no. 12, pp. 3520–3529, 2007.

[34] Jones A.S, Rule J.D, Moore J.S, White S.R, Sottos N.R. Catalyst morphology and dissolution kinetics for self-healing polymers. Chem. Mater. 2006;18:1312–1317.

[35] E. N. Brown, S. R. White and N. R. Sottos: 'Retardation and repair of fatigue cracks in a microcapsule toughened epoxy composite – Part II: In situ self-healing', Compos. Sci. Technol., 2005, 65, 2474–2480.

[36] Kessler MR, Sottos NR, White SR. Self-healing structural composite materials. Composites Part A 2003;34:743-753.

[37] J. D. Rule and J. S. Moore: 'ROMP reactivity endo- and exodicyclopentadiene', Macromolecules, 2002, 35, 7878–7882.

[38] T. C. Mauldin, J. D. Rule, N. R. Sottos, S. R. White and J. S. Moore: 'Self-healing kinetics and stereoisomers of dicyclopentadiene', J. R. Soc. Interface, 2007, 4, 389–393.

[39] Liu X, Lee JK, Yoon SH, Kessler MR. 2006. Characterization of diene monomers as healing agents for autonomic damage repair. J. Appl. Polym. Sci. 101(3):1266–72.

[40] Rule JD, Brown EN, Sottos NR, White SR, Moore JS. Wax-protected catalyst microspheres for efficient selfhealing materials. Adv Mater 2005;17:205–8.

[41] Kamphaus JM, Rule JD, Moore JS, Sottos NR, White SR. A new self-healing epoxy with tungsten (VI) chloride catalyst. J Roy Soc Interface 2008;5:95-103.

[42] Keller M. K., White S. R., Sottos N. R.: A self-healing poly(dimethyl siloxane) elastomer. Advanced Functional Materials, 17, 2399–2404 (2007).

[43] M. Z. Rong, M. Q. Zhang and W. Zhang: 'A novel self-healing epoxy system with microencapsulated epoxy and imidazole curing agent', Adv. Compos. Lett., 2007, 16, 167–172.

[44] Yin T, Rong MZ, Zhang MQ, Yang GC. Self-healing epoxy composites - preparation and effect of the healant consisting of microencapsulated epoxy and latent curing agent. Composite Sci Technol 2007;67:201-212.

[45] Caruso M. M., Delafuente D. A., Ho V., Moore J. S., Sottos N. R., White S. R.: Solvent-promoted self-healing materials. Macromolecules, 40, 8830–8832 (2007).

[46] Quérat E, Tighzert L, Pascault J-P. Microencapsulation of isocyanates. Characterization and storage stability of microcapsules in a polyester a, x-ol. J Coat Technol 1996;68(854):83–90.

[47] Cheong IW, Kim JK. Synthesis of core–shell polyurethane–urea nanoparticles containing 4,40-methylenedi-p-phenyl diisocyanate and isophorone diisocyanate by self-assembled neutralization emulsification. Chem Commun 2004:2484–5.

[48] Yang J, Keller MW, Moore JS, White SR, Sottos NR. Microencapsulation of isocyanates for self-healing polymers. Macromolecules 2008;41:9650–5.

[49] B. Di Credico, M. Levi, S. Turri Eur. Polym. J., 49 (2013), pp. 2467–2476.

[50] C. Suryanarayana, R. K. Chowdoji and D. Kumar, Prog. Org. Coat., 2008, 63, 72.

[51] Cho, S.-Y.; Kim, J.-G.; Chung, C.-M. Sens. Actuators, B 2008, 134, 822−825.

[52] Davis, D. A.; Hamilton, A.; Yang, Y.; Cremar, L. D.; Gough, D. V.; Potisek, S. L.; Ong, M. T.; Braun, P. V.; Martínez, T. J.; White, S. R.; Moore, J. S.; Sottos, N. R. Nature 2009, 459, 68−72.

[53] Lee, C. K.; Davis, D. A.; White, S. R.; Moore, J. S.; Sottos, N. R.; Braun, P. V. J. Am. Chem. Soc. 2010, 132, 16107−16111.

[54] Kingsburry, C.; May, P.; Davis, D. A.; White, S. R.; Moore, J. S.; Sottos, N. R. J. Mater. Chem. 2011, 21, 8381−8388.

[55] Lowe, C.; Weder, C. Adv. Mater. 2002, 14, 1625−1629.

[56] Crenshaw, B.; Weder, C. Chem. Mater. 2003, 15, 4717−4724.

[57] Donati, F.; Pucci, A.; Cappelli, C.; Mennucci, B.; Ruggeri, G. J. Phys. Chem. B 2008, 112, 3668.

[58] Azzaroni, O.; Trappmann, B.; Rijn, P. V.; Zhou, F.; Kong, B.; Huck, W. T. S. Angew. Chem., Int. Ed. 2006, 45, 7440.

[59] Feng, W.; Patel, S.H .; Young, M.-Y.; Zunino, J. L. III; Xanthos, M. Adv. Polym. Technol. 2007, 26, 1−13.

[60] Pang, J. W.; Bond, I. P. Compos. Sci. Technol. 2005, 65, 1791− 1799.

[61] D. Ramachandran, F. Liu and M. W. Urban, Self-repairable copolymers that change color, RSC Adv., 2012, 2, 135.

[62] Odom, S. A.; Jackson, A. C.; Prokup, A. M.; Chayanupatkul, S.; Sottos, N. R.; White, S. R.; Moore, J. S. ACS Appl. Mater. Interfaces 2011, 3, 4547– 4551

[63] Noh et al. – eXPRESS Polymer Letters Vol.7, No.1 (2013) 88–94

[64] Bucknall, C. B., Drinkwater, I. C. & Smith, G. R. Hot plate welding of plastics: Factors affecting weld strength. Polym. Eng. Sci. 20, 432–440 (1980).

[65] Liu, D., Lee, C. Y. & Lu, X. Repairability of Impact-Induced Damage in SMC Composites. J. Compos. Mater. 27, 1257–1271 (1993).

[66] Aïssa, B., Therriault, D., Haddad, E. & Jamroz, W. Self-Healing Materials Systems: Overview of Major Approaches and Recent Developed Technologies. Adv. Mater. Sci. Eng. 2012, 1–17 (2012).

[67] Murphy, E. B. & Wudl, F. The world of smart healable materials. Prog. Polym. Sci. 35, 223–251 (2010).

[68] White, S. R. et al. Autonomic healing of polymer composites. Nature 409, 794–7 (2001).

[69] Cho, S. H., Andersson, H. M., White, S. R., Sottos, N. R. & Braun, P. V. Polydimethylsiloxane-Based Self-Healing Materials. Adv. Mater. 18, 997–1000 (2006).

[70] Ye, L. et al. Self-healing epoxy composites − Preparation and effect of the healant consisting of microencapsulated epoxy and latent curing agent. Compos. Sci. Technol. 67, 201–212 (2007).

[71] Lin, C. B., Lee, S. & Liu, K. S. Methanol-Induced crack healing in poly(methyl methacrylate). Polym. Eng. Sci. 30, 1399–1406 (1990).

[72] Yang, J., Keller, M. W., Moore, J. S., White, S. R. & Sottos, N. R. Microencapsulation of Isocyanates for Self-Healing Polymers. Macromolecules 41, 9650–9655 (2008).

[73] Chung, C.-M., Roh, Y.-S., Cho, S.-Y. & Kim, J.-G. Crack Healing in Polymeric Materials via Photochemical [2+2] Cycloaddition. Chem. Mater. 16, 3982–3984 (2004).

[74] Fortin, J.-P., Gazeau, F. & Wilhelm, C. Intracellular heating of living cells through Néel relaxation of magnetic nanoparticles. Eur. Biophys. J. 37, 223–8 (2008).

[75] Wang, Y., Bolanos, E., Wudl, F., Hahn, T. & Kwok, N. Self-healing polymers and composites based on thermal activation. in 14th Int. Symp. Smart Struct. Mater. Nondestruct. Eval. Heal. Monit. (Dapino, M. J.) 65261I–65261I–12 (International Society for Optics and Photonics, 2007). doi:10.1117/12.715507

[76] Kalista, S. J., Ward, T. C. & Oyetunji, Z. Self-Healing of Poly(Ethylene-co-Methacrylic Acid) Copolymers Following Projectile Puncture. Mech. Adv. Mater. Struct. 14, 391–397 (2007).

[77] Dry CM, Sottos NR. Passive smart self-repair in polymer matrix composite materials. In: Conference on recent advances in adaptive and sensory materials and their applications. Virginia, USA: Technomic; 1992. p. 438–44.

[78] White S. R., Sottos N. R., Geubelle P. H., Moore J. S., Kessler M. R., Sriram S. R., Brown E. N., Viswanathan S.: Autonomic healing of polymer composites. Nature, 409, 794–797 (2001).

[79] Dry C. Procedures developed for self-repair of polymer matrix composite materials. Composite Struct 1996;35:263-269.

[80] Dry C, McMillan W. Three-part methylmethacrylate adhesive system as an internal delivery system for smart responsive concrete. Smart Mater Struct 1996;5:297-300.).

[81] M. Motuku, U.K. Vaidya, G.M. Janowski, Parametric studies on self-repairing approaches for resin infused composites subjected to low velocity impact, Smart Mater Struct, 8 (1999),pp. 623–638.

[82] S.M. Bleay, C.B. Loader, V.J. Hawyes, L. Humberstone, P.T. Curtis, A smart repair system for polymer matrix composites Composites Part A, 32 (2001), pp. 1767–1776.

[83] Toohey KS, Sottos NR, Lewis JA, Moore JS, White SR. 2007. Self-healing materials with microvascular networks. Nat. Mater. 6(8):581–85.

[84] Williams HR, Trask RS, Bond IP. 2007. Self-healing composite sandwich structures. SmartMater. Struct. 16(4):1198–207.

[85] Lewis R. Hart Josephine L. Harries Barnaby W. Greenland, Howard M. Colquhoun and Wayne Hayes Healable supramolecular polymers Polym. Chem., 2013, 4, 4860–4870

[86] Yinlei Lin and Guangji Li*An intermolecular quadruple hydrogen-bonding strategy to fabricate self-healing and highly deformable polyurethane hydrogelsJ. Mater. Chem. B, 2014, 2, 6878–6885

[87] F.R. Kersey, D.M. Loveless, S.L. Craig A hybrid polymer gel with controlled rates of cross-link rupture and self-repair J Roy Soc Interface, 4 (2007), pp. 373–380.

[88] Crano, J. C.; Guglielmetti, R. J.; Editors *Organic Photochromic an Thermochromic Compounds, Volume 1: Main Photochromic Families*; Plenum Press: New York, 1999

[88 89] E. Fischer, Y. Hirshberg, J. Chem. Soc. 1952, 4522.

[90] Data Sheet:FluorolinkP56

http://www.acota.co.uk/assets/datacentre/tds/solvay/P56.pdf.

[91] Brown, M, E. *Introduction to Thermal Analysis: Techniques and Applications*. 59–77 (1988)

[92] J. F. Rabek in 'Radiation Curing in Polymer Science and Technology: Fundamentals and Methods', (Eds J. P. Fouassier and J. F. Rabek), Vol. I, Elsevier Applied Science, London 1993, p. 371]

[93] Coats, A. W. & Redfern, J. P. Thermogravimetric analysis. A review. Analyst 88, 906(1963).

[94] Atkins, P. & De Paula, J. Elements of Physical Chemistry. 459 (2009).

[95] Hof, M. *"Basics of Optical Spectroscopy" in "Handbook of Spectroscopy."*37–152 (Wiley-VCH Verlag GmbH & Co. KGaA, 2003).

[96] Macokso, C. *Rheology : Principles, measurements and applications.* (1994).

[97] Novel Polyurea Microcapsules Using Dendritic Functional Monomer: Synthesis, Characterization, and Its Use in Self-healing and Anticorrosive Polyurethane Coatings

[98] MEHUL M. PATEL* , CHIRAG J. PATEL and NATVAR K. PATEL Study of Thermal Properties on UV-Curable Coatings Derived from Oleochemical Polyols, Chem Sci Trans., 2012, 1(2), 289-296.